HAL
open science

# Finite Element Approach of Electronic Structures

Amélie Fau

## To cite this version:

Amélie Fau. Finite Element Approach of Electronic Structures. Materials and structures in mechanics [physics.class-ph]. Ecole Centrale Paris, 2012. English. NNT : 2012ECAP0049 . tel-00985912

**HAL Id: tel-00985912**

**https://theses.hal.science/tel-00985912v1**

Submitted on 30 Apr 2014

**HAL** is a multi-disciplinary open access archive for the deposit and dissemination of scientific research documents, whether they are published or not. The documents may come from teaching and research institutions in France or abroad, or from public or private research centers.

L'archive ouverte pluridisciplinaire **HAL**, est destinée au dépôt et à la diffusion de documents scientifiques de niveau recherche, publiés ou non, émanant des établissements d'enseignement et de recherche français ou étrangers, des laboratoires publics ou privés.

# Finite Element Approach of Electronic Structures

# THÈSE

présentée et soutenue publiquement le 10 décembre 2012

pour l'obtention du

**Doctorat de l'École Centrale Paris**

**(spécialité mécanique, mécanique des matériaux)**

par

Amélie Fau

sous la direction du Prof. D. Aubry

**Composition du Jury**

| | |
|---|---|
| *Président* : | Prof. P. Cortona (SPMS, École Centrale Paris) |
| *Rapporteurs* : | Prof. F. Chinesta (GeM, École Centrale Nantes) |
| | Prof. S Prudhomme (École polytechnique de Montréal) |
| *Examinateur* : | Prof. D. Aubry (MSSMat, École Centrale Paris) |

**Laboratoire de Mécanique des Sols, Structures et Matériaux - C.N.R.S. U.M.R. 8579**

**2012ECAP0049**

# Acknowledgements

Je remercie les membres du jury pour le regard porté sur ces travaux, et pour les précieux conseils et remarques partagés. Je remercie spécifiquement M. Pietro Cortona pour avoir accepté de présider ce jury, M. Serge Prudhomme et M. Paco Chinesta pour avoir rapporté ce travail, et pour l'attention et l'enthousiasme qu'il y ont apportés.

Je remercie M. Denis Aubry pour m'avoir proposé ce sujet de recherche, et pour ce qu'il m'a appris, tant scientifiquement qu'humainement.

Je remercie l'École Centrale Paris pour la qualité de l'accueil dans sa structure, son école doctorale pour sa vitalité et sa disponibilité, et le Département de Mécanique, pour m'avoir offert des possibilités d'enseigner tout au long de ma thèse notamment M. D. Aubry, M$^{me}$ A.-L. Hamon et M$^{me}$ A. Modaressi. Je pense aussi aux dynamiques équipes des laboratoires, tout particulièrement à celle du laboratoire MSSMat, pour cet environnement d'effervescence scientifique, de rencontres multiples et enrichissantes. Merci pour tous ces échanges et les amitiés qui en sont nées.

Je remercie l'École Normale Supérieure de Cachan pour le support financier fourni pour mettre en œuvre ces travaux, et l'ensemble du personnel de son Département de Génie Civil pour m'avoir accueillie si chaleureusement et constructivement dans leur équipe.

高橋先生
温かくご指導くださり、ありがとうございました。
先生の教え方や生徒との信頼関係の築き方は素晴らしく、お手本になりました。
成功して晴れや かでありながら、
まだ社会経験のない謙虚な年頃の生徒たちと接することができました。
先生に感謝！ 生徒たちに感謝！

Pour mes proches, de ma douce vallée, de la grande capitale, de souvenirs toulousains ou de pays lointains, merci ☺ ! Merci pour votre convivialité enjouée, votre simplicité raffinée, vos projets débridés et toutes les couleurs des blés... C'est une joie d'inventer la route avec vous !

# Contents

**Introduction** **1**

I.1 Multi-scale arrangements in materials . . . . . 1

I.2 Scale of the electrons in the mechanical behavior of materials . . . . . 3

I.3 How to obtain electronic information? . . . . . 5

I.4 Objectives and outline of this dissertation . . . . . 5

**1 An *ab initio* perspective for modeling the mechanical behavior of materials** **7**

1.1 Interest of the nanoscale . . . . . 7

1.1.1 Mechanical quantities of interest . . . . . 8

1.1.2 Electrical quantities of interest . . . . . 9

1.2 Modelization at the nanoscale . . . . . 9

1.2.1 Quantum mechanics model . . . . . 11

1.2.2 Classical mechanics model . . . . . 16

1.3 Our framework . . . . . 18

1.3.1 Stationary cases . . . . . 18

1.3.2 Non-relativistic electrons . . . . . 18

1.3.3 Absolute zero temperature . . . . . 19

1.3.4 Born-Oppenheimer's hypothesis . . . . . 20

1.3.5 Breaking down the wave function . . . . . 20

1.4 Methods to tackle the quantum electronic problem . . . . . 22

1.4.1 Hartree-Fock's methods . . . . . 23

1.4.2 Density functional theory . . . . . 23

1.4.3 Quantum Monte Carlo calculations . . . . . 26
1.5 Summary . . . . . 27

**2 Hartree-Fock's models 29**

2.1 State of the art . . . . . 31
2.1.1 Slater determinants . . . . . 31
2.1.2 The post Hartree-Fock methods . . . . . 32
2.1.3 A mathematical viewpoint of the Hartree-Fock's models . . . . . 33
2.2 The Galerkin method for Hartree-Fock models . . . . . 34
2.2.1 The weak form of the Schrödinger problem . . . . . 34
2.2.2 The Galerkin approximation for the Schrödinger problem . . . . . 35
2.2.3 Weak formulation of the multiconfiguration problem . . . . . 36
2.2.4 The weak form of the Hartree-Fock problem . . . . . 39
2.2.5 Weak formulation of the configuration interaction problem . . . . . 43
2.3 Summary . . . . . 45

**3 Numerical strategy 47**

3.1 State of the art . . . . . 47
3.1.1 Basis functions . . . . . 49
3.1.2 Evaluation of the different functions basis . . . . . 52
3.1.3 The FEM in quantum mechanics . . . . . 54
3.2 The FEM strategy for the Hartree-Fock model . . . . . 56
3.2.1 Galerkin approximation . . . . . 56
3.2.2 Newton method . . . . . 56
3.2.3 Artificial boundary conditions . . . . . 64
3.2.4 Mesh and adaptivity . . . . . 66
3.2.5 Symmetry simplifications for atoms and linear molecules . . . . . 67
3.3 Summary . . . . . 71
3.4 Large scale perspectives . . . . . 73

**4 *Ab initio* quantities of interest** **77**

4.1 The one-electron wave functions . . . . . 77

4.1.1 Geometrical distribution of the individual wave functions . . . . . 77

4.1.2 Individual wave functions in bonds . . . . . 81

4.2 The electronic density . . . . . 83

4.3 Prediction of molecular geometry . . . . . 89

4.4 Mechanical properties . . . . . 91

4.4.1 Stress computation . . . . . 91

4.4.2 Elasticity tensor computation . . . . . 93

4.5 Numerical results . . . . . 94

4.6 Three-dimensional computations . . . . . 94

4.7 Summary . . . . . 95

**5 Error indicator for quantum mechanics quantities of interest** **97**

5.1 How exact are our results ? . . . . . 97

5.1.1 Different quantities of interest . . . . . 98

5.1.2 The various origins of error . . . . . 99

5.2 A very short overview of the state of the art . . . . . 104

5.2.1 Error estimate . . . . . 104

5.2.2 Error estimate for *ab initio* computations . . . . . 105

5.3 A first investigation of error indicators with respect to mechanical and quantum quantities of interest . . . . . 106

5.3.1 Error indicator for the ground energy . . . . . 106

5.3.2 Error indicator for the probability of presence . . . . . 109

5.3.3 Error indicator for the mechanical stresses . . . . . 111

**Conclusions and Perspectives** **113**

**Bibliography** **139**

**Appendices** **143**

**A A brief description of microscopes** **143**

**B Periodic Table** **147**

**C Atomic units** **149**

**D Electron configurations of the atoms** **151**

**E Quantum numbers** **155**

**F The weak form of the Hartree-Fock system** **157**

**G Setting up the Hartree-Fock system** **161**

**H The Two-dimensional equations** **165**

**I Magnetic properties** **167**

**J Crystals: The Bloch theorem** **169**

# Introduction

## I.1 Multi-scale arrangements in materials

Multi-scale organization can be observed for most materials. For example, concrete is studied as a structural beam or as a plate from an engineering point of view. At that macroscopic scale, *i.e.* the length scale on which objects are of a size that is observable by the naked eye, the mechanical behavior of concrete is generally modeled as isotropic, continuous, and homogeneous. Under the elasticity hypotheses, it is characterized by its Young's modulus and its Poisson's ratio. To understand this macroscopic behavior, smaller scales can be explored. Concrete appears to be built from aggregates surrounded by a cement paste. The material at that scale is discontinuous and non homogeneous. Each constituent can be assumed as isotropic, continuous, and homogeneous. To characterize the hydrated cement paste, we look at it from a microscopic scale. The cement paste is composed of different constituents: calcium hydroxide CH, calcium silicate hydrate CSH, and calcium aluminate hydrates CAH. A challenging endeavor is to describe CSH gel [PKS+09, DvB11]. The CSH gel is made up of nuclei and electrons. The study of the nuclei provides information on the behavior of the gel. The behavior of the nuclei themselves depends on the interactions created by the nuclei network and the electronic cloud. The most refined model for a mechanical description consists in looking into the behavior of the electrons.

Similarly, an alloy can be seen as a homogeneous material from an engineering point of view, an assembly of grains at a microscopic scale, an assembly of atoms with a periodic or quasiperiodic arrangement or as a nuclear network surrounded by an electronic cloud. As a third example, the layered structures of a clay are detailed in Table 1.

| | Homogeneous Macroscopic scale | Heterogeneous Mesoscopic scales | | Atomic scale |
|---|---|---|---|---|
| Concrete | | Granulates and cement paste | 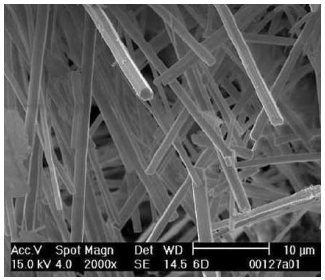  Ettringite (SEM) [vHWvdK03] | 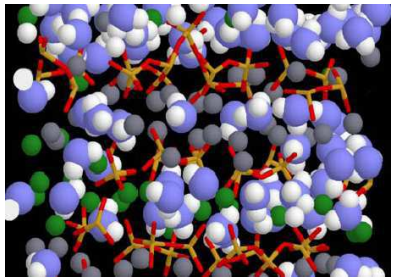 A molecular model of CSH [PKS+09]: ●: oxygen, ○: hydrogen (water molecules), ●: inter and ●: intra-layer calcium ions, ▬: silicon, ▬: oxygen (silica tetrahedra). |
| Alloy | | 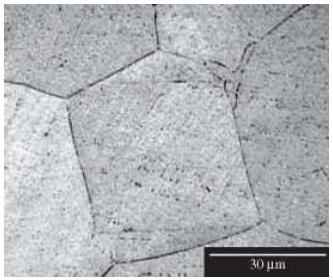  Austenite grains (OM) [NMCO08] | | 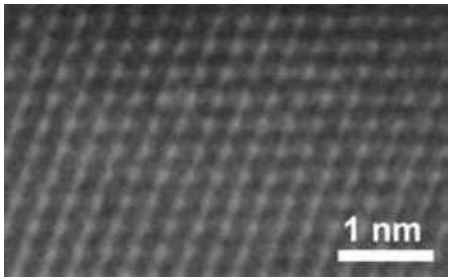  $Al_{111}$ crystal (HRTEM) [RJR+07] |
| Clay | | 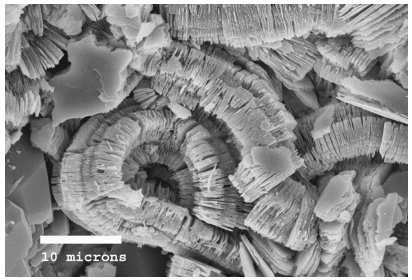  Kaolinite layers (SEM) | | 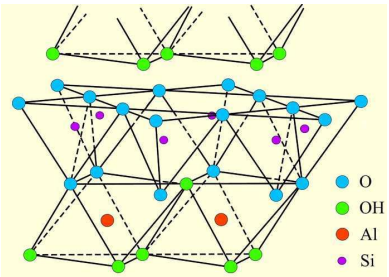  A kaolinite layer (modified from [Gri62]) |

Table 1: Different organization scales of concrete, alloy and clay (OM: Optical Microscope, SEM: Scanning Electron Microscope, HRTEM: High-Resolution Transmission Electron Microscope)

In many application fields, such as aeronautics and civil engineering, engineers have to deal with design problems in which the structures can be several meters large. For these problems, only the structure is of interest, so what could motivate engineers to give a special attention on the electronic scale?

## I.2 Scale of the electrons in the mechanical behavior of materials

To study the mechanical behavior, the scales of interest are between the macroscopic scale and the electronic scale depending on the quantity of interest. At the lowest scale, mechanical characteristics are due to atom displacements associated with the rearrangement of electronic density, especially the density of valence electrons that are involved in chemical bonding. Exploring the intranuclear properties is not needed. Information acquired at the nanoscale is crucial for enhancing strength and interfacial performance of materials. For example, [Tho11] shows that the properties of functional ceramics are largely linked with the local microstructure (defects, grain boundaries, intergranular films, or other precipitations) and with the distribution of these microstructural entities at the mesoscopic or the macroscopic scale. Therefore, electronic studies are useful to obtain a detailed view of classical engineering materials. In addition to these traditional purposes, electronic studies cannot be bypassed to explore new systems that are entirely at the nanoscale.

Nowadays, miniaturization of industrial devices is an important process in manufacturing. Micro-electro-mechanical systems (MEMS) [GD09] and nano-electro-mechanical systems (NEMS) [DBD+00] are expected to significantly impact many areas of technology and science. For those systems, the largest scale is the nanometric one and atomic studies are essential. DNA molecules or nanotubes, whose nanometric structures are presented in Figure 1, are other examples of nanostructures.

Beyond understanding the behavior of materials, nanoscience allows the creation of new materials whose characteristics are dedicated to a specific load or environment. For example, self cleaning glass has been produced; titanium oxyde coats glass and breaks down organic and

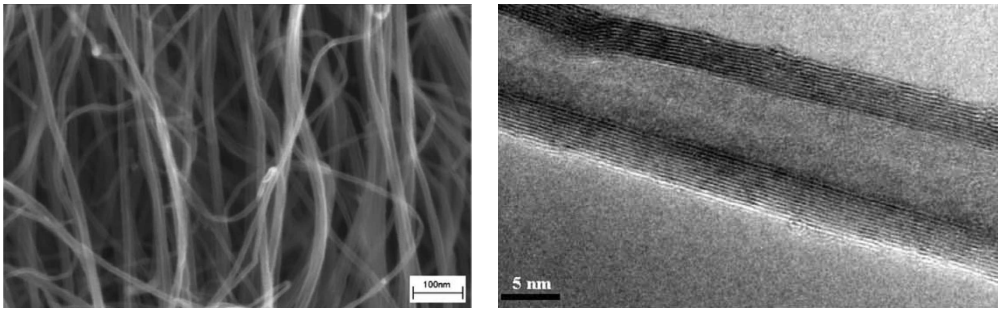


SEM image of CNT Carpet TEM image of graphene layers in CNT

Figure 1: Images of carbon nanotubes (CNT) [BMB09]

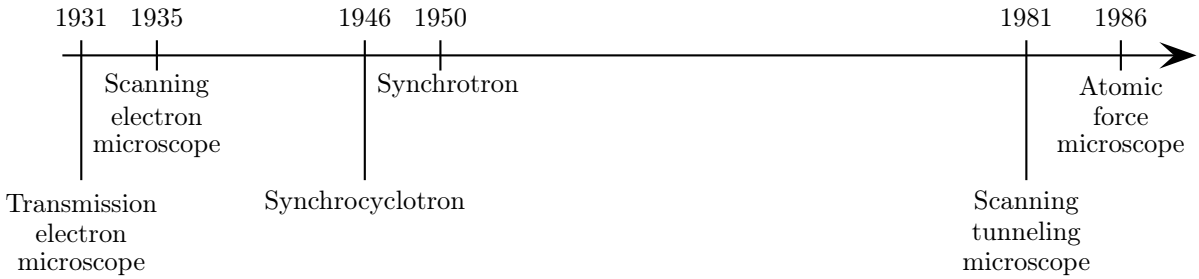


Figure 2: Timeline of microscopy development

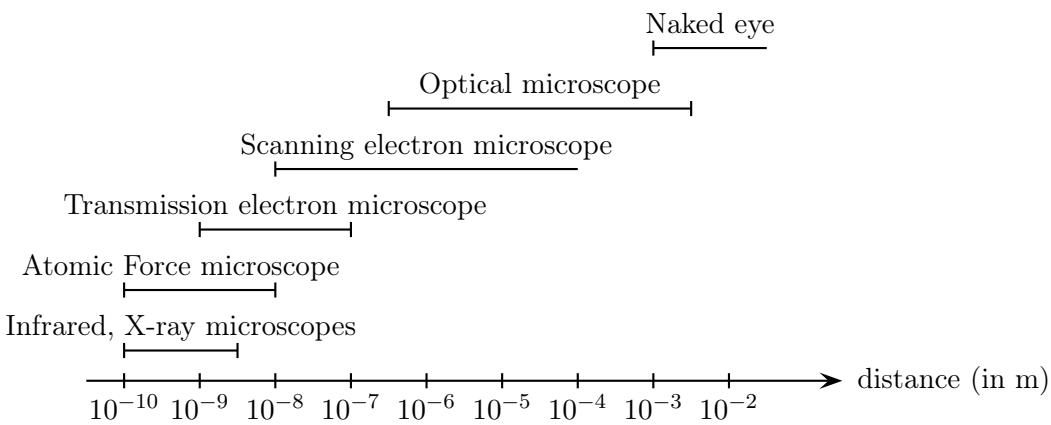


Figure 3: Order of length observable depending on the microscope technologies [FPZ95]

inorganic air polluants by photo-catalytic process [BSI11].

Despite these promising potentialities, the electronic scale has been explored only for the last century due to the difficulties of its observation.

## I.3 How to obtain electronic information?

Electronic systems can be examined by physical experiments or numerical simulations.

Atomic characteristics can be provided by physico-chemical analyses or by observations using a microscope. Appendix A describes the different microscopy technologies invented during the 20th century (Figure 2) with increasing resolution (Figure 3). These devices allow currently the observation of atomic structures. Unfortunately, they generally imply cost prohibitive facilities and require a specific environment, including an air-conditioning system and a large area to install them. They must be handled by specialized scientific experts, and the sample preparation prior to observation is a long and strenuous task.

Numerical simulations and experiments can complement each other. Simulations are based on quantum mechanics theory. They appear as an appealing alternative but they face strong limitations. Because of the high amount of computer memory needed, the problems which can be solved by simulations are still very simple systems. They are interesting for physical studies, but too limited from a mechanical point of view. In recent years, the performance of computational methods and tools increased dramatically, and representative electronic calculations can now be achieved [Ced10].

## I.4 Objectives and outline of this dissertation

This work deals only with numerical simulations of electronic systems. The goal is to collect mechanical information of a material at the nanoscale. These properties of the material are derived from the ground state of any system, *i.e.* the state of the material for which its energy is the lowest. At the atomic level, this ground state is determined by the Schrödinger equation, but

this problem cannot be solved exactly for most systems. We employ the Hartree-Fock methods to simplify the problem. Here we propose to employ localized trial functions, and particularly the finite element method, to approximate the solution. This numerical tool has been widely used in other areas and offer ripe numerical background and tools. We provide error estimates for different quantities of interest with respect to both modeling and numerical sources of error.

The outline of this document is as follows:

- Chapter 1 begins with a brief introduction of nanoscale potentialities and quantum theory. Then, we expose the scope of our study. The exact quantum problem cannot be solved even numerically. The usual methods and approximations to make this problem numerically computable are described.

- Chapter 2 concentrates on the Hartree-Fock hypotheses we chose to approximate the problem. It is shown how the Schrödinger equation is turned into the Hartree-Fock system, and introduces the different post-Hartree-Fock methods, which are derived from the Hartree-Fock method to compute more accurate solutions.

- Chapter 3 begins with a review of the numerical methods proposed in the literature to solve the Hartree-Fock system. These methods are evaluated with respect to their ability to be coupled with larger scales models, the accuracy of their solutions, and their ability to handle large systems. This evaluation hints at using the finite element method. The core of this chapter deals with the details of the numerical strategy that we propose.

- Chapter 4 presents the results obtained for isolated systems: atoms and molecules. Energies of the systems, equilibrium of internuclear distances, and mechanical and electrical properties are computed.

- Chapter 5 focuses on error estimation. The results obtained in Chapter 4 are approximate due to the approximations made to get a computable problem (detailed in Chapter 2) and the employment of numerical tools (detailed in Chapter 3). The goal of the last chapter is to estimate errors with respect to both model and numerical approximations.

# Chapter 1

# An *ab initio* perspective for modeling the mechanical behavior of materials

We discuss, in this chapter, how considering the atomic scale can be relevant to study the mechanical behavior of materials. The choice of this scale influences the selection of the models to work with. Two major classes of models can be considered: either quantum mechanics models or classical mechanics models. We detail the tools employed and the possibilities offered by each class. We opt to utilize quantum models, and expose the framework of our study. The mathematical problem modelizing the system cannot be solved exactly. A brief presentation of the different solution methods proposed in the literature concludes this chapter.

## 1.1 Interest of the nanoscale

This work looks at materials from the atomic point of view. This scale allows the understanding of the local properties which cannot be analyzed by simply studying materials at larger scales *e.g.* the interfaces between two grains, or two materials, the atomic defects, etc. We see in Table 1.1 that the atomic systems have nanometer-order sizes.

| | | |
|---|---|---|
| Van der Waals radius[a] of a H-atom | $1,2.10^{-10}$ m | [Bon64] |
| Covalent radius[b] of a H-atom | $3,2.10^{-9}$ m | [PA08] |
| Length of the O-H bond in the $H_20$ molecule | $0,957854.10^{-10}$ m | [CCF+05] |
| Size of the elementary cell of LiH crystal | $4,0834.10^{-10}$ m | [SM63] |
| Average grain size in a decarburized steel | $2,0.10^{-6}$ m | [Jao08] |

[a]radius of a conventional sphere modeling the atom
[b]half of the distance between two nuclei of identical atoms linked by a covalent bond

Table 1.1: Orders of magnitude of different electronic systems

Throughout this dissertation, we aim at characterizing the mechanical properties of materials at the nanometer level. The size of the numerical samples are in the order of $10^{-8}$ m. At that scale, we can investigate the distribution of nuclei and electrons but not the physical phenomena inside the nuclei, which are beyond the scope of mechanical approaches.

Versatility is an advantage of the electronic approach. At this level, the same entities can describe all types of materials, and a unique framework can define the different characteristics of the material, such as mechanical behavior [NFP+11], electrical behavior [DGD02] or magnetic behavior [LMZ91].

### 1.1.1 Mechanical quantities of interest

We can develop the concept of stress at the atomistic level [Wei02], and derive the mechanical properties of a material at that scale from its total energy $E$ [Sla24, NM85a, God88, IO99].

From uniform displacements $\delta X_{N_j}$ of the nuclei initially located at $X_{N_j}$, we define the homogenized deformation tensor of the nuclear network as:

$$\delta X_{N_j} = \varepsilon \left( X_{N_j} \right) . \tag{1.1}$$

The stress tensor $\sigma$ and the elasticity tensor $C$ can be defined as the derivative of the energy density with respect to the deformation of the nuclear network $\varepsilon$ at the first order and at the

second order [LC88, GM94], respectively:

$$\sigma = \frac{1}{\Omega}\frac{\partial E}{\partial \varepsilon}, \tag{1.2}$$

$$C = \frac{1}{\Omega}\frac{\partial^2 E}{\partial \varepsilon \partial \varepsilon}, \tag{1.3}$$

where $\Omega$ denotes the volume associated with energy $E$.

Quantum mechanics provides the total energy of a system at the nanoscale. Provided one can calculate the derivative of the energy with respect to the deformation $\varepsilon$ and associate a volume $\Omega$ to the energy $E$ computed beforehand, we can derive both mechanical properties from nanoscale calculations [NM85b, SB02, HWRV05].

### 1.1.2 Electrical quantities of interest

Besides mechanical properties, we can also benefit from quantum computations to estimate electrical properties such as the dipole moment or the polarizability tensor [RMG65, JT03, AF05]. Similarly as before, these quantities can be derived from the total energy $E$ when the electric field is taken into account in the Schrödinger equation. The dipolar moment $p$ and the polarizability tensor $\alpha$ can be defined as the derivative of the energy with respect to the electric field $\mathsf{E}^{el}$ at the first order and at the second order respectively:

$$p = \frac{\partial E}{\partial \mathsf{E}^{el}}, \tag{1.4}$$

$$\alpha = \frac{\partial^2 E}{\partial \mathsf{E}^{el} \partial \mathsf{E}^{el}}. \tag{1.5}$$

Here, these material quantities are predicted by solving an atomic problem and determining the ground state of the system, for which the energy is the lowest. They have to be seen as nanoscale quantities because defects and mesoscale organization create some scale effects between nanoscale and macroscale.

## 1.2 Modelization at the nanoscale

At the atomic scale, two kinds of models can be considered: either quantum mechanics models or classical mechanics models.

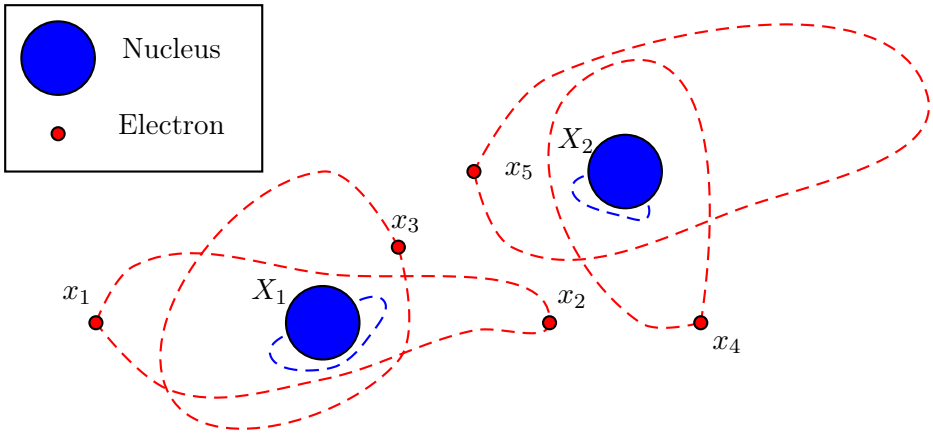


Figure 1.1: Scheme of a nanoscopic system (scale is not respected)

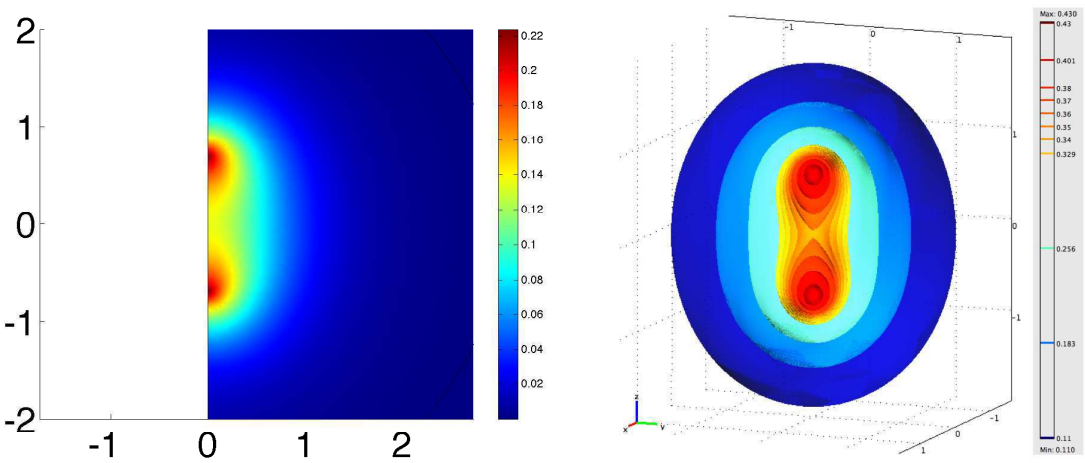


Two-dimensional field Isolevel surfaces

Figure 1.2: Probability of the presence of ground-state electrons in the $H_2$ molecule (length in Bohr radius)

### 1.2.1 Quantum mechanics model

The quantum mechanics problem is only briefly introduced here. The reader is referred to [AF05] or [SO96] for general and detailed presentations, or to [Fou06] for an introduction of the quantum problem in the context of materials science.

Historically, to simulate the system at the nanoscale, the key issue was to establish accurate tools to describe the system. It appeared that at the electronic scale, Newtonian mechanics is not satisfied. The electrons cannot be seen as particles and deterministic mechanics is not accurate. In 1924, Louis de Broglie [de 24] showed that matter exhibits wave properties at the nanoscale. The quantum mechanics models, also called *ab initio* models, are based on this concept and on the Schrödinger equation.

#### The wave function of the system

At the nanometer scale, any material reveals its atomic structure (Figure 1.1). Generally, the number and the nature of atoms in the system are *a priori* known. Each atom is composed of a nucleus surrounded by a number of electrons known from the periodic table (Appendix B). Thus, the entire system is composed of $N_n$ nuclei located at $X_j$ and $N_e$ electrons located at $x_k$. We represent electrons as particles in Figure 1.1 for the sake of simplicity. But, in the context of quantum mechanics, the positions cannot be known in a deterministic manner.

The system formed by the nuclei and electrons is described by the wave function $\Psi$ defined from the $3(N_n + N_e)$-dimensional space into the space of complex numbers:

$$\begin{array}{rcccl} \Psi & : & x = (X_j, x_k) & \longmapsto & \Psi(x) \\ & & \mathbb{R}^{3(N_n+N_e)} & \longrightarrow & \mathbb{C}. \end{array} \tag{1.6}$$

The value of the wave function $\Psi(x)$ has no physical meaning in itself, but the square of the absolute value of the function provides the probability to find each nucleus $j$ at $X_j$ and each electron $k$ at $x_k$ [Bor26]:

$$P(x) = \Psi^*(x)\Psi(x) = |\Psi(x)|^2, \tag{1.7}$$

where $\Psi^*(x)$ denotes the conjugate of $\Psi(x)$. Figure 1.2 represents the field of probability of presence in a two-dimensional and a three-dimensional space for the hydrogen molecule. As the square of its value represents the probability of presence, the wave function must have finite values, but it is not necessarily smooth. Because the probabilities that the system is in each possible state should add up to 1, the norm of the wave function over the whole space must be equal to unity:

$$\int_{\mathbb{R}^{3(N_e+N_n)}} |\Psi|^2 dx = 1. \tag{1.8}$$

The wave function must be squared-integrable over the whole space. Therefore, it is defined in the function space $\mathsf{W}$, subspace of square-integrable function space $\mathbb{L}^2$. The wave function can be multiplied by any constant factor $e^{ik}$ without affecting the values of the probability pf presence $P(x) = \Psi^* e^{-ik} \Psi e^{ik} = \Psi^* \Psi$. This property has no effect on the physical results.

The wave function of a system provides a complete description of the associated physical system. All the other quantities can be derived from it.

In 1926, Schrödinger published several landmark papers [Sch26a, Sch26b]. He established an axiomatic empirical relationship to define the wave function of a system depending on its electric environment: the Schrödinger equation.

### The Schrödinger equation

Any non-relativistic system composed of $N_n$ nuclei and $N_e$ electrons is described by its wave function $\Psi$ which satisfies the Schrödinger equation:

$$-\frac{\hbar^2}{2m_n}\Delta_{X_n}\Psi - \frac{\hbar^2}{2\,m_e}\Delta_{x_e}\Psi + V\Psi = i\hbar\frac{\partial\Psi(x,t)}{\partial t} \tag{1.9}$$

where $\hbar$ is the reduced Planck constant or Dirac constant ($\hbar = 1.054572\,10^{-34}$ J.s), $V$ is the interaction potential, $m_e$ and $m_n$ are the masses of the electrons and the nuclei respectively. The first Laplacian depends on the positions of the nuclei and the second one on the positions of the electrons. They depend respectively on a $3N_n$- and a $3N_e$-dimensional vector. This model does not suppose a local equilibrium but a global one. The Schrödinger equation cannot be written on a portion of space but only on the global space containing all electrons.

For stationary cases which will be detailed in section 1.3.1, $\Psi(x,t) = \Psi(x)\, e^{-\frac{E}{\hbar}it}$, the Schrödinger equation defines the eigenpair wave function/energy of the system $\{\Psi, E\}$:

$$-\frac{\hbar^2}{2m_n}\Delta_{X_n}\Psi - \frac{\hbar^2}{2m_e}\Delta_{x_e}\Psi + V\Psi = E\Psi. \tag{1.10}$$

When using atomic units (Appendix C), the stationary Schrödinger equation reads

$$-\frac{m_e}{2m_n}\Delta_{X_n}\Psi - \frac{1}{2}\Delta_{x_e}\Psi + V\Psi = E\Psi. \tag{1.11}$$

Wave functions appear as eigenmodes of this equation. The solution is not unique. The wave function related to the lowest energy is called the ground state. The others are called excited states. The ground-state system is in a stationary state whereas the lifetime of excited states is in the order of $10^{-10}$ s [FCC96].

If $\Psi_1$ and $\Psi_2$ are solutions of the Schrödinger equation with the same energy $E$, any linear combination $\lambda_1\Psi_1 + \lambda_2\Psi_2$ is also a solution of this equation. The superposition principle may be applied to the wave functions.

### Potential energies

The wave function constituting a system depends on its environment, which is described by the interaction potential energy $V$. It is the sum of the internal and the external interaction potential energies. Particles inside the system determine the internal potential energy. The external potential one is due to external particles and electric or magnetic fields.

**Internal potential energy** Internal potential energy can be divided into three contributions: interactions between nuclei $V_{nn}$, between electrons and nuclei $V_{en}$, or between electrons $V_{ee}$. Nuclei are characterized by their position $X_j$ and their atomic number $Z_j$. Electrons are described by their position $x_k$. Their charge is the elementary charge $e$, equal to one atomic unit. For the sake of clarity, we do not write it explicitly here, but two electrons interact only if they have the same spin-eigenvalue.

Considering only cases when interaction potentials between particles are Coulomb potentials [Cou84], the expressions of the different potential energies are as follow:

$$V_{nn}(X_i, X_j) = \frac{e^2 Z_i Z_j}{4\pi\varepsilon_0 |X_i - X_j|},$$

$$V_{en}(X_j, x_k) = \frac{-e^2 Z_j}{4\pi\varepsilon_0 |X_j - x_k|},$$

$$V_{ee}(x_k, x_l) = \frac{e^2}{4\pi\varepsilon_0 |x_k - x_l|}.$$

In atomic units, the internal potential energies are expressed in Hartree (1 Ha $= 4.360 \times 10^{-18}$ J, see Appendix C). They are estimated by

$$V_{nn}(X_i, X_j) = \frac{Z_i Z_j}{|X_i - X_j|}, \tag{1.12}$$

$$V_{en}(X_j, x_k) = \frac{-Z_j}{|X_j - x_k|}, \tag{1.13}$$

$$V_{ee}(x_k, x_l) = \frac{1}{|x_k - x_l|}. \tag{1.14}$$

Potential energies tend to vanish when the distance between two particles tends to infinity. Potential energy is positive when both particles have the same charge sign (repulsion), whereas it is negative when they have opposite charges (attraction).

**External potential energy** The only external source studied here is the application of a uniform external electric field $\mathsf{E}^{el}$. $V_e^{el}$ is the potential energy caused by the interactions between the external electric field and the electrons:

$$V_e^{el}(x_k) = e x_k . \mathsf{E}^{el}. \tag{1.15}$$

$V_n^{el}$ is the potential energy caused by the interactions between the external electric field and the nuclei:

$$V_n^{el}(X_j) = e Z_j X_j . \mathsf{E}^{el}. \tag{1.16}$$

In atomic units, for a uniform electric field, the expressions of the external electric field potential energies [AF05] read

$$V_e^{el}(x_k) = x_k . \mathsf{E}^{el}, \tag{1.17}$$

$$V_n^{el}(X_j) = Z_j X_j . \mathsf{E}^{el}. \tag{1.18}$$

Non uniform fields would involve interaction with higher multipoles.

The magnetic potential of a system under the application of an external magnetic field B is, similarly as before [NLK86]:

$$V_e^{mag}(x_k) = e\, i\, (\nabla_{x_k} . \wedge B)\, x_k, \tag{1.19}$$

$$V_n^{mag}(X_j) = e\, i\, Z_j\, (\nabla_{x_k} . \wedge B)\, X_j. \tag{1.20}$$

These expressions evaluate the "load" borne by each particle of the system. As stated previously, the total energy is the key information to derive the mechanical properties of the material.

### The total energy of the system

From (1.11), satisfying the normality condition (1.8) and using integration by parts, we get:

$$E = \int_{\mathbb{R}^{3(N_e+N_n)}} \left( \frac{1}{2} \left| \frac{m_e}{m_n} \nabla_{x_n} \Psi \right|^2 + \frac{1}{2} |\nabla_{x_e} \Psi|^2 + V|\Psi|^2 \right) dx. \tag{1.21}$$

The terms $\int_{\mathbb{R}^{3(N_e+N_n)}} \frac{1}{2} \left| \frac{m_e}{m_n} \nabla_{x_n} \Psi \right|^2 dx$ and $\int_{\mathbb{R}^{3(N_e+N_n)}} \frac{1}{2} |\nabla_{x_e} \Psi|^2 dx$ represent respectively the kinetic energies of the nuclei and the electrons. The term $\int_{\mathbb{R}^{3(N_e+N_n)}} V|\Psi|^2 dx$ represents the potential energy.

The total energy appears as the eigenvalue of the Schrödinger equation. The spectrum of eigenvalues can be very large. The mathematical properties of the spectrum are studied in Section 2.1.3. Because some eigenvalues can be degenerated, the dimension of the eigenspace is not necessarily equal to the number of eigenvalues. Hence the system is completely described by its eigenmodes rather than by its eigenvalues.

The ground-state energy provided by these quantum models can be used to define the equilibrium positions of the nuclei or to derive some mechanical, electrical, or magnetic properties, as presented in section 1.1. These models provide advantageously the accurate tools to analyze the electronic properties. Moreover, they do not need - at least theoretically - empirical parameters but only fundamental physical constants. Their major drawback is that they are quite complicated numerically. Therefore, computable systems have a small number of atoms and a small time scale. For stationary cases, simulations are limited to systems of 100 or 1000 atoms [CLM06]. Dynamic simulations are very time consuming, and only short time scale on the order of one picosecond ($10^{-12}$ s) can be computed [CLM06].

Real-world problems are immensely large quantum systems. Therefore, solving problems with a quantum approach requires special strategies [You01]. An attractive alternative is to use empirical models based on classical mechanics.

### 1.2.2 Classical mechanics model

The most usual empirical simulations use molecular dynamics [MH09]. The atoms are considered as material points satisfying Newtonian mechanics [Fre71, Fey99]. Empirical potentials represent interactions between particles. The expressions of the potentials between two electrons $V_{ee}$ are established through preliminary quantum computations or experimental data. Depending on the model refinement, the energy contribution from each pair of interacting particles is considered as a 2-body potential:

$$V_{ee} = \sum_{i=1}^{N_e} \sum_{j=i+1}^{N_e} f_{2b}\left(x_i, x_j\right), \tag{1.22}$$

as a 3-body potential:

$$V_{ee} = \sum_{i=1}^{N_e} \sum_{j=i+1}^{N_e} f_{2b}\left(x_i, x_j\right) + \sum_{i=1}^{N_e} \sum_{\substack{j=1 \\ j\neq i}}^{N_e} \sum_{k>j}^{N_e} f_{3b}\left(x_i, x_j, x_k\right), \tag{1.23}$$

or generally as a N-body potential. The force exerted on a given particle is given by the derivative of the energy with respect to the position of that particle:

$$F_i = -\sum_{j=1}^{N_e} \frac{\partial}{\partial x_i} f_{2b}\left(x_i, x_j\right) - \sum_{j=1}^{N_e} \sum_{k>j}^{N_e} \frac{\partial}{\partial x_i} f_{3b}\left(x_i, x_j, x_k\right). \tag{1.24}$$

This type of model has several drawbacks. Because it uses empirical parameters, it requires a preliminary study of the molecules considered. Therefore, it cannot predict the behavior of new molecular systems, either easily simulate chemical reactions, during which wave functions, and so potentials, are largely modified. In addition, it cannot provide electronic information.

Its major advantage is that it is easier to solve numerically, allowing one to compute a large number of atoms, up to several millions for stationary cases [CWWZ00, KOB+02, HTIF06]. This large number of atoms or molecules can be used in the context of statistical physics.

To sum up, the major difference between *ab initio* and empirical models is that *ab initio* models provide a quantum description due to the wave function of the system, whereas empirical models provide a classical description due to the position and the velocity of the particles. The coexistence of these two models raises two issues. The first is the compatibility between the two modelizations, and the second is how to couple these approaches to benefit from their strong points and minimize their shortcomings.

Ehrenfest's theorem [NP06] states that classical mechanics equations can be derived from quantum mechanics equations by considering particles as localized wave packets [CDL73, BD06]. This hypothesis is satisfied for most macroscopic systems. Thus, quantum mechanics can be seen as a more general theory than classical mechanics. However quantum mechanics is quite special because it requires some concepts of classical mechanics to express some of its principles.

From a numerical point of view, different strategies can be performed to "couple" quantum and empirical models. Praprotnik *et al.* propose a solver equipped with a flexible simulation scheme changing adaptively the model in certain regions of space on demand. Model coupling is a very active research domain which proposes various strategies depending on the problem characteristics. For instance, change of scale from nanoscale to macroscale can be performed by providing information for larger scale models [PSK08], by homogenization [Le 05], by statistical models through Boolean schemes [Mor06], or by an energetic volume coupling method such as the Arlequin method [Ben98]. Brown *et al.* [BTS08] propose a "one-way coupling" of these different models: he performs an *ab initio* calculation to estimate local potentials between some molecules, and then used these potentials as input data in an empirical model. To our knowledge, no "two-way coupling" model has been proposed in the literature until now.

To derive the mechanical properties of materials from the electronic scale, we implement a quantum model whose framework is detailed hereafter.

## 1.3 Our framework

Because the aim of this research is to collect mechanical information, we only focus on stationary cases.

### 1.3.1 Stationary cases

Note that, in the context of quantum mechanics, stationary states involve wave functions depending on time, but whose probability of presence is independent of time:

$$\frac{\partial \Psi(x,t)}{\partial t} \neq 0 \qquad \text{but} \qquad \frac{\partial |\Psi(x,t)|^2}{\partial t} = 0. \tag{1.25}$$

Therefore, $|\Psi(x,t)|^2 = |\Psi(x)|^2$. The general form of the wave function is $\Psi(x,t) = \Psi(x)\, e^{i\alpha t}$. For stationary cases, the total energy $E$ of the system is constant with respect to time. Therefore, the general form of such a solution is $\Psi(x,t) = \Psi(x)\, e^{i\alpha t}$ where $\alpha = -\frac{E}{\hbar}$. This dissertation examines only the amplitude of the wave function that we also denote by $\Psi$.

### 1.3.2 Non-relativistic electrons

We suppose electrons to be non-relativistic. This assumes that the speed of electrons is largely smaller than the speed of light, and therefore the kinetic energy of electrons is negligible compared to the mass energy of electrons $E_m = m_e c^2$ ($c = 299,792.458$ m.s$^{-1}$).

To compute electrons of heavy atoms, and especially their core electrons whose speed is the most important, we would have to apply relativistic models. Desclaux *et al.* [DDE+03] survey the different approaches of relativistic models. The most used one is the Dirac-Fock model [IV01]. The Dirac equation [Dir28] is

$$\left(m_n c^2 \beta + m_e c^2 \beta - i\hbar c \gamma \nabla_{X_n} - i\hbar c \gamma \nabla_{x_e}\right) \Psi = i\hbar \frac{\partial \Psi(x,t)}{\partial t} \tag{1.26}$$

where $\beta$ and $\gamma$ are Dirac's matrices. For stationary cases, the equation turns into

$$\left(m_n c^2 \beta + m_e c^2 \beta - i\hbar c \gamma \nabla_{X_n} - i\hbar c \gamma \nabla_{x_e}\right) \Psi = E\Psi. \tag{1.27}$$

Using the Schrödinger equation, a relativistic approach has been proposed by some authors using a pseudopotential [LCT72] or by an *a posteriori* perturbation [PJS94].

### 1.3.3 Absolute zero temperature

We only focus on systems at 0 K temperature, so that entropy is at a minimum. This hypothesis assumes that the system would be fully removed from the rest of the universe, since it does not have enough energy to transfer to other systems. At this temperature, the wave functions that are solutions of the system are those with the lowest energy.

At a temperature different from 0 K, the system produces a thermal radiation *i.e.* electromagnetic waves [GH07]. To extend to these cases, not only the ground state must be computed but also other states, with higher energies, called excited states. The effect of temperature is described through a statistical distribution between these different states [Kit04, LL05]. Two major statistical distributions are employed depending on the value of the average intermolecular distance with respect to the average de Broglie wavelength. The de Broglie wavelength $\lambda_B$ is the ratio between the Planck constant $h$ and the norm of the momentum of particles $p$: $\lambda_B = \dfrac{h}{|p|}$.

If the average intermolecular distance $\bar{R}$ is smaller than the thermal de Broglie wavelength $\lambda_B$, the Fermi-Dirac distribution is considered. At the absolute temperature $T$, the number $n_i$ of electrons in state $i$, with energy $E_i$ and degenerate degree $g_i$, is given by:

$$n_i = \frac{g_i}{\exp\left(\dfrac{E_i - \mu}{k_B T}\right) + 1} \tag{1.28}$$

where $\mu$ is the chemical potential and $k_B$ is Boltzmann's constant.

If the average intermolecular distance $\bar{R}$ is much greater than the average thermal de Broglie wavelength, the Maxwell-Boltzmann distribution is applied. Among the $N_e$ electrons of the system, the number $n_i$ of electrons in state $i$, with energy $E_i$ and degenerate degree $g_i$, is given by the following expression:

$$n_i = N_e \frac{g_i e^{-\frac{E_i}{k_B T}}}{\sum_{j=1}^{N_e} g_j e^{-\frac{E_j}{k_B T}}}. \tag{1.29}$$

The effect of temperature is beyond the scope of this dissertation. We only compute the ground state of the system from Equation (1.11). This equation, defined in a very large space, requires some simplifications to be solvable for most systems.

### 1.3.4 Born-Oppenheimer's hypothesis

In the Schrödinger equation (1.11), the Laplace operators depend on the $3\,(N_n + N_e)$-dimensional vector $x$ which represents the positions of all the particles in the system. The first Laplacian depends on the positions of the nuclei and the second one on the positions of the electrons. Each nucleus is composed of protons and neutrons. A proton and a neutron are 1836 and 1839 times heavier than an electron, respectively. Therefore, nuclei are much heavier than electrons, between $10^3$ and $10^5$ times depending on the atom. The Born-Oppenheimer hypothesis [BO27] assumes electron motion to be independent of nuclei motion. The kinetic energy of the nuclei $-\dfrac{m_e}{2m_n}\Delta_{x_n}\Psi$ can thus be omitted with respect to the kinetic energy of the electrons $-\dfrac{1}{2}\Delta_{x_e}\Psi$. The Schrödinger equation turns into:

$$-\frac{1}{2}\Delta_{x_e}\Psi + V\Psi = E\Psi. \tag{1.30}$$

Under Born-Oppenheimer's hypothesis, the wave function is still defined in a $3\,(N_e + N_n)$-dimensional space. It is only the dimension of the space of the Laplacian derivation that is reduced.

It is common to extend this hypothesis to break the global wave function down into two independent ones defined in smaller spaces.

### 1.3.5 Breaking down the wave function

We generally assume the global wave function of the system as the product of a $3N_n$-dimensional nuclear wave function $\Psi_n$ and a $3N_e$-dimensional electronic wave function $\Psi_e$ [Thi03, CLM06]:

$$\Psi(X_j, x_k) = \Psi_n(X_j)\Psi_e(x_k), \tag{1.31}$$

$$\begin{array}{lcccc} \Psi & : & \mathbb{R}^{3(N_e+N_n)} & \to & \mathbb{C} \\ \Psi_n & : & \mathbb{R}^{3N_n} & \to & \mathbb{C} \\ \Psi_e & : & \mathbb{R}^{3N_e} & \to & \mathbb{C}. \end{array}$$

Under this assumption, these two wave functions can be solved independently. The nuclear problem is solved using classical mechanics, whereas the electronic problem requires quantum mechanics.

### Nuclear problem solved by classical mechanics

The $N_n$ nuclei are modeled by non-quantum particles characterized by their atomic number $Z_j$. They are described by their position $X_n$ and not by a wave function. Each nucleus has a mass $m_n$. It is submitted to a force $F_n$ derived from the nuclear Coulomb potential $V_n = V_{nn} + V_{en} + V_n^{el}$:

$$F_n = -\nabla_{X_n} V_n = m_n \frac{\partial^2 X_n}{\partial t^2}. \tag{1.32}$$

The positions $X_n$ are estimated using classical deterministic mechanical laws, and the accelerations are estimated by molecular dynamics. To determine the ground state of the system, we minimize the energy functional of the system in which the nuclei positions appear as parameters. The nuclear problem is a geometric optimization on $\mathbb{R}^{3N_n}$ [CLM06].

### Electronic wave function

The $N_e$ electrons are elementary quantum particles. They are described by a wave function $\Psi_e$, which obeys the following electronic Schrödinger equation (in atomic units) defined from a $3N_e$-dimensional space:

$$H_e \Psi_e = -\frac{1}{2}\Delta_{x_e}\Psi_e + V_e \Psi_e = E_e \Psi_e \tag{1.33}$$

where $V_e$ stands for the electronic Coulomb potential: $V_e = V_{en} + V_{ee} + V_e^{el}$ and $H_e$ is the electronic Hamiltonian operator of the system.

Let us examine the properties of the electronic wave function. From equation (1.7), we can establish that the probability distribution of the presence of electrons is the square of the absolute value of the electronic wave function:

$$P_e(x_e, t) = |\Psi_e(x_e, t)|^2. \tag{1.34}$$

From equation (1.8), we deduce that the electronic wave function must satisfy a normality condition over the $3N_e$-dimensional space:

$$\int_{\mathbb{R}^{3N_e}} |\Psi_e|^2 dx = 1. \tag{1.35}$$

The exclusion principle, also called the Pauli principle [Pau25], states that two non-identical electrons may not occupy the same quantum state simultaneously. To satisfy this principle, the electronic wave function solution is chosen as an anti-symmetric function with respect to the permutation of the positions of the electrons $x_i$:

$$\Psi_e(x_{\sigma(1)}, \ldots, x_{\sigma(N_e)}) = \mathrm{sg}\,(\sigma)\,\Psi_e(x_1, \ldots, x_{N_e}) \tag{1.36}$$

where $\sigma$ is a permutation on $[1, N_e]$ and $\mathrm{sg}(\sigma)$ is its signature.

The electronic quantum problem is a partial differential equation defined in $\mathbb{R}^{3N_e}$, for which the positions of the nuclei appear only as parameters. Considering this framework, the total energy $E$ of the system can be divided into a nuclear part $E_n$ and an electronic one $E_e$:

$$E = E_n + E_e. \tag{1.37}$$

Considering the kinetic energy of nuclei to be negligible with respect to the kinetic energy of electrons, the nuclear contribution is only due to the potential energy:

$$E_n = V_{nn} + V_n^{el}. \tag{1.38}$$

Along the same line as previously (section 1.2.1), we can express the electronic energy $E_e$ as

$$E_e = \int_{\mathbb{R}^{3N_e}} \left( \frac{1}{2}|\nabla_{x_e}\Psi_e|^2 + (V_{en} + V_{ee} + V_e^{el})|\Psi_e|^2 \right) dx + \frac{1}{2}\int_{\partial\Omega_e} (\nabla_{n_e}\Psi_e, \Psi_e^*)\, dx. \tag{1.39}$$

Therefore, from the electronic Schrödinger equation (1.33), we can estimate the electronic wave function but this equation can be solved analytically only for very simple cases like the hydrogenoid and the $H_2^+$ ions, systems with only one electron. For general systems, the equation is defined on a highly multi-dimensional domain and cannot be easily solved, even numerically. We briefly present in the next section the different approximations proposed to tackle this problem.

## 1.4 Methods to tackle the quantum electronic problem

Three major families of methods have been proposed to approximate the electronic solution:

- the Hartree-Fock method, where the wave function $\Psi_e$ is assumed to be the product of one-electron wave functions $\varphi_i$. It is referred to as a "rigorous energy/approximate wave function approach" in [DL97];
- the density functional theory, which describes the system through a unique three-dimensional electron density. It is referred to as a "rigorous density/approximate energy approach" in [DL97];
- the Monte-Carlo method, which relies on repeated random sampling and allows for the estimation of the high-multidimensional global wave function.

A classification of these methods and their derivatives is represented in Figure 1.3. Saad *et al.* [SCS10] give a comparative overview of them.

### 1.4.1 Hartree-Fock's methods

The Hartree-Fock method has been developed around 1930. Because it is generally solved using a self-consistent algorithm, it was formerly called self-consistent field method (SCF) [SO96].

Assuming electrons are essentially independent, the form of a determinant is imposed to the global electronic wave function [Sla29]. The resulting solutions behave as if each electron was submitted to the mean field created by the external potential and all the other particles.

Its major drawback is that it disregards the correlation between electrons and it does not guarantee size consistency, *i.e.* it does not guarantee the additivity of energies: for two non-interacting systems $A$ and $B$, the estimation of the energy of the supersystem $A$-$B$ will not be equal to the sum of the energy of $A$ plus the energy of $B$ taken separately. The post-Hartree-Fock methods were proposed later to reduce these estimation errors.

The Hartree-Fock methods are detailed in Chapter 2.

### 1.4.2 Density functional theory

In 1964, Hohenberg and Kohn [HK64] proved that the electron density:

$$\rho\left(x\right) = N_e \int_{\mathbb{R}^{3(N_e-1)}} \left|\Psi_e\right|^2 dx_2 \ldots dx_{N_e} \tag{1.40}$$

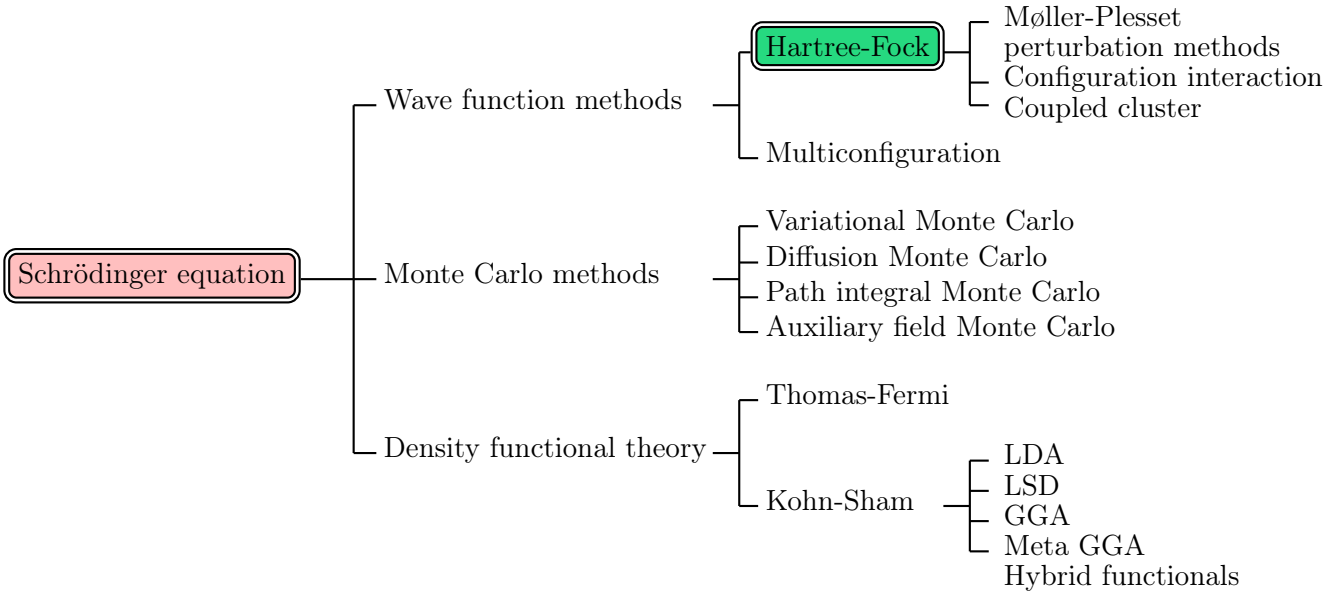


Figure 1.3: Classification of electronic calculation methods (inspired from [CDK+03]) LDA: Local-density approximation - LSD: Local spin density - GGA: Generalized gradient approximation

can thoroughly describe a system. Based on this idea, density functional theory does not evaluate the wave function $\Psi_e$ itself but the electronic density. Therefore, the first advantage of this method is to handle a unique three-dimensional function to describe any system. It is less time-consuming than the Hartree-Fock approach. Another great advantage of this method is that it takes into account the correlation effects, leading to accuracy improvement.

The fundamental state is computed by minimizing the electronic energy functional $E_e^{DFT}$, which depends on the electronic density. This energy functional includes the kinetic energy of the electrons $E_c[\rho(x)]$, the electron-nucleus potential, possibly the potential due to an external electric field, and the Coulomb interactions between the electrons:

$$E_e^{DFT}[\rho(x)] = E_c[\rho(x)] + \int_{\mathbb{R}^3} \rho(x) V_{en}(x) dx + \frac{1}{2} \int_{\mathbb{R}^3} \int_{\mathbb{R}^3} \frac{\rho(x_1)\rho(x_2)}{|x_1 - x_2|} dx_1 dx_2 + E_{xc}[\rho(x)]. \quad (1.41)$$

The last term $E_{xc}[\rho(x)]$, called the exchange-correlation energy functional, cannot be exactly estimated. Establishing the approximate expression of this term is the main difficulty in the DFT method and the key to improve the accuracy of the results [RC04, TCA08b]. The simplest approximation is the local-density approximation (LDA). It is based on the interaction energy for a uniform electron gas. Therefore, it describes the exchange-correlation energy as an analytical function of the electron density $\rho$.

Generalized gradient approximations (GGA) consist in writing the energy as a function of the electron density $\rho$ and the gradient $\nabla\rho$ [PBE96].

Meta GGAs methods consider dependence on $\rho$, $\nabla\rho$, and higher derivatives of $\rho$. Becke proposed to improve the DFT estimation by including the Hartree-Fock exchange in a DFT exchange-correlation functional [Bec93]. Nowadays, such hybrid functionals are largely employed [HCA12].

DFT allows the computation of large systems. Therefore, this method is intensely employed in materials science, both fundamental and industrial research [HWC06]. Improving the accuracy of this method requires material expertise and should be considered for each material specifically.

### 1.4.3 Quantum Monte Carlo calculations

Quantum Monte Carlo calculations have been the less used until now, despite being apparently very powerful. They are adapted to quantum problems since they offer an easy method to integrate over highly multidimensional space. They sample statistically the integrand and average the sampled values. They are suitable for parallel algorithms and can easily be applied to systems containing a thousand or more electrons.

Several quantum Monte Carlo methods exist, some of them are reviewed in [AGL03]. Variational Monte Carlo (VMC) and diffusion Monte Carlo (DMC) are generally the most employed [FMNR01]. They calculate the ground-state wave function of the system and are based on a chosen trial wave function.

Based on the Schrödinger equation (1.33), VMC uses a stochastic integration method over the $3N_e$-dimensional space. Let $R$ be a $3N_e$-dimensional vector where $r_i$ is the position of the $i$th electron. Any value of $R$ is called a walker, a configuration, or a psip in the literature. The probability density of finding the electrons in the configuration $R$ is $P(R)$. We define $\{R_m : m = 1, M\}$ as a set of independent configurations distributed according to the probability distribution $P(R)$. Considering the trial wave function $\Psi_e^{MC}$, the electronic energy

$$E_e^{MC} = \frac{\int \Psi_e^{MC*}(x,P) H_e \Psi_e^{MC}(x,P) dR}{\int \Psi_e^{MC*}(R) \Psi_e^{MC}(R) dR} \tag{1.42}$$

can be estimated by the set of independent configurations through:

$$E_e^{MC} \approx \frac{1}{M} \sum_{m=1}^{M} \Psi_e^{MC^{-1}}(R) H \Psi_e^{MC}(R). \tag{1.43}$$

The accuracy of the results relies on the initial trial wave function, the probability distribution $P(R)$ and the number of walkers.

DMC enhances the predictions using a projection technique with a stochastic imaginary-time evolution to improve the accuracy of the ground-state component of the starting trial wave function.

Path integral Monte Carlo and auxiliary field Monte Carlo compute the density matrix. They can be used to compute systems with many electrons, possibly at finite temperature.

## 1.5 Summary

In this chapter, we have presented the general framework of our study. We will only consider stationary systems at 0 K temperature. We decompose the unique wave function of the system into a nuclear one and an electronic one. The nuclear problem is solved through classical mechanics. The electronic wave function is defined in a $3N_e$-dimensional space and it is estimated using the Schrödinger equation.

This equation can be solved analytically only for very simple cases. Even numerically, it requires a set of hypotheses to be solved for general cases. DFT methods would allow the computation of large systems, but the establishment of accurate exchange-correlation energy functionals requires high-level materials science background. We choose to solve it using the Hartree-Fock approach which is detailed in Chapter 2.

# Chapter 2

# Hartree-Fock's models

Chapter 1 introduced the Schrödinger model. The Schrödinger solution $\Psi_e$ defined from a $3N_e$-dimensional space satisfies the following equations:

$$\begin{cases} E_e\Psi_e = -\dfrac{1}{2}\Delta_x\Psi_e + V_e\Psi_e \\ \Psi_e(x_{\sigma(1)}, \ldots, x_{\sigma(N_e)}) = \mathrm{sg}\,(\sigma)\,\Psi_e(x_1, \ldots, x_{N_e}) \\ \int_{\mathbb{R}^{3N_e}} |\Psi_e|^2 dx = 1. \end{cases} \tag{2.1}$$

This set of equations is defined in a high-dimensional space. This chapter concentrates on the Hartree-Fock methods. They provide a set of hypotheses which allow the Schrödinger equation to be solved numerically. These methods rely on a reduction of the solution space due to specific forms of trial functions.

The ground state of the systems can be found by minimizing the energy functional defined by Equation (1.39), by solving the strong form defined by Equation (2.1), or by solving the weak form of the problem that will be written below. The numerical reasons to compute the solution by the finite element method will be exposed in Chapter 3. When choosing this discretization method, we approximate the weak form of the problem on a finite-dimensional space, which will be described in the second part of this chapter.

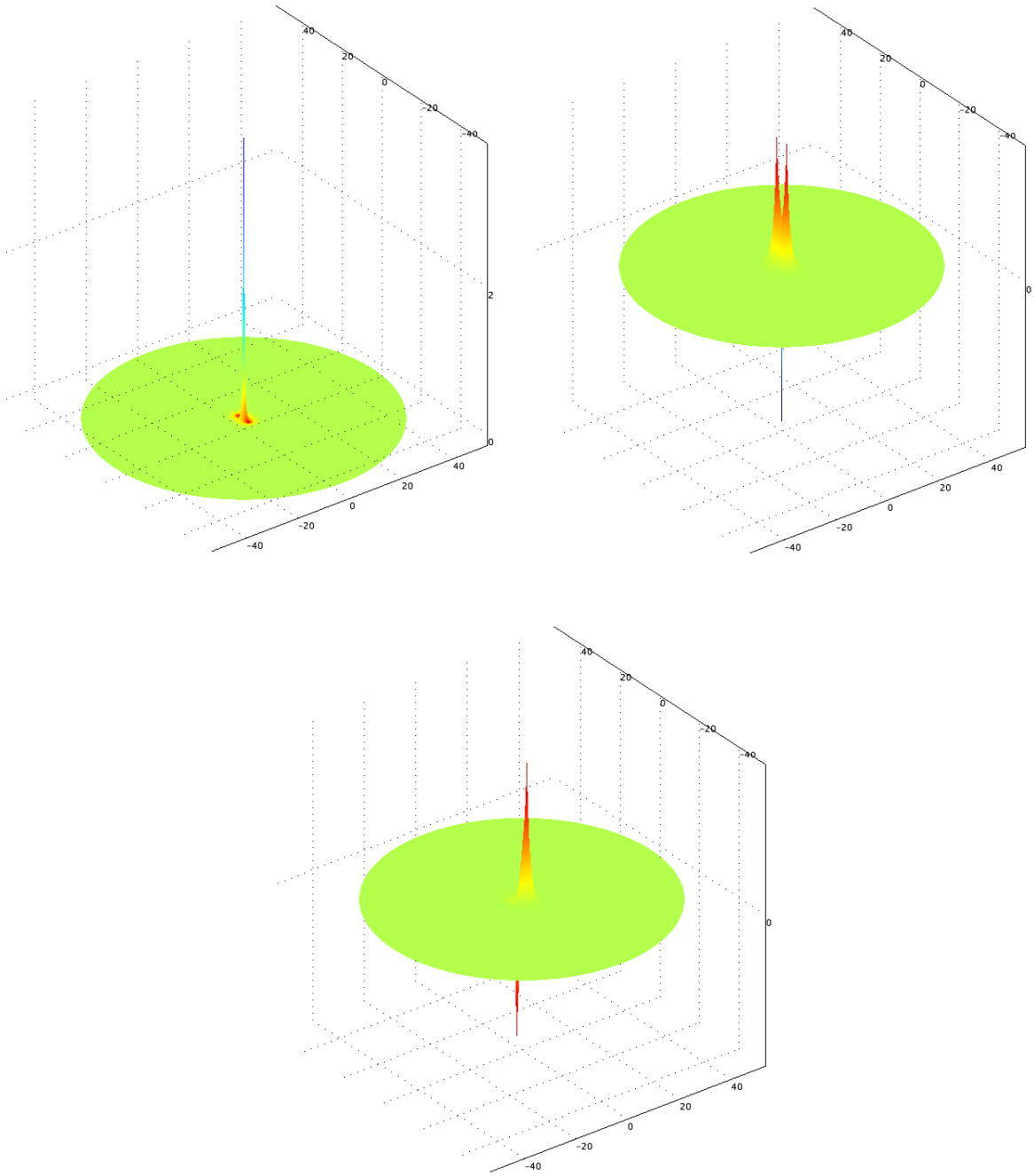


Figure 2.1: Amplitude in the plane $z = 0$ of some one-electron wave functions describing the $BeH_2$ molecule. The positions of the nuclei Be, H and H are given by (0, 0, 0), (0, 2.52, 0), and (0, -2.52, 0), respectively.

## 2.1 State of the art

The Schrödinger solution $\Psi_e$, being an anti-symmetric function, can be expressed as an infinite series of $N_e \times N_e$-dimensional determinants the so-called Slater determinants [Fri03].

### 2.1.1 Slater determinants

The Hartree-Fock methods approximate the Schrödinger solution by a finite series of determinants, called the Slater determinants:

$$\Psi_e \sim \Psi_e^{MC} = \sum_{A=1}^{N_d} \alpha_A \Psi_A = \sum_{A=1}^{N_d} \frac{\alpha_A}{\sqrt{N_e!}} \det\left[\tilde{\Phi}^A\right] \tag{2.2}$$

where $N_d$ is the number of determinants involved in the series. The determinants denoted $\Psi_A$, $A = 1, \ldots, N_d$, are defined in $\mathbb{R}^{3N_e}$; each determinant is built from a matrix, denoted $\tilde{\Phi}^A$, derived from a vector $\Phi^A$ such as:

$$\Psi_A = \frac{1}{\sqrt{N_e!}} \det\left[\tilde{\Phi}^A\right], \quad \tilde{\Phi}^A(x_1, \ldots, x_{N_e}) = \left[\Phi^A(x_1), \cdots, \Phi^A(x_{N_e})\right], \quad \Phi^A(x) = \begin{bmatrix} \varphi_1^A(x) \\ \vdots \\ \varphi_{N_e}^A(x) \end{bmatrix}.$$

Each component of the vectors $\Phi^A$ is defined in $\mathbb{R}^3$ and only depends on the coordinates of one electron. These components are called the one-electron wave functions. Figure 2.1 illustrates some one-electron wave functions which can be used to compute the $BeH_2$ molecule.

For two functions $a : \Omega \to \mathbb{C}$ and $b : \Omega \to \mathbb{C}$, we define the scalar product:

$$(a, b) = \int_\Omega a(x)\, b^*(x)\, dx \tag{2.3}$$

where $b^*$ is the conjugate of $b$. To satisfy the normality of the wave function solution defined by equation (2.1), the determinants are normalized and the coefficients $\alpha_A$ are computed so that $\sum_A |\alpha_A|^2 = 1$. The Slater determinants generally inherit normalization from the orthonormalization of the one-electron wave functions. The series is usually composed of determinants that are orthogonal to each other, but some authors propose series of non-orthogonal determinants [Low55].

The simplest linear combination defined by equation (2.2) is the Hartree-Fock trial function [Sla29], which is constructed from a unique matrix $\tilde{\Phi}(x_e) = [\Phi(x_1) ... \Phi(x_{N_e})]$ of a set $\Phi$ of $N_e$ electronic wave functions $\varphi_i$:

$$\Psi_e^{HF}(x_e) = \frac{1}{\sqrt{N_e!}} \det\left[\tilde{\Phi}(x_e)\right], \quad \Phi(x) = \begin{bmatrix} \varphi_1(x) \\ \vdots \\ \varphi_{N_e}(x) \end{bmatrix}. \tag{2.4}$$

The Hartree-Fock approximation leads to the calculation of $N_e$ one-electron wave functions. The single determinant of the Hartree-Fock model does not allow the accurate representation of the interaction between electrons. The necessary accuracy depends on the phenomena being studied. For instance, bond breaking phenomena need a very accurate energy estimation, which can be provided by post Hartree-Fock methods.

### 2.1.2 The post Hartree-Fock methods

The configuration interaction (CI) method and the multiconfiguration (MC) method enlarge the series of determinants defined by equation (2.2). In MC problems, both coefficients $\alpha_A$ and matrices $\tilde{\Phi}^A$ are simultaneously computed. In CI problems, the matrices $\tilde{\Phi}^A$ are determined first, and then the coefficients $\alpha_A$ are optimized. These two methods will be detailed in the second part of this chapter. They do not guarantee size consistency. Size-consistency means that the energy of two molecules that do not interact (at large distance) calculated directly would be the sum of the energies of the two molecules calculated separately. It is essential to use a size-consistent model to look into bond dissociation in a chemical context. Coupled cluster and perturbation methods are alternatives to supply a series of determinants respecting size consistency. However, these methods are not variational, *i.e.* the solution is not provided by an optimization in a solution space. It thus follows that the total energy obtained can be lower than the true energy.

The coupled cluster method [PB82, BM07, Sch09] relies on an exponential parameterization of a reference wave function. For single-reference coupled cluster method, the reference function is the Hartree-Fock solution $\Psi_e^{HF}$, and the coupled cluster trial function is $\Psi_e^{CC} = \exp^{\mathbf{T}}\left(\Psi_e^{HF}\right)$.

The cluster operator $\mathbf{T}$ acts on the Hartree-Fock wave function to create a linear combination of determinants with excitation rank inferior or equal to $n$: $\mathbf{T} = 1 + \sum_{1}^{n} \mathbf{T_i}$. The operator $\mathbf{T_i}$ is responsible for creating all $i$-rank excitations. For instance, $\mathbf{T_1} = \sum_{i=1}^{N_e} \sum_{j=1}^{N_V} t_i^j \det\left(\Phi^{\hat{i}}, \Phi_V^{\hat{j}}\right)$, and $\mathbf{T_2} = \sum_{i,j=1}^{N_e} \sum_{k,l=1}^{N_V} t_{ij}^{kl} \det\left(\Phi^{\widehat{ij}}, \Phi_V^{\widehat{kl}}\right)$. The exponential operator is expanded into Taylor series $e^T = 1 + T + \frac{T^2}{2} + ...$ and the coefficients $t$ are solved through a non-linear system.

The coupled cluster method provides size extensivity of the solution, *i.e.* correct scaling of the method with the number of electrons. Size consistency depends on the reference wave function.

The Hartree-Fock estimation can also be improved by the perturbation method referred by physicists to as the Møller and Plesset method [MP34, DGG09]. The perturbed wave functions and energies at the order $k$ are series $\left\{\Psi_p = \sum_{i=0}^{k} \lambda^i \Psi_p^i,\ E_p = \sum_{i=0}^{k} \lambda^i E_p^i\right\}$ where the Hartree-Fock solution $\{\Psi_e^{HF}, E_e^{HF}\}$ are considered as the zero-order perturbation $\{\Psi_p^0, E_p^0\}$ and $\lambda^i$ are real coefficients.

### 2.1.3 A mathematical viewpoint of the Hartree-Fock's models

An important research activity has arisen around the existence and the uniqueness of the solution for the different quantum problems. The proof of the existence of a minimizer of the Hartree-Fock equations is presented in [LS77]. The uniqueness of the ground-state minimizer is still an open problem [DL97]. Concerning the spectrum of solutions, Lions proved the existence of infinitely many excited states [Lio87]. Leon also proved the existence of excited states [Leo88] for different definitions of the excited states. One of them defines an excited state as the solution of the minimization of the Hartree-Fock energy functional on a set of normalized Slater determinant wave functions, which are orthogonal to the approximate ground state. The existence of an energy minimum in the multiconfiguration method was established by Friesecke [Fri03]. Lewin proposed another proof for its existence, and proved the existence of saddle points for multiconfiguration methods [Lew02, Lew04]. The application of the Hartree-Fock model for the crystalline phase is studied in [LL05]. Despite of these numerous works, it remains a long list of open problems [DL97].

## 2.2 The Galerkin method for Hartree-Fock models

The Hartree-Fock problem can be solved either by minimizing the Hartree-Fock energy functional [CH95, Szc01], by solving the associated Euler-Lagrange equations, or by solving the weak form of the Euler-Lagrange equations. The Euler-Lagrange equations are generally favored, since algorithms to solve them are more efficient and versatile than optimization techniques in terms of computational effort at least when we are not too far from a solution. However, these algorithms do not ensure convergence *a priori*.

The Galerkin approximation has been formulated and analyzed for density functional theory in [LOS10]. We develop hereafter the weak form of the Hartree-Fock problems to solve them by a Galerkin approach, which will be described and justified in Chapter 3.

### 2.2.1 The weak form of the Schrödinger problem

The weak form of the Schrödinger problem can be obtained by multiplying the Schrödinger equation (eq.2.1) by the virtual term $\delta\Psi_e$, integrating by parts the kinetic term and introducing test multipliers with respect to the normality and anti-symmetry constraints.

Find $\{\Psi_e, E_e, \lambda_\sigma\} \in \mathsf{W} \times \mathsf{W}^{E_e} \times \mathsf{W}^{\lambda}$ such that:

$$\begin{aligned}\frac{1}{2}\left(\nabla_x\Psi_e, \nabla_x\delta\Psi_e\right) + \left(V_e\Psi_e, \delta\Psi_e\right) = E_e\left(\Psi_e, \delta\Psi_e\right) + \frac{\delta E_e}{2}\left[\left(\Psi_e, \Psi_e\right) - 1\right] \\ + \delta\lambda_\sigma\left[\Psi_e(x_{\sigma(1)}, \ldots, x_{\sigma(N_e)}) - \mathrm{sg}\left(\sigma\right)\Psi_e(x_1, \ldots, x_{N_e})\right] \\ + \lambda_\sigma\delta\left(\Psi_e(x_{\sigma(1)}, \ldots, x_{\sigma(N_e)}) - \mathrm{sg}\left(\sigma\right)\Psi_e(x_1, \ldots, x_{N_e})\right), \\ \forall\delta\Psi_e \in \mathsf{W},\ \forall\delta E_e \in \mathsf{W}^{E_e},\ \forall\delta\lambda_\sigma \in \mathsf{W}^{\lambda}, \quad (2.5)\end{aligned}$$

where the test Lagrange multiplier $\delta E_e$ is associated with the constraint $\|\Psi_e\| = 1$ and the test Lagrange multiplier $\delta\lambda_\sigma$ imposes the anti-symmetry of the approximate solution.

This equation cannot be solved exactly in general. We apply the Galerkin approach to approximate the solution.

### 2.2.2 The Galerkin approximation for the Schrödinger problem

Using the Galerkin method, the weak problem is solved in a finite-dimensional basis. The exact solution $\{\Psi_e, E_e\}$ is approximated by an eigenpair $\{\Psi^G, E_G\}$ where

$$\Psi^G = \sum_A \alpha_A \Psi_A. \tag{2.6}$$

The projection of the eigenfunction on each basis function is $\alpha_A = (\Psi^G, \Psi_A)$. The normality of $\Psi^G$ is imposed through the normalization of each $\Psi_A$ and a constraint on the coefficients $\alpha_A$. Consequently, the problem reads:

Find $\{\Psi^G, E_G, \mu, \lambda_\sigma, \lambda^{AB}\}$ such that:

$$\begin{aligned}
\sum_A \alpha_A \left[\frac{1}{2}\left(\nabla\Psi_A, \nabla\delta\left(\alpha_B\Psi_B\right)\right) + \left(V_e\Psi_A, \delta\left(\alpha_B\Psi_B\right)\right)\right] &= E_G \sum_A \alpha_A \left(\Psi_A, \delta\left(\alpha_B\Psi_B\right)\right) \\
+ \delta\mu \left[\sum_A |\alpha_A|^2 - 1\right] &+ \delta\lambda_\sigma \left[\Psi_A(x_{\sigma(1)}, \ldots, x_{\sigma(N_e)}) - \mathrm{sg}\left(\sigma\right)\Psi_A(x_1, \ldots, x_{N_e})\right] \\
&+ \lambda_\sigma \delta\left(\Psi_A(x_{\sigma(1)}, \ldots, x_{\sigma(N_e)}) - \mathrm{sg}\left(\sigma\right)\Psi_A(x_1, \ldots, x_{N_e})\right) \\
&+ \mathrm{tr}\left[\delta\lambda^{AB} \cdot \left(\left(\int \Psi_A \otimes \Psi_B^*\right) - \delta_{AB} I\right)\right], \\
&\forall\delta\alpha_B \in \mathsf{W}^\alpha,\ \forall\delta\Psi_B \in \mathsf{W},\ \forall\delta\lambda_\sigma \in \mathsf{W}^{\lambda_\sigma},\ \forall\delta\mu \in \mathsf{W}^\mu,\ \forall\delta\lambda^{AB} \in \mathsf{W}^{\lambda^{AB}},
\end{aligned} \tag{2.7}$$

where tr denotes the trace of a square matrix and $\delta_{AB}$ is the Kronecker delta, *i.e.* $\delta_{AB} = 1$ if $A = B$ and $\delta_{AB} = 0$ if $A \neq B$. The test Lagrange multiplier $\delta\lambda_\sigma$ imposes the anti-symmetry of the solution, $\delta\lambda^{AB}$ imposes the orthonormalization of the basis wave functions, and $\delta\mu$ constraints the coefficients $\alpha_A$ to satisfy $\sum_A |\alpha_A|^2 = 1$. Now the problem can be decomposed as follows:

Find $\{\Psi_A, \alpha_A, \mu, \lambda_\sigma, \lambda^{AB}\}$ such that:

$$\begin{aligned}
\sum_A \alpha_A\alpha_B \left[\frac{1}{2}\left(\nabla\Psi_A, \nabla\delta\Psi_B\right) + \left(V_e\Psi_A, \delta\Psi_B\right)\right] + \alpha_A \left[\frac{1}{2}\left(\nabla\Psi_A, \nabla\Psi_B\right)_X + \left(V_e\Psi_A, \Psi_B\right)_X\right]\delta\alpha_B \\
= E_G \sum_A \alpha_A\alpha_B \left(\Psi_A, \delta\Psi_B\right) + E_G \sum_A \alpha_A \left(\Psi_A, \Psi_B\right)_X \delta\alpha_B + \delta\mu \left[\sum_A |\alpha_A|^2 - 1\right] \\
+ \delta\lambda_\sigma \left[\Psi_A(x_{\sigma(1)}, \ldots, x_{\sigma(N_e)}) - \mathrm{sg}\left(\sigma\right)\Psi_A(x_1, \ldots, x_{N_e})\right]
\end{aligned}$$

$$+ \lambda_\sigma \delta \left( \Psi_A(x_{\sigma(1)}, \ldots, x_{\sigma(N_e)}) - \mathrm{sg}\,(\sigma)\, \Psi_A(x_1, \ldots, x_{N_e}) \right)$$
$$+ \mathrm{tr} \left[ \delta\lambda^{AB}. \left( \left( \int \Psi_A \otimes \Psi_B^* \right) - \delta_{AB} I \right) \right],$$
$$\forall \delta\Psi_B \in \mathsf{W},\ \forall \delta\lambda^{AB} \in \mathsf{W}^{\lambda^{AB}},\ \forall \delta\lambda_\sigma \in \mathsf{W}^{\lambda_\sigma},\ \forall \delta\alpha_B \in \mathsf{W}^{\alpha},\ \forall \delta\mu \in \mathsf{W}^{\mu}. \quad (2.8)$$

It can be seen from (2.8) that the coefficients $\alpha_A$ are the eigenvalues of the matrix $H_{G_{AB}}$ defined by $H_{G_{AB}} = \left[ \frac{1}{2} \left( \nabla\Psi_A, \nabla\Psi_B \right)_X + \left( V_e \Psi_A, \Psi_B \right)_X \right]$.

### 2.2.3 Weak formulation of the multiconfiguration problem

We consider first the MC which gives a general approach and will derive next the Hartree-Fock (HF) and Configuration Interaction (CI) from it. The multiconfiguration model considers the trial function $\Psi_e^{MC}$:

$$\Psi_e^{MC} = \sum_{A=1}^{N_d} \alpha_A \Psi_A, \quad (2.9)$$

where $\Psi_A$ are determinants built from one-electron wave functions:

$$\Psi_A = \frac{1}{\sqrt{N_e!}} \det \left[ \tilde{\Phi}^A \right]. \quad (2.10)$$

Consequently the constraint of anti-symmetry of the basis functions associated with the Lagrange multipliers $\delta\lambda_\sigma$ is satisfied. Both the set of coefficients $\alpha_A$ and the one-electron wave functions $\Phi^A$ are computed simultaneously [WM80, MMC90].

#### General form of the equations system

As presented in equation (2.8), the coefficients $\alpha_A$ are computed as eigenvalues of the matrix $H_G$. To guarantee *a priori* the orthonormality of the functions $\Psi_A$ and the normality of the solution $\Psi_e^{MC}$, we impose through Lagrange multipliers on the one-electron wave functions:

$$\int_{\mathbb{R}^3} \Phi^A \otimes \Phi^B = \delta_{AB} I. \quad (2.11)$$

From equation (2.8), we compute the one-electron wave functions $\Phi^A$ by:

$$\sum_A \alpha_A \alpha_B \left[ \frac{1}{2} \left( \nabla \det\tilde{\Phi}^A, \nabla \delta \det\tilde{\Phi}^B \right) + \left( V_e \det\tilde{\Phi}^A, \delta \det\tilde{\Phi}^B \right) \right] = E_G \sum_A \alpha_A \alpha_B \left( \det\tilde{\Phi}^A, \delta \det\tilde{\Phi}^B \right)_X$$

$$+\,\delta\left[\mathrm{tr}\left(\frac{\Lambda^{AB}}{2}.\left(\int_{\mathbb{R}^3}\Phi^A\otimes\Phi^B-\delta_{AB}I\right)\right)\right]. \quad (2.12)$$

From elementary algebra, we can show that:

$$\delta\mathrm{det}\tilde{\Phi}=\sum_{q=1}^{N_e}\det\left(\Phi\left(x_1\right),\ldots,\delta\Phi\left(x_q\right),\ldots,\Phi\left(x_{N_e}\right)\right). \quad (2.13)$$

Because of the orthonormality of the one-electron wave functions, the products $\left(\mathrm{det}\tilde{\Phi}^A,\delta\mathrm{det}\tilde{\Phi}^B\right)$ vanish. Problem (2.12) can thus be reduced to:

Find $\{\Phi^A,\Lambda^{AB}\}\in\mathsf{W}^\Phi\times\mathsf{W}^\Lambda$ such that:

$$\sum_{A=1}^{N_d}\alpha_A\alpha_B\left[\frac{1}{2}\left(\nabla_{x_e}\mathrm{det}\tilde{\Phi}^A,\nabla_{x_e}\delta\mathrm{det}\tilde{\Phi}^B\right)_{x_e}+\left(\left(V_{en}+V_{ee}\right)\mathrm{det}\tilde{\Phi}^A,\delta\mathrm{det}\tilde{\Phi}^B\right)_{x_e}\right]=\left(\Lambda^{AB}\Phi^A,\delta\Phi^B\right)_{x_e}$$
$$+\,\mathrm{tr}\left[\frac{\delta\Lambda^{AB}}{2}.\left(\int_{\mathbb{R}^3}\Phi^A\otimes\Phi^B-\delta_{AB}I\right)\right],$$
$$\forall\delta\Phi^B\in\mathsf{W}^\Phi,\ \forall\delta\Lambda^{AB}\in\mathsf{W}^\Lambda. \quad (2.14)$$

### Computations of the integrals over $\mathbb{R}^3$

Integrals defined on $\mathbb{R}^{3N_e}$ are turned into integrals defined on $\mathbb{R}^3$ due to the form of the multi-configuration trial functions.

- First, we concentrate on the product $\left(\nabla_{x_e}\mathrm{det}\tilde{\Phi}^A,\nabla_{x_e}\delta\mathrm{det}\tilde{\Phi}^B\right)_{x_e}$. It is recast using the one-electron wave functions as:

$$\varepsilon_i\varepsilon_j\left[\left(\varphi^A_{i_1}\left(x_1\right),\varphi^B_{j_1}\left(x_1\right)\right)\ldots\left(\frac{\partial\varphi^A_{i_m}\left(x_m\right)}{\partial x_m},\frac{\partial\delta\varphi^B_{j_m}\left(x_m\right)}{\partial x_m}\right)\ldots\left(\varphi^A_{i_{N_e}}\left(x_{N_e}\right)\varphi^B_{j_{N_e}}\left(x_{N_e}\right)\right)\right.$$
$$+\left(\varphi^A_{i_1}\left(x_1\right),\varphi^B_{j_1}\left(x_1\right)\right)\ldots\left(\frac{\partial\varphi^A_{i_m}\left(x_m\right)}{\partial x_m},\frac{\partial\varphi^B_{j_m}\left(x_m\right)}{\partial x_m}\right)\ldots$$
$$\left.\ldots\left(\varphi^A_{i_n}\left(x_n\right),\delta\varphi^B_{j_n}\left(x_n\right)\right)\ldots\left(\varphi^A_{i_{N_e}}\left(x_{N_e}\right),\varphi^B_{j_{N_e}}\left(x_{N_e}\right)\right)\right].$$

Due to the orthogonality of the one-electron wave functions, the first term of this sum vanishes. The second remains non zero only if $A=B$ and $i_k=j_k$, $\forall k\in[1;N_e]$. Therefore, we find:

$$\left(\nabla_{x_e}\mathrm{det}\tilde{\Phi}^A,\nabla_{x_e}\delta\mathrm{det}\tilde{\Phi}^B\right)_{x_e}=\left(\nabla_x\Phi^A,\nabla_x\delta\Phi^A\right)_x. \quad (2.15)$$

- Secondly, we focus on the interactions between nuclei and electrons $\left(V_{en}\left(X_M, x_q\right)\det\tilde{\Phi}^A, \delta\det\tilde{\Phi}^B\right)$ and write them using the one-electron wave functions:
$\varepsilon_i\varepsilon_j\left(\varphi^A_{i_1}\left(x_1\right), \varphi^B_{j_1}\left(x_1\right)\right)\ldots\left(V_{en}\left(x_M, x_q\right)\varphi^A_{i_q}\left(x_q\right), \delta\varphi^B_{j_q}\left(x_q\right)\right)\ldots\left(\varphi^A_{i_{N_e}}\left(x_{N_e}\right), \varphi^B_{j_{N_e}}\left(x_{N_e}\right)\right).$
The orthonormality of the one-electron wave functions (eq. 2.11) leads to $A = B$, $i_m = j_m$ $\forall m \in [1; N_e]$ and :

$$\left(V_{en}\left(X_M, x_q\right)\det\tilde{\Phi}^A, \delta\det\tilde{\Phi}^B\right) = \left(V_{en}\left(x_M, x\right)\Phi^B, \delta\Phi^B\right).$$

- Thirdly, we turn to the interactions between electrons $\left(V_{ee}\left(x_p, x_q\right)\det\tilde{\Phi}^A, \delta\det\tilde{\Phi}^B\right)$ and establish it can be written as:

$$\left(\left(\frac{\Phi^A\left(x_p\right)}{\left|x_p - x_q\right|}, \Phi^B\left(x_p\right)\right)_{x_p}\Phi^A\left(x_q\right), \delta\Phi^B\left(x_q\right)\right)_{x_q} - \left(\left(\frac{\Phi^A\left(x_p\right)}{\left|x_p - x_q\right|}\otimes\Phi^B\left(x_p\right)\right)\Phi^A\left(x_q\right), \delta\Phi^B\left(x_q\right)\right).$$

We introduce the interaction matrix $G^{AB}$ whose terms are:

$$G^{AB}\left(x\right) = \int_{\mathbb{R}^3}\frac{\Phi^{A^*}(y)\otimes\Phi^B(y)}{|x-y|}dy. \tag{2.16}$$

Therefore,

$$\left(V_{ee}\left(x_p, x_q\right)\det\tilde{\Phi}^A, \delta\det\tilde{\Phi}^B\right) = \left(\left(\mathrm{tr}\left(G^{AB}\right)I - G^{AB}\right)\Phi^A\left(x_q\right), \delta\Phi^B\left(x_q\right)\right)_{x_q}.$$

We note that the interaction matrix $G$ is a convolution with a Coulomb kernel. It can be defined as the solution of Green's partial differential equations:

$$\mathrm{tr}\left[\nabla G^{AB}\cdot\nabla\delta G^{AB^T}\right] = 4\pi\,\mathrm{tr}\left[\left(\Phi^A\otimes\Phi^{B^*}\right)\cdot\delta G^{AB^T}\right], \qquad \forall\delta G^{AB}\in\mathsf{W}^G. \tag{2.17}$$

Finally, the multiconfiguration system reads:

Find $\left\{\alpha_A, \Phi^A, \Lambda^{AB}, G^{AB}\right\}$ such that:

$$\sum_A\alpha_A\alpha_B\left[\frac{1}{2}\left(\nabla\Phi^A, \nabla\delta\Phi^B\right)_x + \left(V_{en}\Phi^A, \delta\Phi^B\right)_x\right] + \left(\left(\mathrm{tr}\left(G^{AB}\right)I - G^{AB}\right)\Phi^A, \delta\Phi^B\right)_x$$

$$
\begin{aligned}
&+ \alpha_A \left[\frac{1}{2}\left(\nabla\Psi_A, \nabla\Psi_B\right)_X + \left(V_e\Psi_A, \Psi_B\right)_X\right]\delta\alpha_B - E_e^{MC}\sum_A \alpha_A\left(\Psi_A, \Psi_B\right)_X \delta\alpha_B \\
&+ \delta\mu\left[\sum_A |\alpha_A|^2 - 1\right] - \left(\Lambda^{AB}\Phi^A, \delta\Phi^B\right)_x + \operatorname{tr}\left[\frac{\delta\Lambda^{AB}}{2}.\left(\int_{\mathbb{R}^3}\Phi^A\otimes\Phi^B - \delta_{AB}I\right)\right] \\
&\quad + \operatorname{tr}\left[\nabla G^{AB}\cdot\nabla\delta G^{AB^T}\right] - 4\pi\operatorname{tr}\left[\left(\Phi^A\otimes\Phi^{B^*}\right)\cdot\delta G^{AB^T}\right] = 0, \\
&\quad \forall\delta\alpha_B \in \mathsf{W}^\Phi,\ \forall\delta\Phi^B \in \mathsf{W}^\Phi,\ \forall\delta\Lambda^{AB} \in \mathsf{W}^\Lambda,\ \forall\delta G^{AB} \in \mathsf{W}^G,\ \forall\delta\mu \in \mathsf{W}^\mu. \qquad (2.18)
\end{aligned}
$$

The set $\left\{\delta\alpha_A, \delta\Phi^A, \delta\Lambda^{AB}, \delta G^{AB}\right\}$ denotes the test functions. $\Lambda^{AB}$ appears as a Lagrange multiplier associated with the unit norm of the determinants $\Psi^A$. This system of non-linear eigenmatrices will be solved by an iterative numerical scheme introduced in the next chapter.

- Finally, the approximate energy for the multiconfiguration approximation is obtained as:

$$
E_e^{MC} = \sum_{A=1}^{N_d}\sum_{B=1}^{N_d} c_A^* c_B\left(H_e\det\left[\tilde{\Phi}^A(x)\right], \det\left[\tilde{\Phi}^B(x)\right]\right). \qquad (2.19)
$$

This model has also been presented in [Fri03] and in [Lew04]. It involves a very large number of degrees of freedom and is often restricted to the Hartree-Fock trial function.

### 2.2.4 The weak form of the Hartree-Fock problem

We specify now the multiconfiguration formulation to Hartree-Fock as a special case. The Hartree-Fock method considers a single Slater determinant as the trial function (see definition (2.4)). The Hartree-Fock solution $\Psi_e^{HF}$ is derived from a unique vector $\Phi$ of $N_e$ one-electron wave functions. $\{\Phi, \Lambda\}$ satisfy the following system which is derived directly from the above multiconfiguration equations:

Find $\{\Phi, \Lambda\}$ such that:

$$
\begin{cases}
\frac{1}{2}\left(\nabla\Phi, \nabla\delta\Phi\right) + \left(\left(\left(V_{en} + \operatorname{tr}(G)\right)I - G\right)\Phi, \delta\Phi\right) = \left(\Lambda\Phi, \delta\Phi\right), & \forall\delta\Phi \in \mathsf{W}^\Phi, \\
\operatorname{tr}\left[\left(I - \int_{\mathbb{R}^3}\Phi\otimes\Phi^*\right)\cdot\delta\Lambda^T\right] = 0, & \forall\delta\Lambda \in \mathsf{W}^\Lambda,
\end{cases}
\qquad (2.20)
$$

where $\Lambda$ appears as a matrix of Lagrange multipliers associated with the orthonormalization of the one-electron wave functions, and $\delta\Lambda$ as a test Lagrange-multiplier. We have to solve

a self-consistent integro-differential system where the diagonal of the matrix $\Lambda$ contains the eigenvalues. Appendix F details how this weak form is directly established. The terms of the interaction matrix $G$ are:

$$G(x) = \int_{\mathbb{R}^3} \frac{\Phi^*(y) \otimes \Phi(y)}{|x-y|} dy \tag{2.21}$$

that can also be defined as the solution of Laplace's partial differential equations:

$$\operatorname{tr}\left[\nabla G \cdot \nabla \delta G^T\right] = 4\pi \operatorname{tr}\left[(\Phi \otimes \Phi^*) \cdot \delta G^T\right], \qquad \forall \delta G \in \mathsf{W}^G. \tag{2.22}$$

The Hartree-Fock strategy considers a system of $N_e$ independent wave functions. Even if it is only a result of the mathematical hypotheses, this approach reveals expressions of the electronic energies. The diagonal of the matrix $\Lambda$ contains the energies of the modes. They can be linked approximately to the ionization energies by Koopman's theorem. The accuracy of this approximation depends on the specific system. The term $\frac{1}{2}(\nabla\Phi, \nabla\Phi)$ represents the kinetic energies of the wave functions. The term $(V_{en}\Phi, \Phi)$ represents the electrostatic interactions between nuclei and electrons. Inter-electron repulsion is embedded in the term $(\operatorname{tr}(G)\Phi, \Phi)$. The term $(-G\Phi, \Phi)$ has a quantum origin: it comes from the anti-symmetry of the wave function. The terms $\operatorname{tr}(G)$ and $G$ are commonly noted $J$ and $K$ and are referred to as the Coulomb operator and the exchange operator. The Hartree-Fock electronic energy reads:

$$E_e^{HF} = \left(-\frac{1}{2}\nabla\Phi, \nabla\Phi\right) + V_{en}|\Phi|^2 + \left[\operatorname{tr}(G) I.\Phi - G.\Phi\right]\Phi. \tag{2.23}$$

The strong form of the Hartree-Fock problem is classic and is obtained from the weak form (2.20) as (see Appendix G):

$$\begin{cases} -\dfrac{1}{2}\Delta_{x_e}\Phi + V_{en}\Phi + \left[\operatorname{tr}(G) I - G\right]\Phi = \Lambda\Phi \\ \triangle_x G = -4\pi\Phi \otimes \Phi^* \\ \int_{\mathbb{R}^3} \Phi \otimes \Phi^* \, dx = I. \end{cases} \tag{2.24}$$

Remark: The influence of an electric potential can be incorporated into the Hartree-Fock equation. To investigate interactions between electrons and an external electric field creating an

external potential energy $V_e^{el}$, the Hartree-Fock system reads:

$$\begin{cases} \left(-\frac{1}{2}\nabla\Phi, \nabla\delta\Phi\right) + \left(\left(\left(V_{en} + V_e^{el} + \mathrm{tr}\,(G)\right) I - G\right)\Phi, \delta\Phi\right) = (\Lambda\Phi, \delta\Phi)\,, & \forall\delta\Phi \in \mathsf{W}^{\Phi}, \\ \mathrm{tr}\left[\nabla G \cdot \nabla\delta G^T\right] = \mathrm{tr}\left[(4\pi\Phi\otimes\Phi^*)\cdot\delta G^T\right], & \forall\delta G \in \mathsf{W}^{G}, \\ \mathrm{tr}\left[(I - \int_{\mathbb{R}^3}\Phi\otimes\Phi^*)\cdot\delta\Lambda^T\right] = 0 & \forall\delta\Lambda \in \mathsf{W}^{\Lambda}. \end{cases} \tag{2.25}$$

### Remarks about spins

Two electrons interact only if they have the same spin eigenvalue. For the sake of clarity, the spin eigenvalues are not made explicit in this dissertation, but they are taken into account in computations. Each electronic wave function $\varphi_i$ is characterized by its spin eigenvalue $\sigma_i$, which can be $\frac{1}{2}$ or $-\frac{1}{2}$. Since electrons are fermions, two different electrons (one with the spin eigenvalue $\frac{1}{2}$ and the other one with the spin eigenvalue $-\frac{1}{2}$) can occupy the same eigenmode. For some systems, since all eigenmodes are occupied by two electrons, the Hartree-Fock system can be simplified. The system of $N_e$ electrons can be described by $\frac{N_e}{2}$ pairs of electrons. The Hartree-Fock system is simplified into the Restricted Hartree-Fock (RHF) system of $\frac{N_e}{2}$ components. Systems describable by this restricted model have necessarily an even number of electrons, but all systems with an even number of electrons cannot be described by this model, *e.g.* the Oxygen atom. Electronic structures for which the Hartree-Fock system cannot be simplified must be described by $N_e$ wave functions and the Unrestricted Hartree-Fock (UHF) system.

Among the different eigenmodes solutions of the Hartree-Fock system, we know from the *aufbau* principle that the eigenmodes which are occupied by electrons are those with the lowest eigenvalues [AF05]. The list of occupied modes is called the electron configuration. For our computations, the electron configuration is established using the literature. It imposes the number of wave functions defining the system and the model describing the system, either the restricted Hartree-Fock or the unrestricted Hartree-Fock model. Appendix D lists the electron configurations of the isolated atoms.

Solving the Hartree-Fock problem

$\downarrow$

Computing an arbitrary number of virtual functions

$\downarrow$

Deriving some determinants from these two sets of functions

$\downarrow$

Computing coefficients $\alpha_A$

$\downarrow$

Estimating the CI energy

Figure 2.2: Scheme of the configuration interaction strategy

**Properties of the Hartree-Fock solutions**

The Hartree-Fock system has symmetric properties. Let $C$ be an orthogonal matrix, the transformation $\tilde{\Phi} = C\Phi$ transforms the system (2.24) into a system of the same form, $\Lambda$ being replaced by $C\Lambda C^T$. One can always find a $C$ such that the transformed $\Lambda$ becomes a diagonal matrix.

Let us examine two distinct wave functions $\varphi_k$ and $\varphi_l$ (with $k \neq l$ and $(k,l) \in [1;N_e]^2$), which are assumed solutions of the Fock system (2.24). We multiply the $k$-th equation by $\varphi_l^*$ and the $l$-th equation by $\varphi_k^*$. Integrating over $\mathbb{R}^3$ the difference of both terms and considering the basis in which $\Lambda$ is a diagonal matrix, we show that if $\Lambda_{kk} \neq \Lambda_{ll}$, for $k \neq l$, then $\varphi_k$ and $\varphi_l$ are necessarily orthogonal.

A way to improve the estimate of the Hartree-Fock problem without solving a problem as complex as the multiconfiguration one is computing the configuration interaction problem.

### 2.2.5 Weak formulation of the configuration interaction problem

The configuration interaction approach is in fact a two-stage scheme for MC where the one-electron wave functions are computed first as in HF, new trial waves are computed from them and the associated $\alpha_i$ are finally computed. The configuration interaction strategy uses the same trial function as the multiconfiguration problem:

$$\Psi_e^{CI} = \frac{1}{\sqrt{N_e!}} \sum_{A=1}^{N_d} \alpha_A \det\left[\tilde{\Phi}^A\right]. \tag{2.26}$$

The one-electron wave functions $\Phi^A$ are determined separately from the coefficients $\alpha_A$. The coefficients $\alpha_A$ are obtained by equation (2.8). The determination of the vectors $\Phi_A$ is simplified when compared with the multiconfiguration problem. It is divided into three steps:

- First, the Hartree-Fock problem (eq.2.20) is solved, the first vector $\Phi^1$ contains its solution.
- Then, an auxiliary vector containing any number $N_v$ of one-electron wave functions is computed.
- Finally, the vectors $\Phi^A$ (for $A \in ]1;N_d]$) are built combining some one-electron wave functions of $\Phi^1$ and some components of the vector $\Phi^V$.

The one-electron wave functions $\varphi_{Vi}$ contained in the vector $\Phi^V$ are called virtual wave functions. The pair $\{\Phi^V, \Lambda^V\}$ is defined as the solution of:

$$\begin{cases} \left(-\frac{1}{2}\nabla\Phi^V, \nabla\delta\Phi^V\right) + \left(\left(\left(V_{en} + \mathrm{tr}\left(G\right)\right) I - G^V\right)\Phi^V, \delta\Phi^V\right) = \left(\Lambda^V\Phi^V, \delta\Phi^V\right), & \forall\delta\Phi^V \in \mathsf{W}^\Phi, \\ \mathrm{tr}\left[\nabla_{x_e} G^V \cdot \nabla_{x_e}\delta G^{V^T}\right] = \mathrm{tr}\left[\left(4\pi\Phi^V \otimes \Phi^*\right) \cdot \delta G^{V^T}\right], & \forall\delta G^V \in \mathsf{W}^G, \\ \mathrm{tr}\left[\left(I - \int_{\mathbb{R}^3} \Phi^V \otimes \Phi^{V^*}\right) \cdot \delta\Lambda^{V^T}\right] = 0, & \forall\delta\Lambda^V \in \mathsf{W}^\Lambda, \end{cases} \tag{2.27}$$

where $\Lambda^V$ appears as a Lagrange multiplier associated with the orthonormalization of the one-electron virtual wave functions, and $\delta\Lambda^V$ as a test Lagrange-multiplier. The diagonal of the matrix $\Lambda^V$ contains the eigenvalues related to the electron energies of the virtual modes $\varphi_i^V$. The virtual wave funcions $\varphi_i^V$ are orthogonal between each other, and orthogonal to the Hartree-Fock wave functions $\varphi_i$.

The vectors $\Phi^A$ are constructed by replacing some one-electron wave functions of vector $\Phi$ by some virtual wave functions. For instance, considering a system described by three one-electron wave functions, three vectors $\Phi^A$ can be:

$$\Phi^1\left(x\right) = \begin{bmatrix} \varphi_1\left(x\right) \\ \varphi_1^V\left(x\right) \\ \varphi_3\left(x\right) \end{bmatrix}, \quad \Phi^2\left(x\right) = \begin{bmatrix} \varphi_1\left(x\right) \\ \varphi_1^V\left(x\right) \\ \varphi_2^V\left(x\right) \end{bmatrix}, \quad \Phi^3\left(x\right) = \begin{bmatrix} \varphi_2^V\left(x\right) \\ \varphi_1^V\left(x\right) \\ \varphi_3\left(x\right) \end{bmatrix}.$$

Using two virtual wave functions, 18 vectors $\Phi^A$ could be built: 6 vectors involve only one virtual wave function and 12 vectors involve both virtual wave functions simultaneously. Then, the determinants are derived from the matrices $\tilde{\Phi}^A$ built from the vectors $\Phi^A$. The Slater determinants constructed using $k$ virtual wave functions are called excited states at the order $k$.

Since the one-electron wave functions are orthonormal, the determinants derived from these are orthonormal. The maximum number of determinants $N_{d,max}$ involved in the series depends on the number of components of the vector $\Phi$ and on the number of virtual wave functions. Using the maximum number of available determinants guarantees size consistency (see page 32).

The configuration interaction strategy is summed up by Figure 2.2. First, the Hartree-Fock problem is solved, then a number of virtual functions is chosen, and these functions are

computed. Some determinants are derived from the wave functions contained in the vectors $\Phi$ and $\Phi^V$. Finally, the coefficients $\alpha$ are computed, and the approximate energy is estimated by equation (2.19).

## 2.3 Summary

In this chapter, we have presented the family of Hartree-Fock methods, also called the wave function methods. Supposing that the wave function has the form of Slater determinants, the Hartree-Fock strategy turns a unique equation defined from a very large space into several equations defined only from a three-dimensional space. Regrettably, it neglects electronic correlation. The post-Hartree-Fock methods were introduced to improve results by increasing the space of trial functions. In that case, trial functions are linear combinations of Slater determinants with the Hartree-Fock determinant included.

The Hartree-Fock method has been used to solve quantum mechanics problems since the 1930s. During the first decades, only small systems with very few electrons could be solved using this method because the Hartree-Fock system is non-linear and can involve a large number of degrees of freedom. To solve it for general cases, it requires an efficient numerical strategy. In the next chapter, we present different numerical methods to overcome these difficulties.

The post-Hartree-Fock methods provide a hierarchy of trial functions to estimate the electronic state of any system. Considering the hierarchy of the different solution spaces $\mathsf{W}^{HF} \subset \mathsf{W}^{CI} \subset \mathsf{W}$, the exact energy $E_e$ is lower than the multiconfiguration energy $E_e^{CI}$ which is lower than the Hartree-Fock energy $E_e^{HF}$:

$$E_e \leqslant E_e^{CI} \leqslant E_e^{HF}. \tag{2.28}$$

Energy estimates become more accurate when the trial function space is enlarged. In Chapter 5, we construct error estimation tools to compare the accuracy of the different trial function spaces.

# Chapter 3

# Numerical strategy

In this work, we apply the Hartree-Fock and the configuration interaction methods (introduced in Chapter 2) to approximate solutions of the Schrödinger equation. For the sake of simplicity, the numerical strategy is presented here for the Hartree-Fock system considered as the reference problem. The same tools and approach are used to solve the configuration interaction problem.

As discussed in the previous chapter, the Hartree-Fock problem is a non linear eigenvalue problem and involves a large number of degrees of freedom. Therefore, solving it requires powerful numerical tools to ensure convergence, to tackle large systems and to provide accurate approximations of the solutions. The first part of this chapter overviews the different strategies set up in the literature to tackle the problem. Most involve a variational discretization based on a finite-dimensional space of trial functions. The evaluation of the different basis sets aims at using the finite element method to solve the Fock system. The second part of this chapter details our finite element strategy to solve efficiently the weak form of the Fock system.

## 3.1 State of the art

As mentioned before, solving the Hartree-Fock problem can be done by several approaches: minimizing the Hartree-Fock energy functional, solving the strong form of the problem, or solving the weak form of the system. Whatever the approach, the solver requires an $N_b$-finite-dimensional

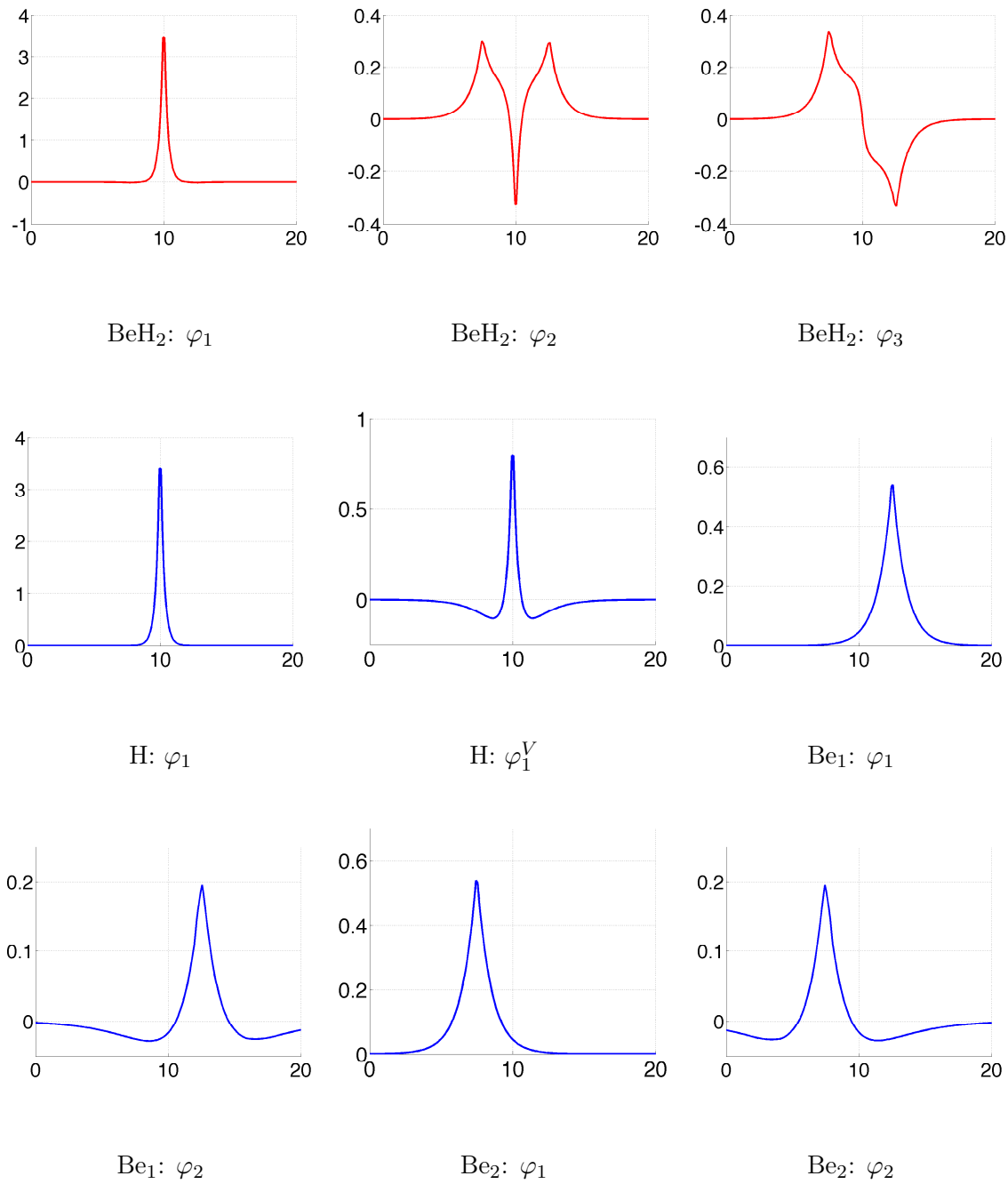


Figure 3.1: Some atomic orbitals relative to the Be and the H atoms (in blue) which can be employed as a basis set to compute the $BeH_2$ molecule whose one-electron eigenfunctions are represented in red. All the wave functions are represented on the axis $z$ (*i.e.* $\{x = 0, y = 0\}$ considering the following positions of the atoms: H(0;0;7.48), Be(0;0;10), and H(0;0;12.52).

space $\nu$. Each wave function $\varphi_j$ is expanded as a linear combination of basis functions $\{\chi_i\}_{i\in[1;N_b]}$ of $\nu$:

$$\forall j \in [1; N_e], \qquad \varphi_j = \sum_{i=1}^{N_b} C_{ji}\chi_i \qquad \text{where} \qquad C_{ji} = (\chi_i, \varphi_j)_{\mathbb{R}^3}\,. \tag{3.1}$$

$C$ is a matrix that contains the coefficients of the linear combination of $\chi_i$ to build $\varphi_j$.

The choice of the basis functions and their number $N_b$ will affect the accuracy of the numerical results. In order to optimize the convergence, Cancès *et al.* [CLM06] highlight the importance of adapting the basis functions to the problem at hand. In the literature, different sets of trial functions have been proposed.

### 3.1.1 Basis functions

As quantum operators are Hermitian, eigenfunctions form a basis on which all the solutions can be developed. Using this idea, the first atomic simulations were developed on atomic orbitals sets. Such an approach can be related to the Rayleigh-Ritz method which is very often used in mechanics [Gou95].

#### Atomic orbitals

Atomic orbitals $\chi_a$ are eigenfunctions of isolated atoms. Figure 3.1 shows a set of atomic orbitals relative to the Be and the H atoms which can be used as a basis set to compute the $BeH_2$ molecule. These trial functions are centered on each nucleus, and their number $N_b$ is greater or equal to the number of fundamental wave functions for the isolated atoms considered. In addition to the atomic orbitals centered on real atoms, some authors introduce ghost atoms and ghost atomic orbitals to enlarge the discretization basis [OM76].

Atomic orbitals can be described by different mathematical functions, such as hydrogen-like atomic orbitals, Gaussian orbitals or Slater-type orbitals, which are detailed below.

For molecular or crystal simulations, atomic orbitals can be employed as a basis set to build molecular orbitals [Hal91]. The Linear Combination of Atomic Orbitals (LCAO) method defines molecular orbitals $\chi_{mol}$ as:

$$\chi_{mol} = \sum_a C_{ia}\chi_a. \tag{3.2}$$

The coefficients $C_{ia}$ of the linear combination are determined by a variational approach [SO96, AF05].

In the following paragraphs, we list some mathematical functions proposed in the literature to approximate atomic orbitals.

**Slater-type orbitals** In 1930, Slater introduced Slater-type orbitals, also called STOs [Sla30, Sla32]. They are generally divided in a radial and an angular part expressed in cylindrical coordinates $(r, \theta, \varphi)$. These two parts are independent, and are solved separately.

The angular part is usually the real part of spherical harmonics $Y_l^m$. The radial part $\chi_{STO}^r$ is assumed to decay exponentially at long range, and has the following form:

$$\chi_{STO}(r) = C_{STO}|r|^{n-1}e^{-\zeta|r|} \tag{3.3}$$

where $C_{STO}$ is a normalization constant, and $n$ is the principal quantum number defined in the brief introduction to quantum numbers in Appendix E. Models for atoms and molecules allow the determination of the effective nuclear charge $\zeta$ [OPNZ00].

For example, Crystal [Cry11] is a commercial software that provides the solution of the Hartree-Fock system using a basis of Slater-type orbitals.

**Gaussian functions** In 1950, Boys [Boy50] proposed Gaussian functions as atomic orbitals. They can be called Gaussian orbitals, Gaussian type orbitals or GTOs. Alike STOs, they are divided into independent radial and angular parts and the real part of the spherical harmonics is used as the angular part. The radial part has the following form:

$$\chi_{GTO}(r) = C_G r^l e^{-\alpha r^2} \tag{3.4}$$

where $C_G$ is a normalization constant, and $l$ is the angular quantum number (defined in Appendix E).

Crystal [Cry11], Jaguar [Sch11] and Gaussian [Gau11] are examples of software that solve the Hartree-Fock system with a Gaussian basis.

Without using atomic orbitals *i.e.* eigensolutions of atomic problems, trial functions can also be mathematical constructs suitable for the Hartree-Fock simulations.

### Plane or spherical waves

The electronic problem can be expanded on an orthonormal basis of plane waves [dLPZ79]. The basis functions $\chi_{PW}$ are expressed as a function of the Cartesian coordinate $x$ in case of plane waves:

$$\chi_{PW}(x) = \sum_k c_k e^{ikx} \tag{3.5}$$

where $c_k$ are normalization constants. Spherical waves are functions of the distance $r$ between the electron and the nucleus:

$$\chi_{SW}(r) = \sum_k c_k e^{ikr}. \tag{3.6}$$

For localized systems, such as the first row elements or transition metals, where the vacuum area can be large, this method generally requires a large number of basis functions. To solve this problem, some authors propose to employ adaptive coordinates. General curvilinear coordinates are arranged in order to be dense where the wave functions are localized [DCAJ94].

The software VASP [VAS11] is equipped with such a basis set.

### Wavelets

Some authors [CAJL93] suggest a basis of wavelets. These oscillations provide an orthonormal basis with respect to the inner product defined by eq.(2.3), localized in both real and Fourier spaces [Cha05].

DFT++ [Cor11], MADNESS [Com11] or BigDFT [Eur11] can solve the electronic problem with wavelets basis.

### Finite element basis functions

The finite element method (FEM) provides another approach to build a basis of localized trial functions. This discrete numerical method is widespread in the contexts of structural mechanics, fluid mechanics, acoustics, among other domains in which partial differential equations need to

be solved. Approximate solutions are found from discretization of the weak form of the problem. This method is detailed in [ZT05] or in [Joh09].

The domain $\Omega$ of the FEM is segmented into $M$ tetrahedra (in 3D). Polynomials $\omega_j^p$ of order $p$ are defined on each tetrahedron $j$. They constitute a basis of local functions, continuous on $\Omega$. Numerical solutions $\varphi_i^p$, approximation of the exact solutions $\varphi_i$, are estimated on this partition $\left\{\omega_j^p,\, j \in [1, M]\right\}$:

$$\varphi_i \approx \varphi_i^p = \sum_{j=1}^{M} C_{ij}\, \omega_j^p. \tag{3.7}$$

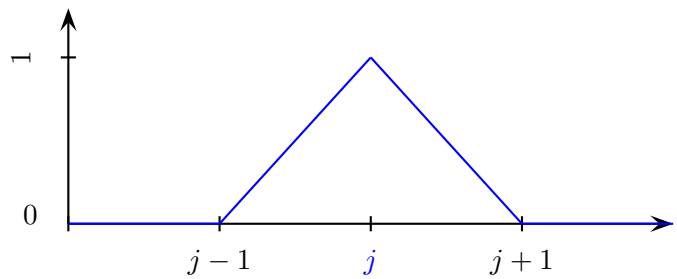


Figure 3.2: A FEM basis function: $\omega_j^1$ of order 1

We use Lagrangian finite elements. Each polynomial takes the value 1 only at a certain node and all the other basis functions vanish for the considered node. Therefore, approximate functions are continuous piecewise polynomials on subdomains called "finite elements". The coefficients $C_{ij}$ are the values of the approximate wave functions $\varphi_i$ at the corresponding nodes. They are estimated numerically applying the Galerkin method to the weak form of the Hartree-Fock electronic problem presented in Chapter 2. The quality of finite element approximations depends on the form and the density of the mesh involved.

### 3.1.2 Evaluation of the different functions basis

Tsuchida and Tsukada [TT98] list the properties required for an ideal basis set: simplicity, sparsity, high parallelizability, possibility to use non-periodic boundary conditions, possibility to expand wave functions in real space efficiently, with non-uniformity, with computational effort scaling linearly with the number of variables.

First, let us compare the different atomic orbitals between them. The general form of the Gaussian functions is not as accurate as the form of Slater-type orbitals. Therefore, they generally require a larger number of basis functions and are not widely used for atomic or crystal computations.

For molecular cases, a drawback of Slater-type orbitals is the fact that products of two Slater-type orbitals of distinct atoms are difficult to compute. Gaussian orbitals are preferred because the product of two Gaussian functions centered on different atoms can be expressed as a Gaussian function centered on a point along the axis connecting the two atoms.

Now, let us compare atomic orbitals with other basis functions. Any kind of atomic or molecular orbitals is disadvantageous because it needs preliminary knowledge of the expressions of atomic orbitals, specific to the atoms considered. Moreover, any atomic orbital, such as hydrogen-like atomic orbitals, Slater-type orbitals, Gaussians or exponential-type orbitals, imposes a general form to the approximate wave functions over the entire domain. To estimate the total energy of the system, the most influential area is in the neighborhood of the nuclei. Such methods tend to represent accurately the wave functions in these areas and to poorly represent them far from the nuclei. Globally defined basis sets cannot improve the estimation of the wave functions near the nuclei without causing effects far from them. This limitation encourages the use of locally defined basis sets.

The finite element method and wavelets do not impose a special form of the wave function and use real-space computations. Therefore, they allow for a local refinement of the approximate wave function. A fine discretization is used near the nuclei where the potential varies rapidly [LS85]. Moreover, algorithms using localized basis functions provide a linear scaling complexity [GP92, MGC93, ODMG95]. Besides, in the long term, coupling a FEM microscale or mesoscale model with a FEM nanoscale model appears more natural than coupling a FEM microscale or mesoscale model with a nanoscale model based on atomic orbitals.

We choose to use the FEM. In the next section, we give an overview of the works which solve quantum problems by the FEM.

### 3.1.3 The FEM in quantum mechanics

The FEM is traditionally employed to compute the deformations of materials. Works on the application of the FEM to atomic problems first appeared in 1975 [Ask75]. Askar presented an approach to solve the stationary problem of the hydrogen atom using finite elements. He compared theoretically this method with the finite difference method and Rayleigh-Ritz's method, and computed the energies of the ground state and the first excited states for the hydrogen atom within 0.1 % error.

Then, several authors performed FEM solution of one- or two-dimensional problems [FRRT78, NB76]. In 1985, Levin and Shertzer published the first work applying the FEM to three-dimensional problems [LS85]. They solved the Helium ground state with a 324-node three-dimensional grid. Their low error on the average positions of the electrons $\langle x_e \rangle$ and $\langle x_e^2 \rangle$, as compared to the literature, offered promising perspectives for the FEM in the quantum context. The memory of their computer limited the accuracy of their results for large systems. Braun *et al.* [BSH93] also computed the Helium atom ground state and some excited states of spherical symmetry. They used parallelepipedal elements, and took advantage of wave functions' symmetry or antisymmetry to reduce the domain by half. They reached around 23 000 degrees of freedom, and noted a strong dependence of the results on the number of nodes considered. Contrary to the results obtained by other methods, they showed that the relative error on $\langle x_e \rangle$ and $\langle x_e^2 \rangle$ is not consistently larger than the relative error on energies.

Ackerman [Ack95] tested the influence of $R$, the radius of the two-dimensional FEM domain. For Helium ground state, the effect of $R$ on the results is obvious between $6.0\,a_0$ and $9.0\,a_0$ but there is not any significant influence of the domain radius on the results between $12.0\,a_0$ and $15.0\,a_0$. He also performed three-dimensional computations for the Helium atom and the hydrogen ion $H^-$, and faced instability of the Gaussian numerical integration and a divergence of the results due to the singularity of the potential term. He proposed to solve this problem by changing the coordinate system into Hylleraas coordinates $s_{ij}$, $t_{ij}$ and $u_{ij}$ defined from $r_i$ and $r_j$ the first polar coordinates of the electrons $i$ and $j$: $s_{ij} = r_i + r_j$, $t_{ij} = r_i - r_j$ and $u_{ij}$ the distance between the electrons $i$ and $j$ [KM93, Rui05a, Rui05b]. Scrinzi [Scr95] studied the influence of the coordinate system and showed the substitution $r$ into $\exp(i\alpha r)$ where $0 < \alpha < \frac{\pi}{2}$

provides a higher accuracy with many fewer basis functions when comparing to classical FEM computations. Other authors [AR93, AER94] proposed an alternative by using self-adaptive meshes.

Tsuchida and Tsukada used the FEM, in LDA framework (see page 25), to solve the hydrogen molecule [TT95b] and performed some pseudopotential calculations for silicium in the diamond structure [TT95a]. They took advantage of the FEM to compute systems with large vacuum regions, where a rough mesh is well adapted. These authors improved the method by using non-uniform grids thanks to the adaptive curvilinear coordinates [TT96, TT98]. A review on the use of the FEM to solve the Kohn-Sham equations of density functional theory was written by Pask and Sterne [PS05].

In 1990, Sundholm and Olsen employed the FEM to compute only the radial part of the electronic wave function in the framework of the Hartree-Fock method [SO90a]. They used this numerical strategy to calculate the nuclear quadrupole moments of different systems [SO90b, SO93, TSP98], and the electron affinities of various elements like manganese [SO95]. Alizadegan *et al.* [AHM10] applied a "divide and conquer" algorithm to the finite element Hartree-Fock calculations to supply parallelization and explore larger systems in the future.

The FEM has also been employed to solve directly the Schrödinger equation for lithium ground state in a six-dimensional space [ZYD04].

Since the FEM has been so widely used in other areas, including in the industry, there is a lot of expertise on the corresponding numerical solvers, optimization,... so numerical tools and background are very ripe. The major drawback of the FEM is the need for extensive computer core memory. The FEM also needs bounded domains whereas the quantum problem is defined on an unbounded domain. In the following section, we present how we set up the finite element method to solve the Hartree-Fock problem.

## 3.2 The FEM strategy for the Hartree-Fock model

Chapter 2 detailed how the Galerkin approximation allows the reduction of the Schrödinger problem into the Hartree-Fock problem. Using the finite element method, the Galerkin approximation is applied a second time to solve the Hartree-Fock problem in a finite-dimensional space.

### 3.2.1 Galerkin approximation

The unknowns $\{\Phi_h, \Lambda_h, G_h\}$ are estimated solving the weak form of the system in the finite-dimensional spaces $\mathsf{W}^\Phi$, $\mathsf{W}^\Lambda$ and $\mathsf{W}^G$:

$$\frac{1}{2}\left(\nabla\Phi_h, \nabla\delta\Phi_h\right) + \left(\left(\left(V_{en} + \operatorname{tr}\left(G_h\right)\right) I - G_h\right)\Phi_h, \delta\Phi_h\right) - \left(\Lambda_h\Phi_h, \delta\Phi_h\right) + \operatorname{tr}\left[\left(I - \int_{\mathbb{R}^3} \Phi_h \otimes \Phi_h^*\right) \cdot \delta\Lambda_h^T\right]$$
$$+ \operatorname{tr}\left[\nabla G_h \cdot \nabla\delta G_h^T\right] - 4\pi \operatorname{tr}\left[\left(\Phi_h \otimes \Phi_h^*\right) \cdot \delta G_h^T\right] = 0,$$
$$\forall\delta\Phi_h \in \mathsf{W}^\Phi, \forall\delta\Lambda_h \in \mathsf{W}^\Lambda, \forall\delta G_h \in \mathsf{W}^G. \quad (3.8)$$

An *a priori* analysis implies that this method converges to the solution [CLM06]. This problem is a discrete nonlinear "eigenmatrix" problem. Here, the trial functions are based on Lagrange polynomial functions of degree 2, and the numerical integration is done using Gaussian integration [Joh09]. We detail in the following section the iterative solution method.

### 3.2.2 Newton method

The ideal algorithm to solve the Hartree-Fock problem should ensure global convergence with a fast convergence rate and a low memory requirement. A lot of works have been done in this domain to analyze and evaluate the existing algorithms and propose new alternatives [Can98]. Here we briefly overview the current propositions. We refer to [CLM06] for an introduction to the topic, or to [DDE+03] for detailed explanations.

Two main types of solvers have been proposed to solve the quantum problem. The first is the fixed-point methods such as Roothan's algorithm [Roo51], level-shifting algorithm [SH73] or DIIS algorithm [P.P82]. They are based on a generalized eigenvalue problem where for two matrices $R$ and $M$ the eigenpair $\{\lambda, x\}$ satisfies:

$$R.x = \lambda M.x \qquad \text{with} \qquad x \neq 0.$$

Roothan's algorithm was historically the first algorithm used to tackle quantum problems. It either converges towards a stationary point or oscillates between two states, none of them being solution to the HF system. Currently, the most commonly used algorithm is the Direct Inversion in the Iterative Subspace (DIIS) algorithm. It turns out to be very efficient in most cases, but does not converge for some cases without rigorous explanation for that [CDK+03].

The second category of algorithms has been developed to solve the constraint optimization problem. Different optimization algorithms are proposed in [CLM06]. They all consist in building a sequence of iterates $x$ which converges to the global minimizer of $E$. The next iterate $x_{n+1}$ from $x_n$ is based on two choices: the choice of the direction $d_n$, and the choice of the length $t_n$ along this direction. These algorithms always converge but rarely towards the global minimum for large systems or large function bases.

### Full Newton method

Here we propose to apply Newton's method to solve the system (3.8). The Newton method has already been used by [FMS73] as an alternative to classical algorithms for solving the eigenvalue problem . We detail the algorithm hereafter. For the sake of clarity, we describe it in the case of the strong form of the system.

Starting from initial values $\left\{\Phi^0, \Lambda^0, G^0\right\}$, the iterative process consists in building a series of increments $0, 1, 2, \ldots, n$ while convergence is not reached. We present here how the increments are defined at the step $n+1$ from the values of the unknowns at step $n$. Let us first define the residuals at iteration $n$:

$$\begin{cases} r_\Phi^n = -\dfrac{1}{2}\Delta_x \Phi^n + V_{en}\Phi^n + \left(\operatorname{tr}\left(G^n\right) I - G^n\right)\Phi^n - \Lambda^n \Phi^n, \\ R_G^n = -\Delta G^n - 4\pi \Phi^{n^*} \otimes \Phi^n, \\ R_\Lambda^n = \int_{\mathbb{R}^3} \Phi^{n^*} \otimes \Phi^n - I. \end{cases} \tag{3.9}$$

The Newton method stems from a linearization of the system around the last iterate $\{\Phi^n, \Lambda^n, G^n\}$.

At step $n+1$, the small increments $\{d\Lambda, d\Phi, dG\}$ must satisfy:

$$\begin{cases} 0 = r_\Phi^{n+1} = r_\Phi^n + d\Lambda\left(\Phi^n\right) + \Lambda^n\left(d\Phi\right) + \dfrac{1}{2}\Delta_x d\Phi - V_{en} d\Phi - \left(\mathrm{tr}\left(dG\right) I - dG\right)\Phi^n \\ \qquad\qquad - \left(\mathrm{tr}\left(G^n\right) I - G^n\right) d\Phi, \\ 0 = R_G^{n+1} = R_G^n + \Delta_G dG + 4\pi\left(d\Phi \otimes \Phi^{n^*} + \Phi^n \otimes d\Phi^*\right), \\ 0 = R_\Lambda^{n+1} = R_\Lambda^n - \int_{\mathbb{R}^3}\left(d\Phi \otimes \Phi^{n^*} + \Phi^n \otimes d\Phi^*\right) dx. \end{cases} \tag{3.10}$$

The problem consists in finding $\{d\Lambda, d\Phi, dG\}$ while $\dfrac{|d\Lambda| + |d\Phi| + |dG|}{|\Lambda| + |\Phi| + |G|} \geq \mathtt{tol}^{\mathtt{max}}$ where $|\Lambda| = \sqrt{\mathrm{tr}\left(\Lambda.\Lambda^T\right)}$ and $|G| = \sqrt{\mathrm{tr}\left(G.G^T\right)}$.

The increments $\{d\Lambda, d\Phi, dG\}$ are defined from the solution of the linear system at step $n$. For more clarity, we suppress indexes $n$:

Find $\{d\Lambda, d\Phi, dG\}$ such that:

$$\begin{cases} -d\Lambda\left(\Phi\right) + \left(\mathrm{tr}\left(dG\right) I - dG\right)\Phi + \underbrace{\left(-\dfrac{1}{2}\Delta_x \bullet + V_{en} I + \mathrm{tr}\left(G\right) I - G - \Lambda\right)}_{F}.d\Phi = r_\Phi, \\ \Delta_G dG + 4\pi\left(d\Phi \otimes \Phi^* + \Phi \otimes d\Phi^*\right) = R_G, \\ \int_{\mathbb{R}^3}\left(d\Phi \otimes \Phi^* + \Phi \otimes d\Phi^*\right) dx = R_\Lambda. \end{cases} \tag{3.11}$$

where $F$ is the operator underlined in eq.(3.11). It is possible to eliminate successively $dG$:

$$dG = -\Delta_G^{-1} R_G - \Delta_G^{-1}\left(4\pi\left(d\Phi \otimes \Phi^* + \Phi \otimes d\Phi^*\right)\right) = G_R + G_\Phi\left(d\Phi\right). \tag{3.12}$$

The increment $dG$ has two origins: $G_R$ the inverse Green function of the residual $R_G$, and $G_\Phi\left(d\Phi\right)$ an increment proportional to the increment $d\Phi$. Then, the increment $d\Phi$ can also be eliminated:

$$d\Phi = F^{-1}\left(r_\Phi + d\Lambda\left(\Phi\right) - \left(\mathrm{tr}\left(dG\right) I - dG\right)\Phi\right) = \Phi_r + \Phi_G + \Phi_\Lambda d\Lambda. \tag{3.13}$$

It has three origins: $\Phi_r$ the image of the residual $r_\Phi$ by the inverse of the Fock operator, $\Phi_G$ an increment linked with the increment $dG$ and $\Phi_\Lambda\left(d\Lambda\right)$ an increment proportional to the increment $d\Lambda$. Finally, $d\Lambda$ reads:

$$\int_{\mathbb{R}^3}\left(\Phi_\Lambda d\Lambda\right) \otimes_s \Phi\, dx = R_\Lambda - \int_{\mathbb{R}^3}\left(\Phi_r + \Phi_G\right) \otimes_s \Phi\, dx. \tag{3.14}$$

These loops are iterated until the convergence target error $\texttt{tol}^{\texttt{max}}$ is reached. We generally consider $\texttt{tol}^{\texttt{max}}_{\texttt{gr}} = 10^{-6}$. One of the difficulties to solve the Hartree-Fock system is the very large number of degrees of freedom. Figure 3.3 represents the number of functions to be evaluated for atomic systems. For an unrestricted Hartree-Fock (UHF) strategy (see page 41), it increases proportionally to the number of electrons $N_e$ as $N_e^{1.6}$. This drastic increase is due to the numerous interaction terms $G_{ij}$. For cases where a restricted Hartree-Fock (RHF) strategy can be set up, the increase is reduced and proportional to $N_e^{1.3}$. For instance, the study of Chlorine, an atom of 17 electrons, requires a UHF strategy and the estimation of 97 functions. Computing the fundamental state of Argon, an atom of 18 electrons, requires only the estimation of 46 functions by the RHF strategy.

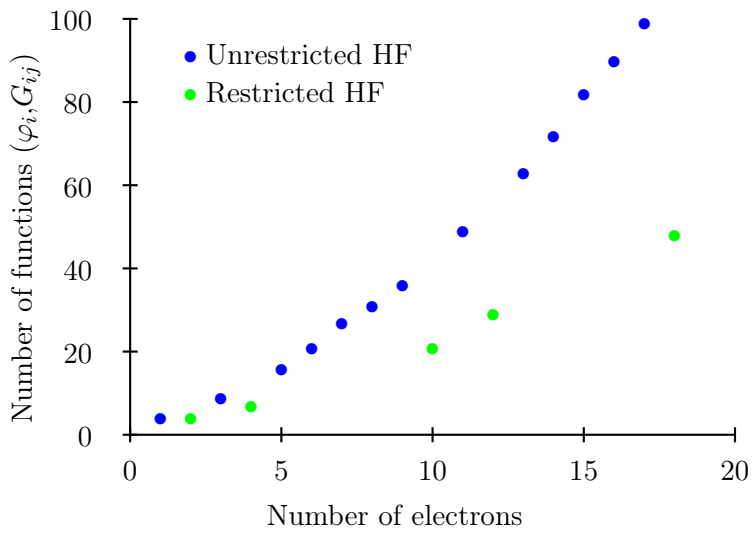


Figure 3.3: Number of degrees of freedom in three-dimensional computations depending on the number of electrons for atomic systems in RHF or UHF conditions

### Staggered Newton method

Due to the number of unknowns, stiffness matrices associated with the vector $\Phi$ and the matrix $G$ are very large and their consideration in linear solvers can demand a lot of memory. A staggered strategy is set up to reduce memory requirements. For each step towards convergence,

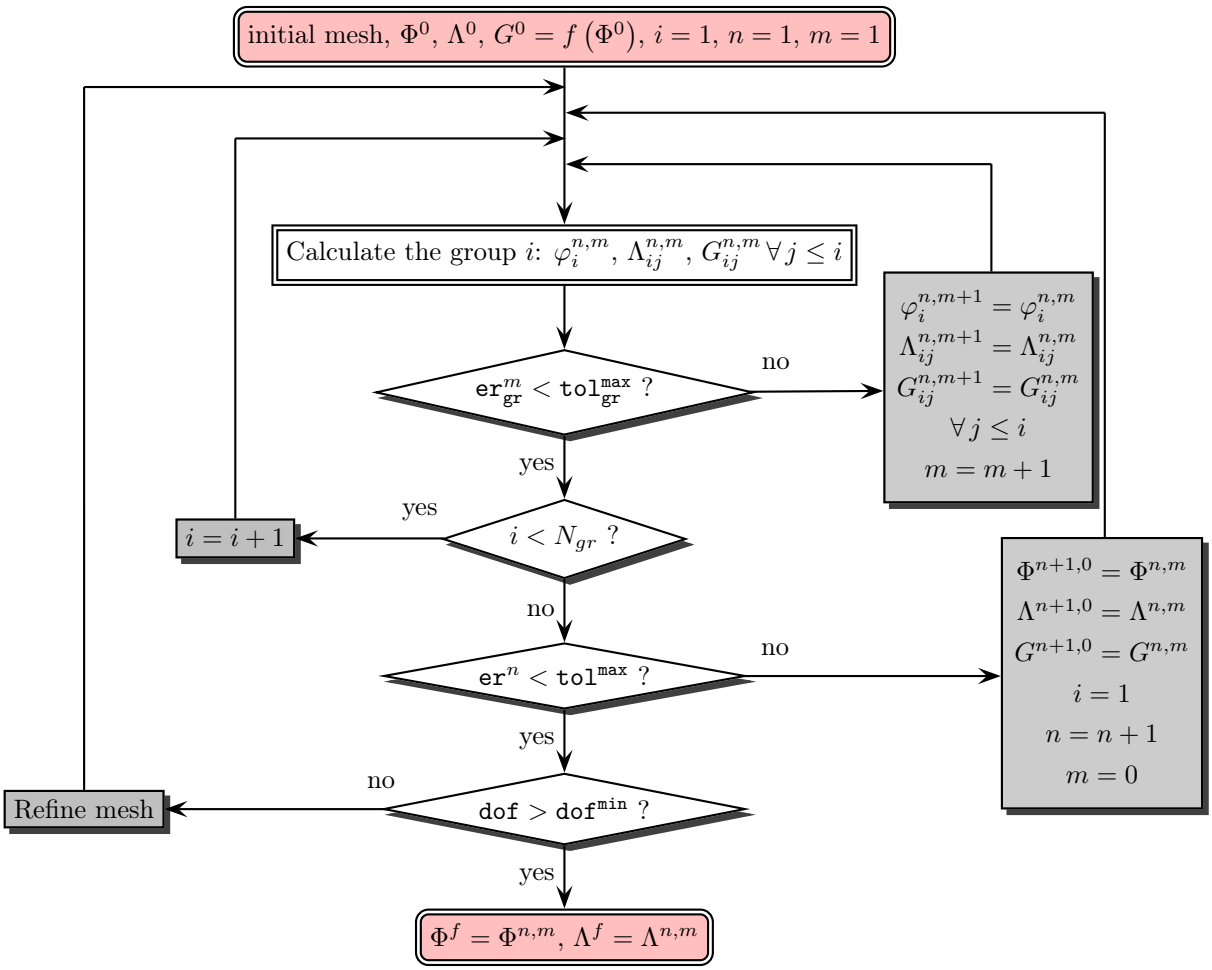


Figure 3.4: Scheme of the numerical strategy applied to the Hartree-Fock problem

the variables related to the same wave function $i$ $\{\varphi_i, \Lambda_{ji}, G_{ji}$ if $j \leqslant i\}$ are lumped together in $N_{gr}$ groups.

$$\begin{aligned} H_{11}^{n+1}\Phi_1^{n+1} + H_{12}^{n}\Phi_2^{n} &= \Lambda_1^{n+1}\Phi_1^{n+1} \\ H_{12}^{n}\Phi_1^{n} + H_{22}^{n+1}\Phi_2^{n+1} &= \Lambda_2^{n+1}\Phi_2^{n+1} \end{aligned}$$

Each group is estimated independently from the other ones. Therefore, the submatrices to be inverted are much smaller. For the same memory cost, the number of nodes of the mesh can be increased, and the accuracy of the results is improved. To optimize the accuracy of the results, we can impose a constant number of functions by group and increase the number of groups, but this alternative leads to an increase of the computation time.

It is important to note that all the components of the stiffness matrix relative to the matrix $G$ are identical. Memory requirement is reduced by saving the stiffness matrix and solving simultaneously for different right-hand sides of the equation.

Figure 3.4 sums up the solution strategy. We use a staggered strategy and begin any computation by determining the number of segregation groups $N_{gr}$. Then, three loops follow one another. The first one estimates the unknowns relative to each group, when the other ones have a fixed expression; the superscript $m$ numbers the iteration, and the loop is stopped when the error is inferior to the target error $\texttt{tol}_{\texttt{gr}}^{\texttt{max}}$. Once all the groups have been computed separately, the error is estimated over all the unknowns. The second loop is iterated until the convergence target error $\texttt{tol}^{\texttt{max}}$ is reached. The iterations are numbered by $n$. The last loop controls the number of degrees of freedom used to estimate any field $\varphi_i$ or $G_{ji}$ and forces it to be superior to $\texttt{dof}^{\texttt{min}}$.

Fixing the convergence criteria is a delicate task. Even if some authors propose results with a high precision such as [OT11] which present results to the nearest $10^{-15}$ Ha, in most of the litterature, energy estimates are provided experimentally or numerically to the nearest $10^{-3}$ Ha [TCA08a, MHH12]. Usually, we choose $\texttt{tol}_{\texttt{gr}}^{\texttt{max}} = 10^{-6}$, $\texttt{tol}^{\texttt{max}} = 10^{-7}$ and $\texttt{dof}^{\texttt{min}} = 100000$, and provide results to the nearest $10^{-4}$ Ha.

We now turn to the initial guesses applied to the iterative numerical method.

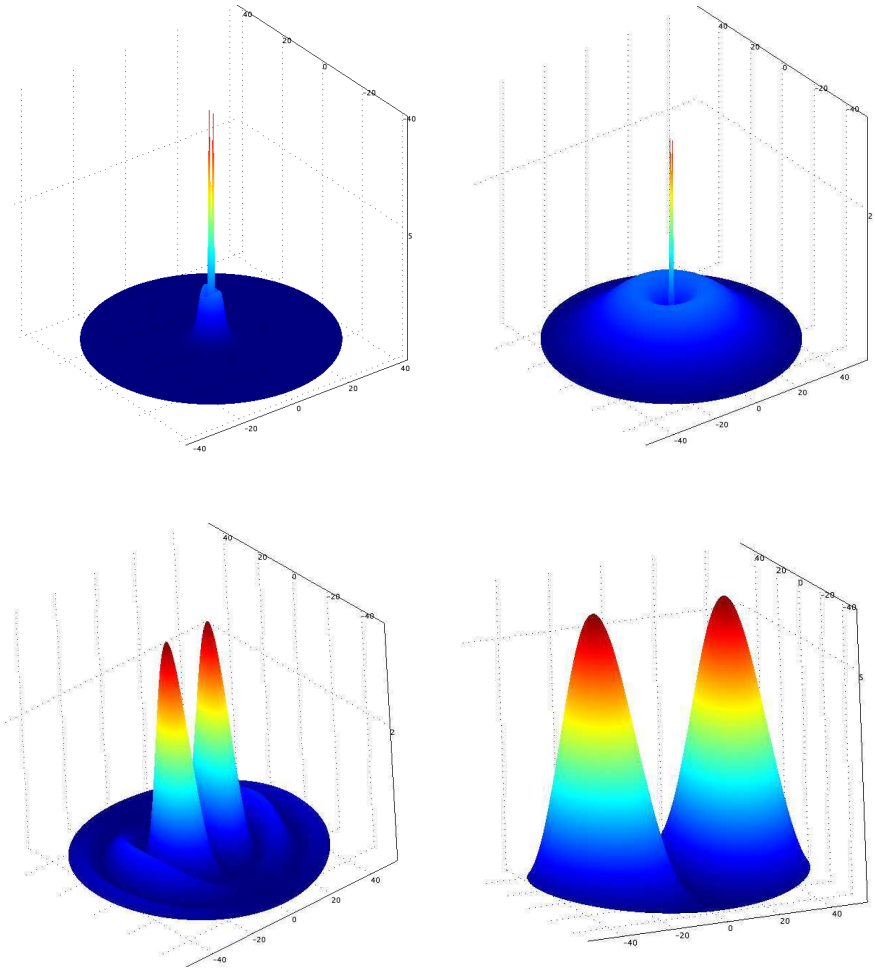

Figure 3.5: Individual probability of presence for some eigenmodes of the $H_2$ molecule

### Starting values of the unknowns

It has been proven that the Hartree-Fock system has a discrete spectrum of several eigenvalues and eigenfunctions [Lio87]. The Newton method used here provides only one solution. The algorithm does not guarantee that this solution is the ground state solution. Fonte *et al.* proved in [FMS73] the existence and the local uniqueness of a solution of the Hartree-Fock equations by the Newton iteration algorithm in some specific mathematical conditions which depend on the modes provided as initial guesses. We can check *a posteriori* that approximate wave functions are the ground-state solution by examining the number of nodes of the solutions *i.e.* the number of points where the wave function has minimal amplitude. If the approximate solution is not the ground state, it can be any eigenmode of the eigenmode spectrum. Figure 3.5 illustrates different eigenmodes of the $H_2$ molecule.

In the case of atoms or molecules with ionic bonds, we impose as initial guesses the ground state hydrogen-like atomic orbitals. We list them below using the spherical coordinate system and denoting $\mathrm{Z_{eff}}$ the effective nuclear charge that is the positive charge experienced by an electron taking into account the shielding effect due to the other electrons:

$$
\begin{aligned}
&\text{Mode 1s:} && \chi_{1s}(r) &&= \frac{1}{\sqrt{\pi}}\mathrm{Z}_{\mathrm{eff}}^{\frac{3}{2}}\exp\left(-\mathrm{Z}_{\mathrm{eff}}\, r\right),\\
&\text{Mode 2s:} && \chi_{2s}(r) &&= \frac{1}{2\sqrt{2\pi}}\mathrm{Z}_{\mathrm{eff}}^{\frac{3}{2}}\left(1-\frac{\mathrm{Z}_{\mathrm{eff}}\, r}{2}\right)\exp\left(-\frac{\mathrm{Z}_{\mathrm{eff}}\, r}{2}\right),\\
&\text{Mode 2p}_x\text{:} && \chi_{2p_x}(r,\theta,\varphi) &&= \frac{1}{4\sqrt{2\pi}}r\mathrm{Z}_{\mathrm{eff}}^{\frac{5}{2}}\exp\left(-\frac{\mathrm{Z}_{\mathrm{eff}}\, r}{2}\right)\sin\theta\cos\varphi,\\
&\text{Mode 2p}_y\text{ :} && \chi_{2p_y}(r,\theta,\varphi) &&= \frac{1}{4\sqrt{2\pi}}r\mathrm{Z}_{\mathrm{eff}}^{\frac{5}{2}}\exp\left(-\frac{\mathrm{Z}_{\mathrm{eff}}\, r}{2}\right)\sin\theta\sin\varphi,\\
&\text{Mode 2p}_z\text{:} && \chi_{2p_z}(r,\theta) &&= \frac{1}{4\sqrt{2\pi}}r\mathrm{Z}_{\mathrm{eff}}^{\frac{5}{2}}\exp\left(-\frac{\mathrm{Z}_{\mathrm{eff}}\, r}{2}\right)\cos\theta,\\
&\text{Mode 3s:} && \chi_{3s}(r) &&= \frac{1}{3\sqrt{3\pi}}\mathrm{Z}_{\mathrm{eff}}^{\frac{3}{2}}\left(1-\frac{2\mathrm{Z}_{\mathrm{eff}}\, r}{3}+\frac{2\mathrm{Z}_{\mathrm{eff}}^2\, r^2}{27}\right)\exp\left(-\frac{\mathrm{Z}_{\mathrm{eff}}\, r}{3}\right),\\
&\text{Mode 3p}_x\text{:} && \chi_{3p_x}(r,\theta,\varphi) &&= \frac{4}{27\sqrt{2\pi}}\mathrm{Z}_{\mathrm{eff}}^{\frac{3}{2}}\left(\mathrm{Z}_{\mathrm{eff}}\, r-\frac{\mathrm{Z}_{\mathrm{eff}}^2\, r^2}{6}\right)\exp\left(-\frac{\mathrm{Z}_{\mathrm{eff}}\, r}{3}\right)\sin\theta\cos\varphi,\\
&\text{Mode 3p}_y\text{:} && \chi_{3p_y}(r,\theta,\varphi) &&= \frac{4}{27\sqrt{2\pi}}\mathrm{Z}_{\mathrm{eff}}^{\frac{3}{2}}\left(\mathrm{Z}_{\mathrm{eff}}\, r-\frac{\mathrm{Z}_{\mathrm{eff}}^2\, r^2}{6}\right)\exp\left(-\frac{\mathrm{Z}_{\mathrm{eff}}\, r}{3}\right)\sin\theta\sin\varphi,\\
&\text{Mode 3p}_z\text{:} && \chi_{3p_z}(r,\theta) &&= \frac{4}{27\sqrt{2\pi}}\mathrm{Z}_{eff}^{\frac{3}{2}}\left(\mathrm{Z}_{\mathrm{eff}}\, r-\frac{\mathrm{Z}_{\mathrm{eff}}^2\, r^2}{6}\right)\exp\left(-\frac{\mathrm{Z}_{\mathrm{eff}}\, r}{3}\right)\cos\theta.
\end{aligned}
$$

For molecules with covalent bonds, we can apply a linear combination of hydrogen-like orbitals, but predicting this linear combination is cumbersome for complex systems. Therefore, initial values of the unknowns for molecules with covalent bonds are obtained as solutions of the linearized system. The non-linear part is introduced gradually increasing the coefficient $\alpha$ from 0 to 1 like in a continuation method and we get for each $\alpha$, $\{\Phi(\alpha), \Lambda(\alpha), G(\alpha)\}$ defined by:

$$\begin{cases} \left(+\frac{1}{2}\nabla\Phi, \nabla\delta\Phi\right) + \left(\left(V_{en} + \alpha\left(\mathrm{tr}\left(G\right) I - G\right)\right)\Phi, \delta\Phi\right) = \left(\Lambda\Phi, \delta\Phi\right), & \forall\delta\Phi \in \mathsf{W}^{\Phi}, \\ \mathrm{tr}\left[\nabla G.\nabla\delta G^{T}\right] = \mathrm{tr}\left[\left(4\pi\Phi\otimes\Phi^{*}\right).\delta G^{T}\right], & \forall\delta G \in \mathsf{W}^{G}, \\ \mathrm{tr}\left[\left(I - \int_{\mathbb{R}^3}\Phi\otimes\Phi^{*}\right).\delta\Lambda^{T}\right] = 0, & \forall\delta\Lambda \in \mathsf{W}^{\Lambda}. \end{cases} \tag{3.15}$$

The first computation is made with $\alpha = 0$. Then, the solution obtained is used as the initial values of the functions for a computation considering $\alpha = \delta\alpha$. Iteratively, solutions obtained when $\alpha = (n-1)\,\delta\alpha$ are used as initial values for computations with $\alpha = n\,\delta\alpha$ until $\alpha = 1$. Generally, we impose $\delta\alpha = 0.2$.

### 3.2.3 Artificial boundary conditions

The Hartree-Fock system is a set of equations defined on a three-dimensional unbounded space whereas the FEM is conventionally designed to work on bounded domains. Even if infinite elements [Ast00, Kum00], or generalized finite element method [NB76] can be possible strategies to solve such problems, we choose to apply the FEM on bounded domains with special boundary conditions.

For isolated systems, the FEM domain $\Omega$ is a sphere whose radius is $R$. To reduce parasite effects of the external boundaries, the spherical boundary of the domain is chosen to be far from the different nuclei. To limit the volume of computation to a sphere not too large, we introduce artificial boundary conditions [EM77].

Far from the nuclei, we approximate wave functions as spherical waves:

$$\varphi_i|_{r\to\infty} = \varphi_0 \exp^{ik_i r}. \tag{3.16}$$

Neglecting the effect of Coulombian potentials in this area, we establish from the Hartree-Fock system (2.24) that $k_i^2 = 2\Lambda_{ii}$. Therefore, in cases of materials at ground state (with negative electronic energies), the boundary conditions for the wave functions $\Phi$ are:

$$\left.\frac{\partial \varphi_i}{\partial r}\right|_{r\to\infty} = -\sqrt{-2\Lambda_{ii}}\varphi_i. \tag{3.17}$$

The interaction terms $G_{ij}$ are approximate solutions of Laplace's equations whose second terms involve themselves the wave functions $\varphi_i$ and $\varphi_j$. The radial approximation at the boundary is difficult to establish. We write it from the convolution form defined by eq.(2.16):

$$\left.\frac{\partial G_{ij}}{\partial r}\right|_{r\to\infty} = \left(-\sqrt{-2\Lambda_{ii}} - \sqrt{-2\Lambda_{jj}}\right) G_{ij}. \tag{3.18}$$

External boundary conditions imply some parasite effects, especially when the size of the FEM domain gets smaller. In Table 3.2, we compare the energy estimates for the Helium atom applying aforesaid conditions and Dirichlet conditions that impose approximate wave functions to vanish on the spherical boundary. In the case of the Helium atom, we conclude that a radius greater than 20 $a_0$ is large enough to cancel the effect of the type of boundary conditions. However, the boundary can have an effect due to the estimation of the energy defined by the integral on a bounded domain of Equation (2.23), whereas the quantum problem is defined on an unbounded domain.

| Radius of the domain ($a_0$) | Order of magnitude of the difference in estimates of electronic energy between radiative and Dirichlet conditions (Ha) |
|---|---|
| 5 | $10^{-4}$ |
| 10 | $10^{-9}$ |
| 15 | $10^{-15}$ |
| $\geq 20$ | $< 10^{-15}$ |

Table 3.2: Influence of the boundary conditions on the estimation of the energy of the Helium atom for different radii of the FEM domain

### 3.2.4 Mesh and adaptivity

We use tetrahedrons to partition the three-dimensional FEM domain. For axisymetrical modes as explained below, triangular elements mesh the FEM domain. With real-space methods, localized refinement seems appealing to optimize the number of degrees of freedom, and perform large scale *ab initio* calculations. As wave functions present a singularity near the nuclei, we impose an initial mesh refined in these critical zones. Another approach would be to use generalized finite element method [NB76].

Adaptive coordinate transformations [TT96, TT98] or self-adaptive meshing [AR93] allow to locally refine the estimation of the wave functions. To improve the quality of the numerical solution, we employ a mesh adaptivity method and ensure that a minimum number of degrees of freedom $\texttt{dof}^{obj}$ is used to estimate any function. The mesh is optimized with respect to the local error.

Adaptivity can be set up for different quantities of interest and different norms. We use the $\mathcal{L}_2$ norm. The mesh and so the results depend on the quantity considered to refine the mesh.

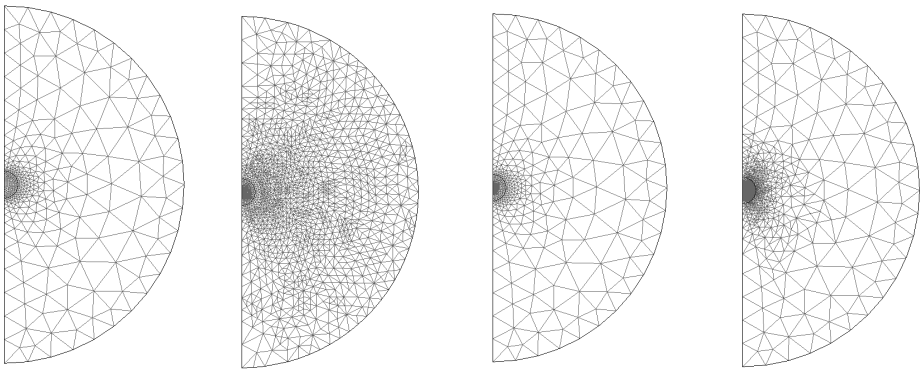

| (a) Initial mesh | (b) Adaptivity on all the unknowns | (c) Adaptivity on the 2s mode | (d) Adaptivity on the $2p_z$ mode |
|---|---|---|---|
| 19 453 dof | 109 081 dof | 150 017 dof | 131 621 dof |

Figure 3.6: Meshes of adaptive computations for the Neon atom on a FEM domain of radius 40 $a_0$: Initial mesh (a) and different meshes obtained after two adaptive iterations (b,c,d)

Figure 3.6 presents different meshes obtained after two iterative steps for different quantities

of interest. Considering all unknowns, new nodes are evenly added into the FEM domain. Considering a localized wave function such as the 2s mode, the new nodes are localized in a small area near the nucleus. For a less localized wave function such as the $2p_z$ mode, nodes are added in a larger area around the nucleus. Considering the error on the interaction terms $G_{ij}$, the mesh is refined far from the nucleus.

As the error estimator is not unique, the choice of an accurate estimator is crucial. Chapter 5 focuses on this topic. For the first calculations presented here, error is estimated with respect to all unknowns using the Euclidian norm based on the local residual.

### 3.2.5 Symmetry simplifications for atoms and linear molecules

In the case of atoms and linear molecules *i.e.* molecules in which all bond angles are 180 degrees, all one-electron wave functions can be broken up into two independent functions: in-plane functions $\varphi_i^{rz}$ depending on the two dimensions $r$ and $z$, and axial functions $\varphi_i^{\theta}$ depending only on the angle $\theta$ [Bre30]:

$$\varphi_i(r,\theta,z) = \varphi_i^{\theta}(\theta)\varphi_i^{rz}(r,z). \tag{3.19}$$

In these cases, axial functions $\varphi_i^{\theta}$ are spherical harmonics that depend on the magnetic quantum number $m_i$ (defined in Appendix E) of the wave function considered:

$$\varphi_i^{\theta}(\theta) = e^{im_i\theta}. \tag{3.20}$$

For more general cases, a spherical harmonics development would be possible. The "building-up" principle, also called the Aufbau principle, allows for the knowledge *a priori* of the second quantum number $m_i$ of each one-electron wave function, and so the electron configuration of the different atoms (Appendix D).

The FEM domain can be reduced to a two-dimensional one, a half-disk whose radius is denoted $R$: $\Omega = \{(r,z),\, r \geq 0,\, \sqrt{r^2+z^2} \leqslant R\}$. In some peculiar cases, due to the symmetry of the wave functions, we could use only a quarter of a disk.

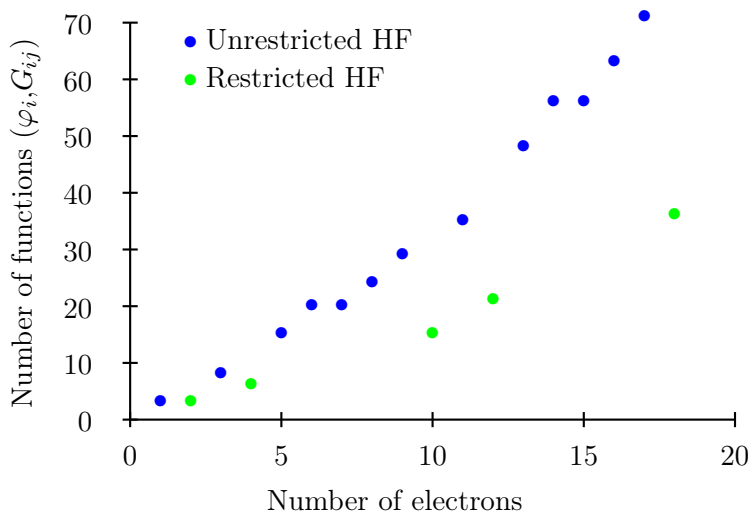


Figure 3.7: Number of degrees of freedom by node in two-dimensional computations depending on the number of electrons for atomic systems in RHF or UHF conditions

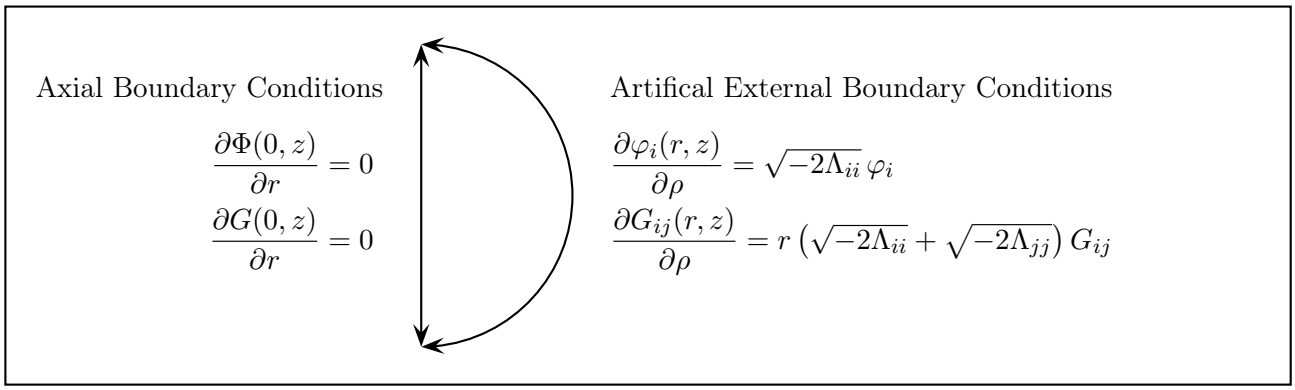


Figure 3.8: Boundary conditions considered on the 2D FEM domain

In the two-dimensional space $(r, z)$, find $(\varphi_i^{rz}, \Lambda_{ij})$ such that:

$$\begin{aligned}
&\left(\sum_{j=1}^{N_e} e^{i(m_j-m_i)\theta}\Lambda_{ij}\varphi_j^{rz}, \delta\varphi_i^{rz}\right) = -\frac{1}{2}\left[(\nabla_{rz}\varphi_i^{rz}, \nabla_{rz}\delta\varphi_i^{rz}) - \left(\frac{m_i^2}{r^2}\varphi_i^{rz}, \delta\varphi_i^{rz}\right)\right] \\
&\qquad\qquad + \left(\left(V_{en} + \operatorname{tr} G^{rz} - \sum_{j=1}^{N_e} G_{ji}^{rz}\right)\varphi_i^{rz}, \delta\varphi_i^{rz}\right), \\
&\operatorname{tr}\left(\nabla_{rz}G_{ij}^{rz}.\nabla_{rz}\delta G_{ij}^{rz}\right) - \frac{(m_i-m_j)^2}{r^2}\left(G_{ij}^{rz}, \delta G_{ij}^{rz}\right) = \operatorname{tr}\left(\left(4\pi\varphi_i^{rz}\otimes\varphi_j^{rz^*}\right).\delta G_{ij}^{rz^T}\right), \\
&\operatorname{tr}\left(\left(I_{ij} - e^{i(m_i-m_j)}\int_{\mathbb{R}^3}\varphi_i^{rz}\otimes\varphi_j^{rz^*}\right).\delta\Lambda_{ij}^T\right) = 0, \\
&\qquad\qquad \forall\delta\varphi_i \in \mathsf{W}^{\varphi},\ \forall\delta G_{ij} \in \mathsf{W}^{G_{ij}},\ \forall\delta\Lambda_{ij} \in \mathsf{W}^{\Lambda_{ij}}.
\end{aligned} \tag{3.21}$$

The derivation of the weak formulation in two-dimensional space is detailed in Appendix H. We have calculated systems for which the second quantum number is equal to -1, 0 or 1. These three values of the second quantum number match three degenerate eigenmodes. The equations are identical for the values $+m$ or $-m$ of the second quantum number. We choose to calculate only the eigenmodes for the non-negative values of $m_i$. This strategy leads to a decrease of the number of functions to be computed and to get rid of degeneracy between the three modes. Figure 3.7 shows how the number of unknowns is reduced considering only the positive values of $m_i$.

For instance, to compute the fundamental state of argon, the number of functions to be evaluated is reduced from 46 to 35. Figure 3.9 shows how the three-dimensional solutions are built once the two-dimensional modes have been computed.

For the axial boundary ($r = 0$), supposing $\varphi_i = e^{im_i\theta}\varphi_i^{rz}(r, z)$, the boundary conditions depend on the parity of $m_i$ for the one-electron wave function $\varphi_i$:

$$\begin{cases} \exists k \in \mathbb{N} \quad m_i = 2k & \dfrac{\partial\varphi_i(0,z)}{\partial r} = 0, \\ \exists k \in \mathbb{N} \quad m_i = 2k+1 & \varphi_i(0,z) = 0. \end{cases} \tag{3.22}$$

and for the components $G_{ij}$ of the matrix $G$:

$$\begin{cases} \exists\{k, k'\} \in \mathbb{N}^2,\ m_i = 2k \quad \text{and} \quad m_j = 2k', & \dfrac{\partial G_{ij}(0,z)}{\partial r} = 0, \\ \qquad\qquad \text{else}, & G_{ij}(0,z) = 0. \end{cases} \tag{3.23}$$

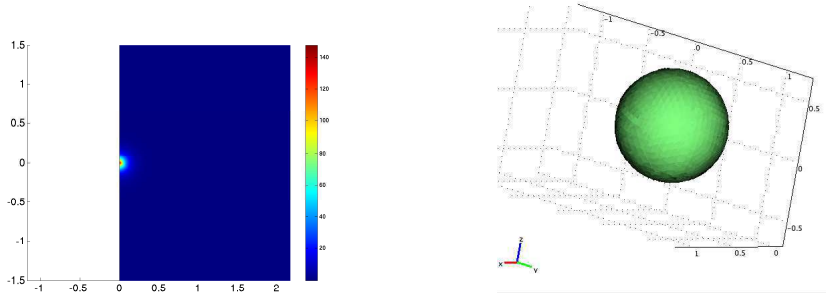

2D 1st and 2nd modes $\Longrightarrow$ 3D 1st and 2nd modes ($|\varphi_1|^2 = 0.13$)

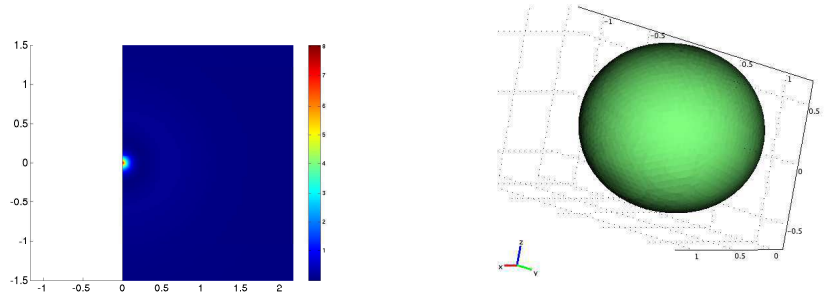

2D 3rd and 4th modes $\Longrightarrow$ 3D 3rd and 4th modes ($|\varphi_3|^2 = 0.13$)

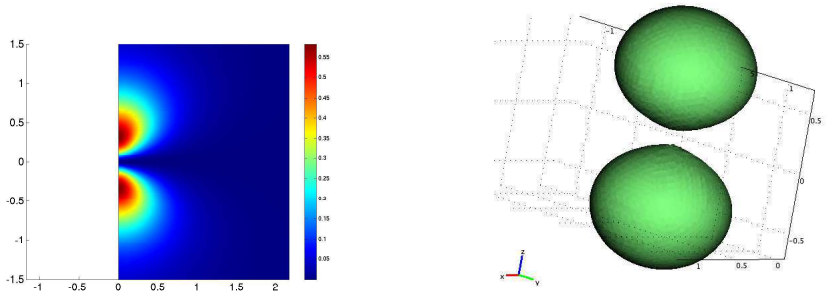

2D 5th and 6th modes $\Longrightarrow$ 3D 5th and 6th modes ($|\varphi_5|^2 = 0.13$)

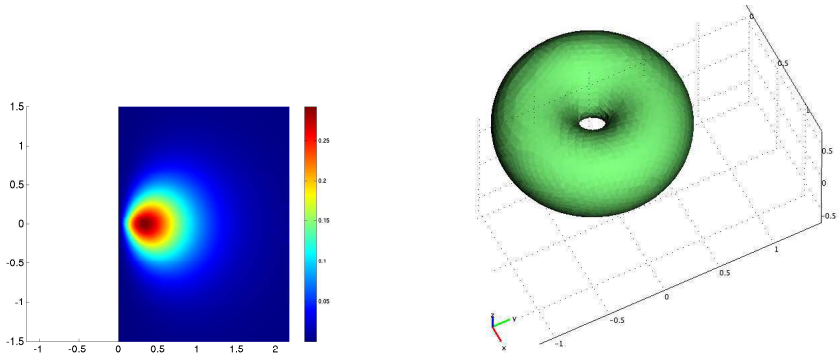

2D 7th and 8th modes $\Longrightarrow$ 3D 7th and 8th modes ($|\varphi_7|^2 = 0.13$)

Figure 3.9: Probability of presence of the different modes of the Oxygen atom in two-dimensional $(r, z)$ and three-dimensional $(r, \theta, z)$ spaces

For the circular external boundary ($\rho = R$), as developed for three-dimensional cases, we use a plane wave approximation far from the nuclei and we subject the one-electron wave functions $\varphi_i$ to the following boundary condition:

$$\frac{\partial \varphi_i(r,z)}{\partial \rho} = \sqrt{-2\Lambda_{ii}}\,\varphi_i, \tag{3.24}$$

and the components $G_{ij}$ of the matrix $G$, solution of Laplace's equations, to:

$$\frac{\partial G_{ij}(r,z)}{\partial \rho} = r\left(\sqrt{\frac{m_i^2}{r^2} - 2\Lambda_{ii}} + \sqrt{\frac{m_j^2}{r^2} - 2\Lambda_{jj}}\right) G_{ij}. \tag{3.25}$$

Figure 3.8 illustrates the boundary conditions for the vectors $\Phi$ and $G$ in the particular case of all the wave functions have a second quantum number which equals 0.

## 3.3 Summary

In this chapter, the finite element method strategy used to solve the Hartree-Fock system is presented. This numerical method combines the advantages of both basis-oriented and real-space-grid approaches. We choose as the iterative method the Newton method and evaluate residuals at each step. The calculation is stopped when convergence on a quantity of interest (such as the total energy, or the wave function itself...) is obtained.

Difficulties in solving the Hartree-Fock system lie in the number of degrees of freedom, the singularities of the wave functions and the different eigenfunctions which can be solution of the system. To overcome difficulties due to the number of degrees of freedom, the algorithm integrates a staggered solver and mesh adaptivity. Initial guesses are hydrogen orbitals or the solutions of the linearized problem. But, the algorithm does not guarantee to provide a global optimizer. The number of nodes of the solution wave functions is checked *a posteriori* for being equal to the number of nodes of the expected modes.

This chapter has introduced the numerical strategy for the Hartree-Fock problem. The same approach is used to compute the virtual modes and estimate the CI energy. The CI model is used to increase the accuracy of the estimation and needs a large FEM domain, and a large number of degrees of freedom to be pertinent. But, with a large radius of the FEM domain, it is difficult to obtain convergence of the virtual modes.

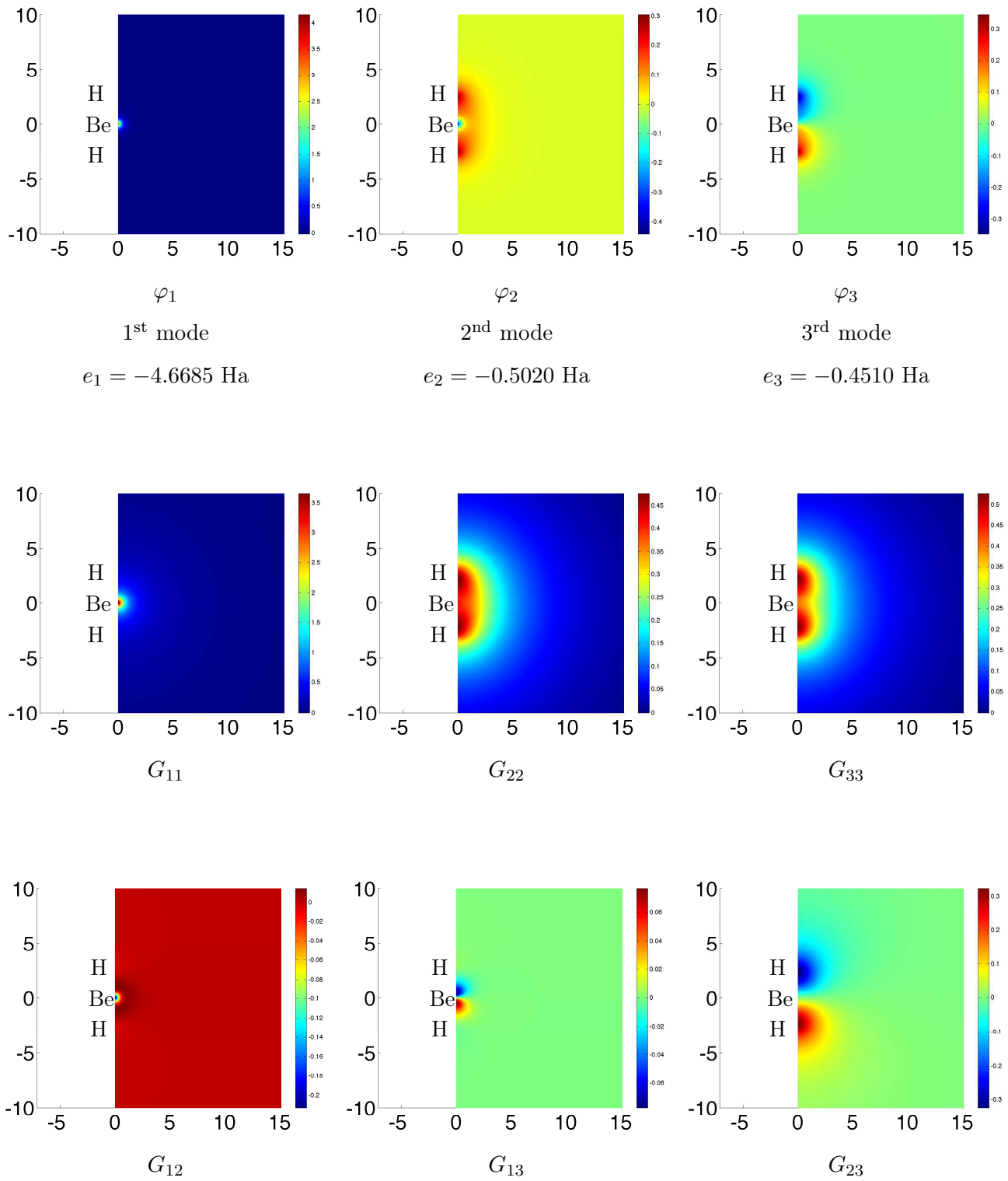


Figure 3.10: Fields computed for the Hartree-Fock modelization of the ground state of the $BeH_2$ molecule

Figure 3.10 shows the different two-dimensional fields computed to characterize the $BeH_2$ molecule (composed of three atoms and six electrons): three one-electron wavefunctions $\varphi_1$, $\varphi_2$, $\varphi_3$ and six interaction terms $G_{11}$, $G_{22}$, $G_{33}$, $G_{12}$, $G_{13}$ and $G_{23}$.

## 3.4 Large scale perspectives

The Hartree-Fock or post-Hartree-Fock problems are generalized eigenvalues problems. These problems have cubic complexity, which is the bottleneck in dealing with many electron systems. Different strategies have been developed to overcome this difficulty [CA08].

To circumvent the curse of dimensionality, a reduced basis approximation method is suggested by Maday and Razafison [MR08]. They consider a space of approximation smaller than the usual Hartree-Fock space, it is spanned by a small number of well chosen solutions. Other authors propose a separated representation strategy [AMCK06a, AMCK06b, AC08] or Proper Generalized Decomposition [Nou10]. This strategy can be seen as elaborate derivative of the decomposition on atomic orbitals basis.

By a modal analysis, a first strategy consists in computing only the significant modes. Only the modes that can participate in the formation of chemical bonds are involved in material properties, they are called valence modes [vBG80]. Modes that are not perturbed by the surrounding atoms such as the first mode of the Beryllium atom (Figure 3.11) are called core modes. An idea to reduce the complexity of the calculation is to compute only the valence modes. Core electrons are included into nuclear potentials through pseudopotentials or core effective potentials [Pic89]. These potentials are established by preliminary computations on isolated atoms. Technical aspects of this method are explained in [PTA+92].

Solutions of electronic problems are generally localized and pertinent information is only given by the valence modes outside the regions surrounding nuclei [YC82]. To take advantage of this property, Slater proposed in 1937 a localized model refinement called the muffin-tin approximation to treat periodic materials [Sla37]. Potentials between nuclei and electrons were supposed to

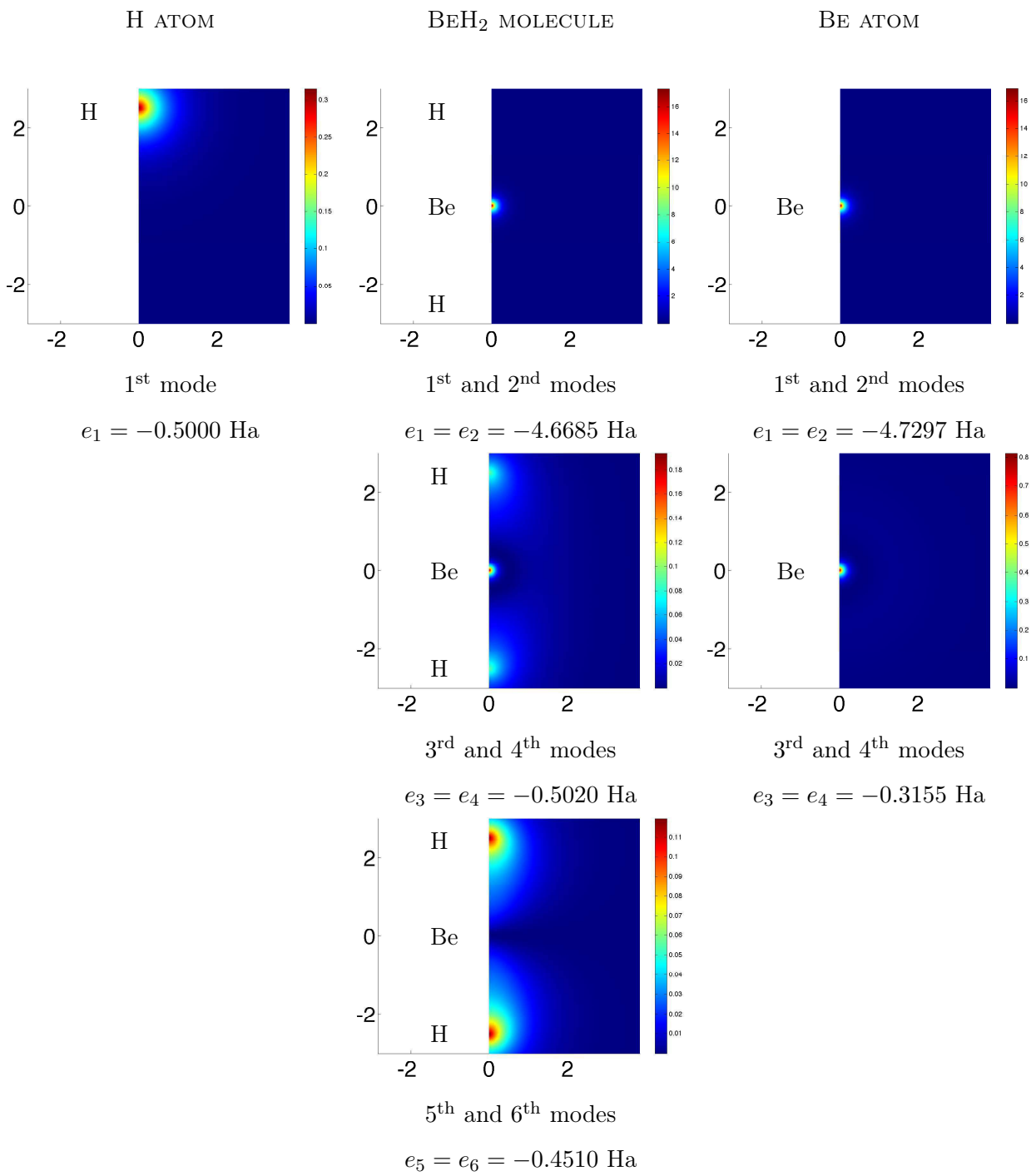


Figure 3.11: Core and valence modes: core modes are not very perturbed by the surrounding atoms such as the first mode of the Be atom (individual probabilities of presence for the one-electron modes of the Be atom, the H atom and the $BeH_2$ molecule)

be spherically symmetrical within spheres surrounding the atoms, and constant outside. Wave functions were expanded in spherical harmonics and radial solutions of the wave equations within the spheres, and in plane waves outside the spheres, joining continuously at the surface.

Recently, Barrault [Bar05, BCHLB07] applied a technique of domain decomposition and turned the unique problem into several localized minimization problems under constraint. He showed a localized convergence of the algorithm, scalability up to 1000 processors in 1D and possible extension to 2D/3D domains. The domain decomposition method provides linear complexity with respect to the number of electrons in the system.

# Chapter 4

# *Ab initio* quantities of interest

This chapter is devoted to the numerical results obtained by the Hartree-Fock method described in Chapter 2 and the numerical strategy detailed in Chapter 3. First, we focus on the individual electronic wave functions that completely describe any atomic system. Then, we exploit them to provide other physical information: mechanical quantities such as bonding forces, bond stiffness, or electric properties such as dipolar moment and polarizability tensor.

## 4.1 The one-electron wave functions

Quantum mechanical computations provide the wave function of the system. In the case of the Hartree-Fock model, we compute the one-electron wave functions. In two-dimensional computations, each one-electron wave function is described by its field in the plane $(r, z)$ and its magnetic quantum number.

We only examine the one-electron wave functions of the ground state.

### 4.1.1 Geometrical distribution of the individual wave functions

Figure 4.1 and Figure 4.2 represent, respectively, the probability of presence of the one-electron wave functions of the Beryllium and the Oxygen atoms. In both cases, the nucleus of the atom is located in $(0; 0)$. We note that all individual wave functions are localized in an area near the nucleus. The probability of presence decreases rapidly to almost vanish far from the nucleus. To

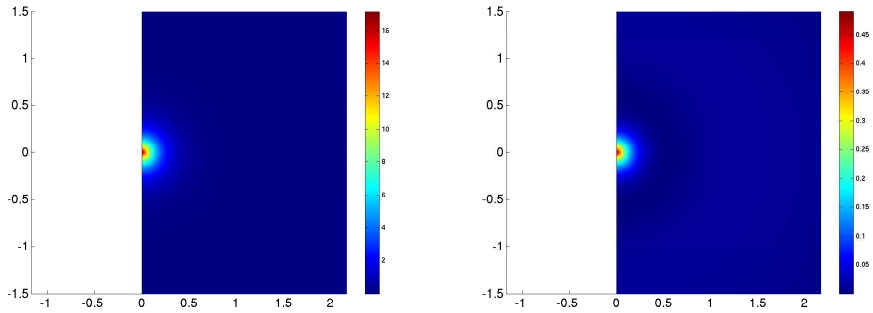


$1^{\text{st}}$ and $2^{\text{nd}}$ modes ($m_1$=$m_2$=0)

$e_1 = e_2 = -4.7297$ Ha

$R_{99,1} = R_{99,2} = 1.11\, a_0$

$3^{\text{rd}}$ and $4^{\text{th}}$ modes ($m_3$=$m_4$=0)

$e_3 = e_4 = -0.3155$ Ha

$R_{99,3} = R_{99,4} = 5.53\, a_0$

Figure 4.1: Individual probability of presence for the ground-state modes of the Beryllium atom (HF model)

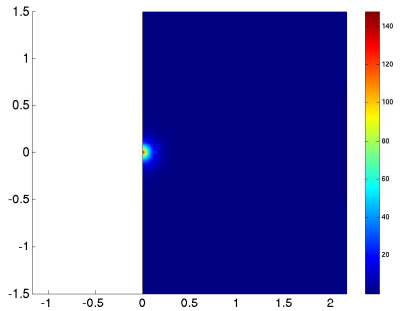

$1^{\text{st}}$ and $2^{\text{nd}}$ modes ($m_1$=$m_2$=0)

$e_1 = -20.7343$ Ha

$e_2 = -20.6594$ Ha

$R_{99,1} = R_{99,2} = 0.4959\, a_0$

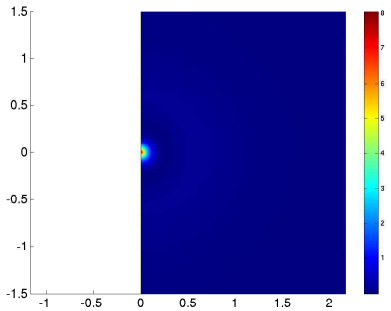

$3^{\text{rd}}$ and $4^{\text{th}}$ modes ($m_3$=$m_4$=0)

$e_3 = -1.4293$ Ha

$e_4 = -1.0939$ Ha

$R_{99,3} = 2.3880\, a_0$

$R_{99,4} = 2.4796\, a_0$

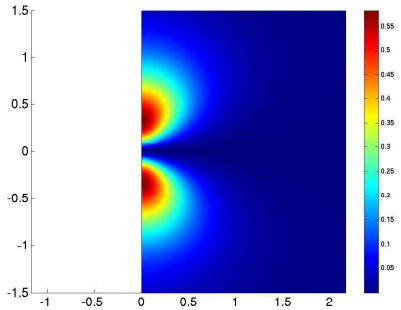

$5^{\text{th}}$ and $6^{\text{th}}$ modes ($m_5$=$m_6$=0)

$e_5 = -0.6265$ Ha

$e_6 = -0.5389$ Ha

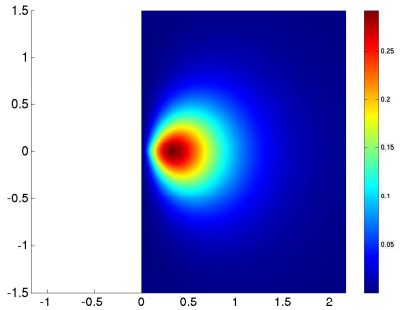

$7^{\text{th}}$ ($m_7$=1) and $8^{\text{th}}$ ($m_8$=−1) modes

$e_7 = e_8 = -0.6335$ Ha

Figure 4.2: Individual probability of presence for the different modes of the Oxygen atom (HF model)

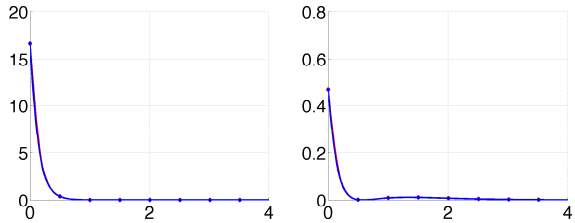


$e_1 = -4.7297$ Ha $\quad$ $e_2 = -0.3155$ Ha

$m_1 = 0$ $\quad$ $m_2 = 0$

Be atom

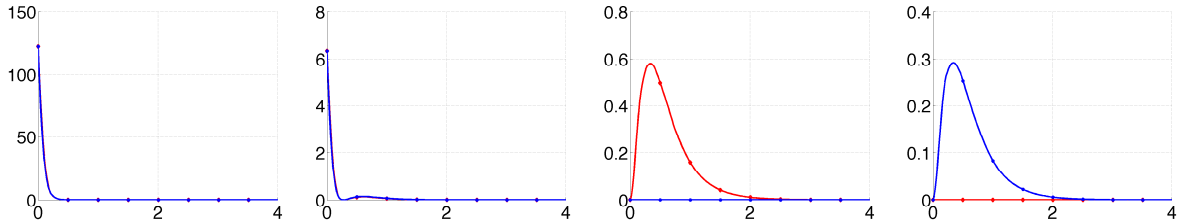


$e_1 = -20.7343$ Ha $\quad$ $e_3 = -1.4293$ Ha $\quad$ $e_5 = -0.6265$ Ha $\quad$ $e_7 = e_8 = -0.6335$ Ha

$e_2 = -20.6594$ Ha $\quad$ $e_4 = -1.0939$ Ha $\quad$ $e_6 = -0.5389$ Ha

$m_1 = 0$ $\quad$ $m_2 = 0$ $\quad$ $m_3 = 0$ $\quad$ $m_4 = 1$

O atom

Figure 4.3: Profiles of the one-electron wave functions in the $r$ direction (in blue) and in the $z$ direction (in red) for the Beryllium atom and the Oxygen atom (HF model)

characterize the extent of the modes, we define a distance $R_{99}$ as the radius of a sphere in which the probability of presence of all the electrons is 99%.

The Beryllium atom comprises four electrons whereas the Oxygen atom contains eight electrons. We can see that when the number of electrons in the atom increases, the new occupied modes are more diffused far from the nucleus.

Comparing the different modes of a same atom in Figure 4.3, we observe that the more diffused modes are those with the highest eigenvalues. The number of nodes, zeros of the wave functions, increases with the frequency of the stationary system and so with the energy of the modes.

Among all the stable natural elements, we focus our study on the isolated atoms of the elements between the hydrogen and calcium atoms in the periodic table because these elements are preponderant in the chemical makeup of traditional materials. Results are introduced in Table 4.1. For instance, let us examine the estimation for the Helium atom. The energy of the Helium atom is estimated to be $-2.86412$ Ha which is far from the experimental estimation $-2.901$ Ha [DHC91] considered as "exact" estimation. The configuration interaction approximation improves the estimation to $-2.86413$ Ha using 10 determinants. Comparing with other numerical solutions of the Hartree-Fock problem ($-2.8552$ Ha [JGP93] and $-2.8612$ Ha [Kob12]), we can see that our result is in concordance with the literature data. A better accuracy would need a refined model considering dynamic and relativistic effects. For other atoms, the comparison is similar. For instance, [JGP93] provides for the Lithium atom the HF total energy 7.4314 Ha whereas our estimation is 7.4351 Ha (experimental estimation: 7.47821 Ha [DHC91]).

Beyond isolated atoms, we investigate the one-electron wave functions of systems in which different nuclei are linked to form an isolated molecule.

### 4.1.2 Individual wave functions in bonds

In the case of molecules, the one-electron wave functions allow for an understanding of the bonding state of the molecule and how the different electrons are involved in the bond. In

| **Atom** | **Z** | $1^{st}$ mode | $2^{nd}$ mode | $3^{rd}$ mode | $4^{th}$ mode | $5^{th}$ mode | $6^{th}$ mode |
|---|---|---|---|---|---|---|---|
| **H** | 1 | -0.5000 | | | | | |
| **He** | 2 | -0.9185 | | | | | |
| **Li** | 3 | -2.4786 | -0.1983 | | | | |
| **Be** | 4 | -4.7297 | -0.3155 | | | | |
| **B** | 5 | -7.69275 | -0.5033 | -0.3208 | | | |
| **C** | 6 | -11.3263 | -0.7077 | -0.4389 | | | |
| **N** | 7 | -15.6539 | -0.9595 | -0.5477 | | | |
| **O** | 8 | -20.6969 | -1.2616 | -0.5996 | | | |
| **F** | 9 | -26.32485 | -1.5571 | -0.746125 | | | |
| **Ne** | 10 | -32.8242 | -1.9622 | -0.8082 | | | |
| **Na** | 11 | -40.3591 | -2.7646 | -1.6000 | -0.1868 | | |
| **Mg** | 12 | -49.4694 | -4.1683 | -2.6193 | -0.1263 | | |
| **Al** | 13 | -58.3814 | -4.8939 | -3.3419 | -0.4027 | -0.2379 | |
| **Ar** | 18 | -118.6267 | -12.3322 | -9.4544 | -1.2929 | -0.5867 | |
| **Ca** | 20 | -152.941 | -17.0782 | -13.4365 | -2.2930 | -1.3202 | -0.2127 |

Table 4.1: Estimation of the electronic energy for ground-state one-electron modes for isolated atoms (in hartree) considering $R = 2\,000\,a_0$ and 200 000 dof by function

Figures 4.4, 4.5, 4.6 and 4.7, we represent respectively the one-electron wave functions of the LiH, HF, $C_2$ and $BeH_2$ molecules, and of the isolated atoms that compose them.

Some one-electron wave functions in the molecules have a very similar shape and energy to those of the isolated atoms. The electrons associated with those wave functions are core electrons of the atoms which are very stable and little disturbed by their surroundings. On the other hand, some modes in the molecule have been largely disturbed when compared with those of isolated atoms. The electrons associated with those modes are the valence electrons; they create the bond between the atoms to form the molecule. The way the valence electrons behave to form the bond characterizes the material. For prevailing covalent character of the bond, the one-electron wave functions are "shared" between atoms (for instance in $C_2$, $BeH_2$ or $O_2$ molecules). If some one-electron wave functions initially centered around one nucleus are delocalized around another nucleus, the bond is considered as ionic such as in the HCl, NaH or HF molecules.

Studying the one-electron wave functions is cumbersome due to the number of fields to be examined, and assessment of the results is strenuous. To overcome these problems, we can focus on the global electronic density of the system.

## 4.2 The electronic density

The electron density defined by equation (1.40) provides a unique field to analyze and understand the bonding state of the system. Its approximation by the Hartree-Fock model reads:

$$\rho_{HF}(x) = |\Phi|^2. \tag{4.1}$$

Using the CI model (see Chapter 2), it is evaluated by:

$$\rho_{CI}(x) = \sum_{k=1}^{N_d} |\alpha_k|^2 |\Phi^k|^2 + \sum_{K=1}^{N_d} \sum_{\substack{L=1 \\ L\neq K}}^{N_d} \alpha_K \alpha_L^* \delta_{\varphi_1^K \varphi_1^L} \dots \varphi_a^K \varphi_a^{L^*} \dots \delta_{\varphi_{N_e}^K \varphi_{N_e}^L}. \tag{4.2}$$

where $\delta_{\varphi_i^K \varphi_i^L} = 1$ if $\varphi_i^K = \varphi_i^L$ and $\delta_{\varphi_j^K \varphi_i^L} = 0$ if $\varphi_i^K \neq \varphi_i^L$. Figure 4.9 illustrates these electronic densities, and so the bonding character, in the $H_2$, LiH, $BeH_2$, HF, NaH, HCl, and $C_2$ molecules. It can be compared with experimental results obtained by analyzing diffraction results. New techniques are developped to measure directly the wave functions [LSP+11]. We present here only results for isolated systems, for which we cannot provide diffraction results.

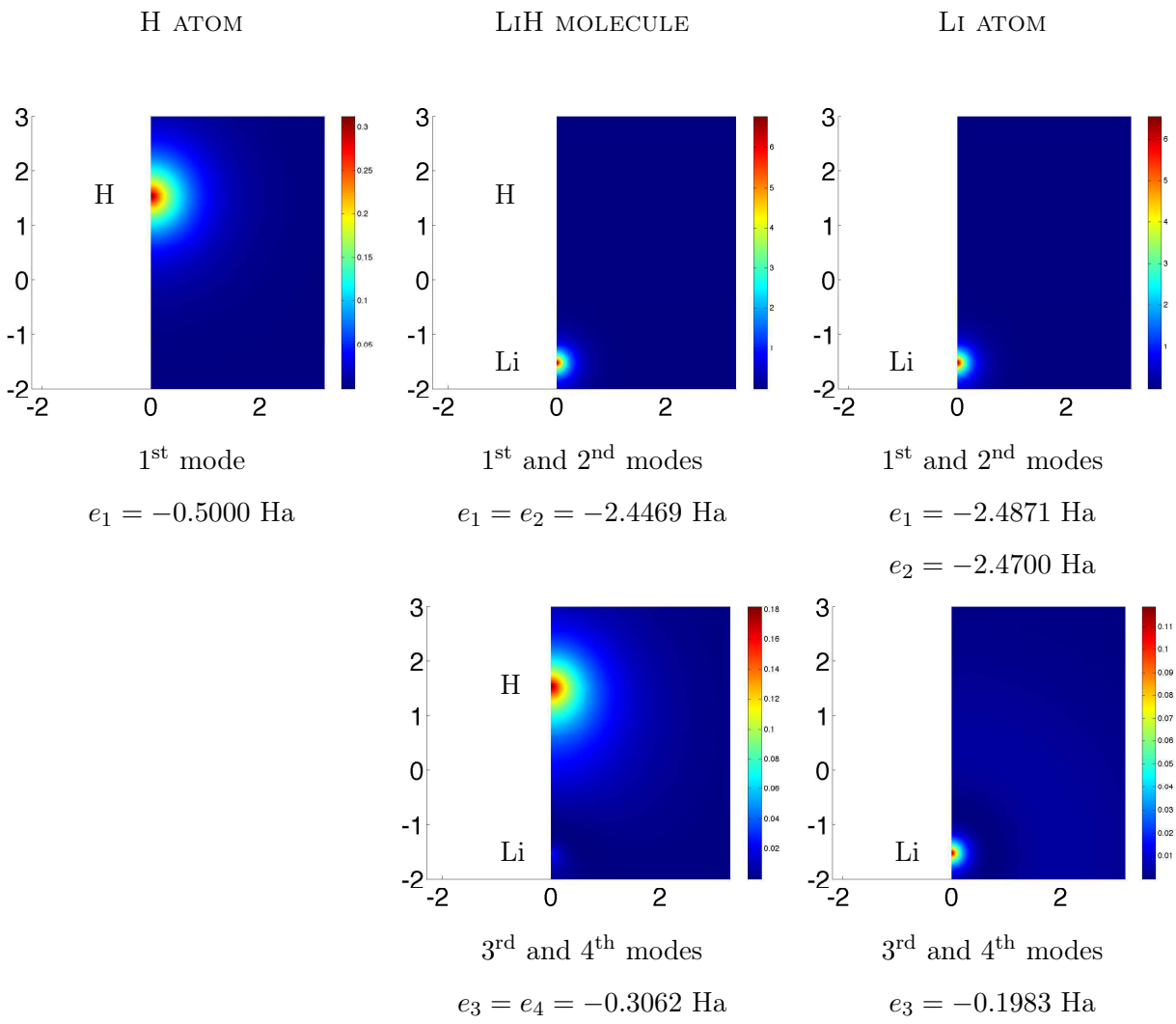


Figure 4.4: Individual probability of presence for the different modes of the H atom, the Li atom and the LiH molecule (HF model)

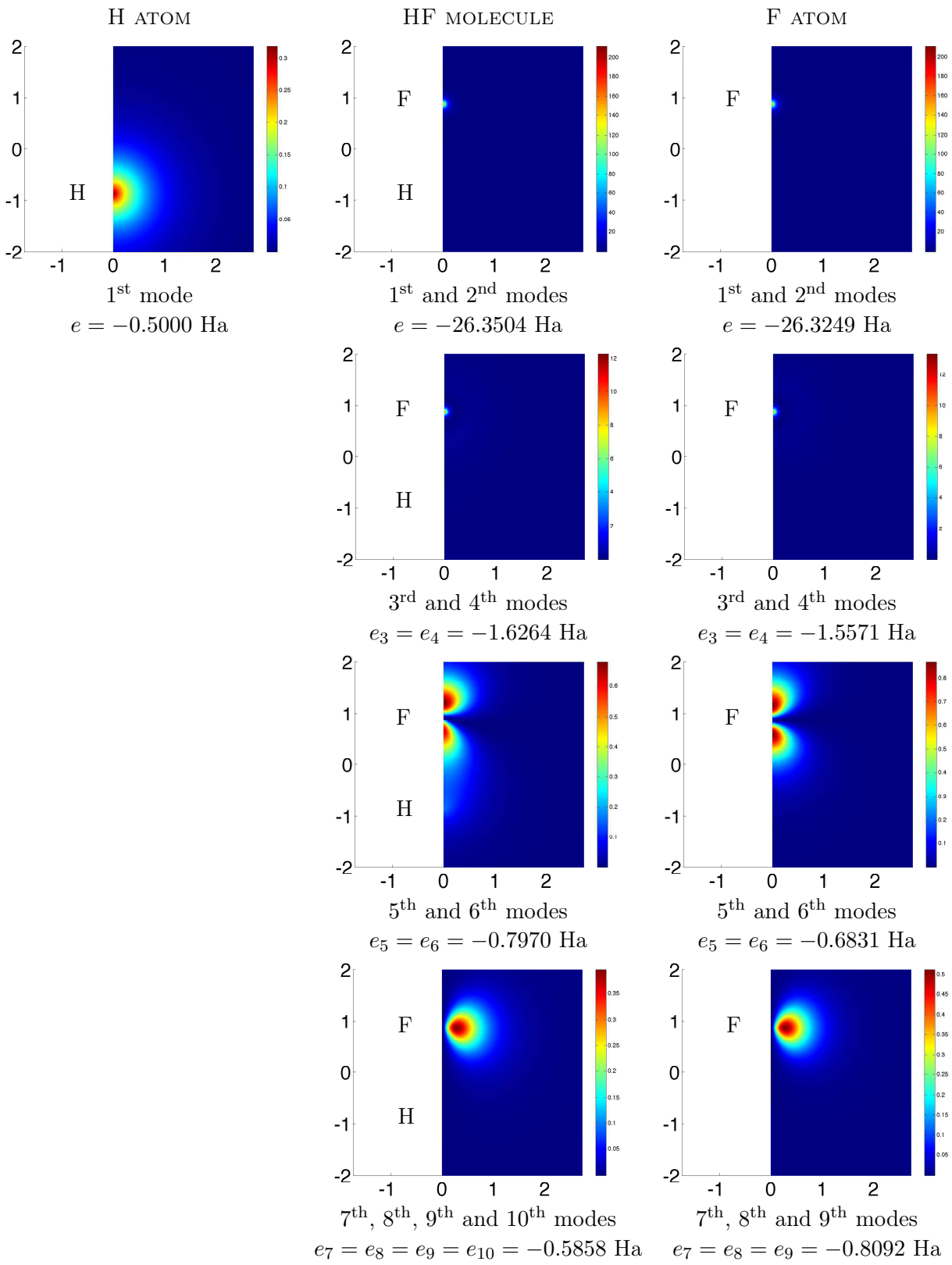


Figure 4.5: One-electron probability of presence of the H atom, the F atom and the HF molecule (HF model)

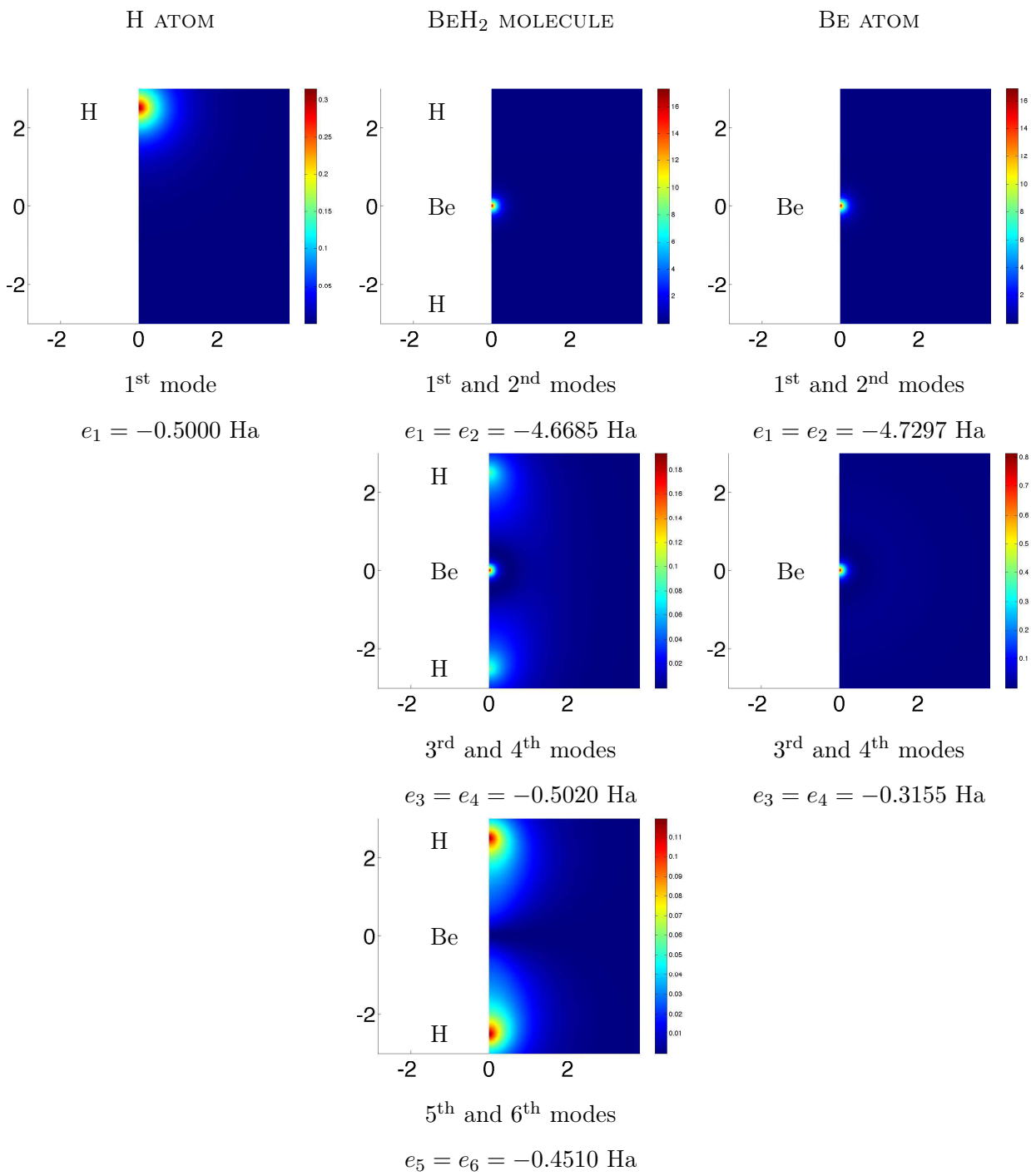


Figure 4.6: Covalent bond: individual probability of presence for the modes of the Be atom, the H atom and the $BeH_2$ molecule (HF model)

C ATOM

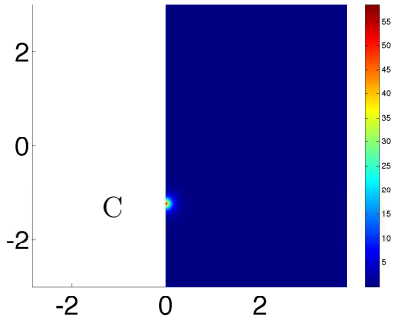


$1^{st}$ and $2^{nd}$ modes

$e_1 = -11.3487$ Ha

$e_2 = -11.3038$ Ha

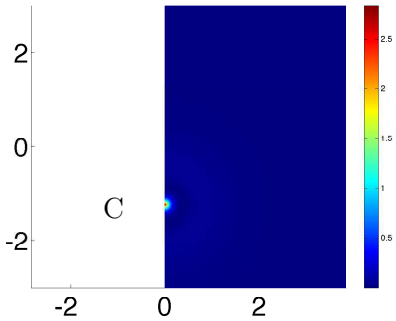


$3^{rd}$ and $4^{th}$ modes

$e_3 = -0.8303$ Ha

$e_4 = -0.5851$ Ha

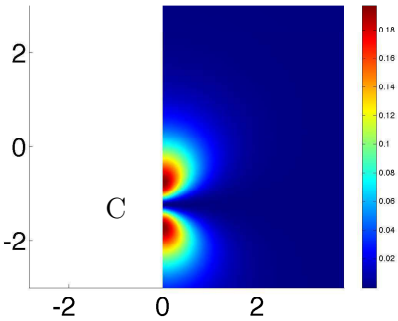


$5^{th}$ mode

$e_5 = -0.4420$ Ha

$C_2$ MOLECULE

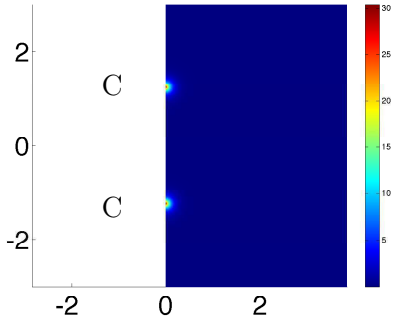


$1^{st}$ and $2^{nd}$ modes

$e_1 = e_2 = -11.3653$ Ha

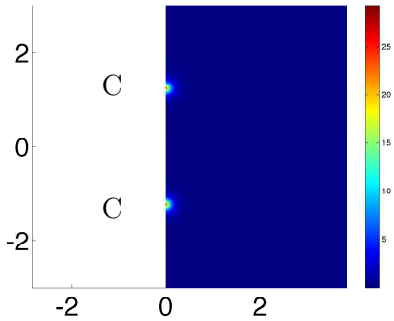


$3^{rd}$ and $4^{th}$ modes

$e_3 = e_4 = -11.3287$ Ha

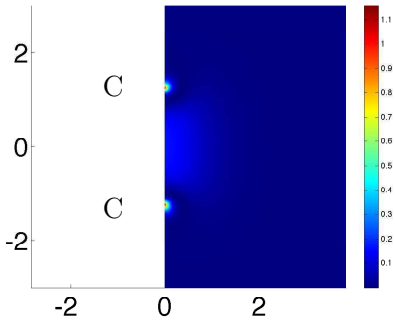


$5^{th}$ and $6^{th}$ modes

$e_5 = e_6 = -0.9321$ Ha

C ATOM

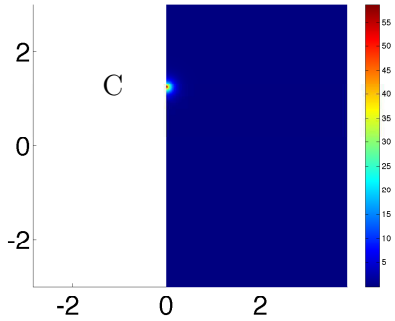


$1^{st}$ and $2^{nd}$ modes

$e_1 = -11.3487$ Ha

$e_2 = -11.3038$ Ha

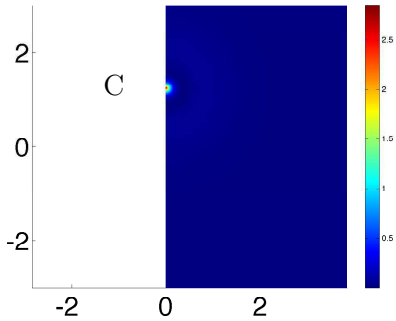


$3^{rd}$ and $4^{th}$ modes

$e_3 = -0.8303$ Ha

$e_4 = -0.5851$ Ha

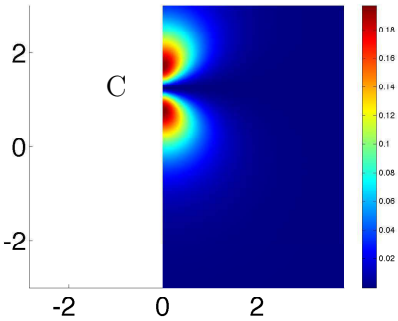


$5^{th}$ mode

$e_5 = -0.4420$ Ha

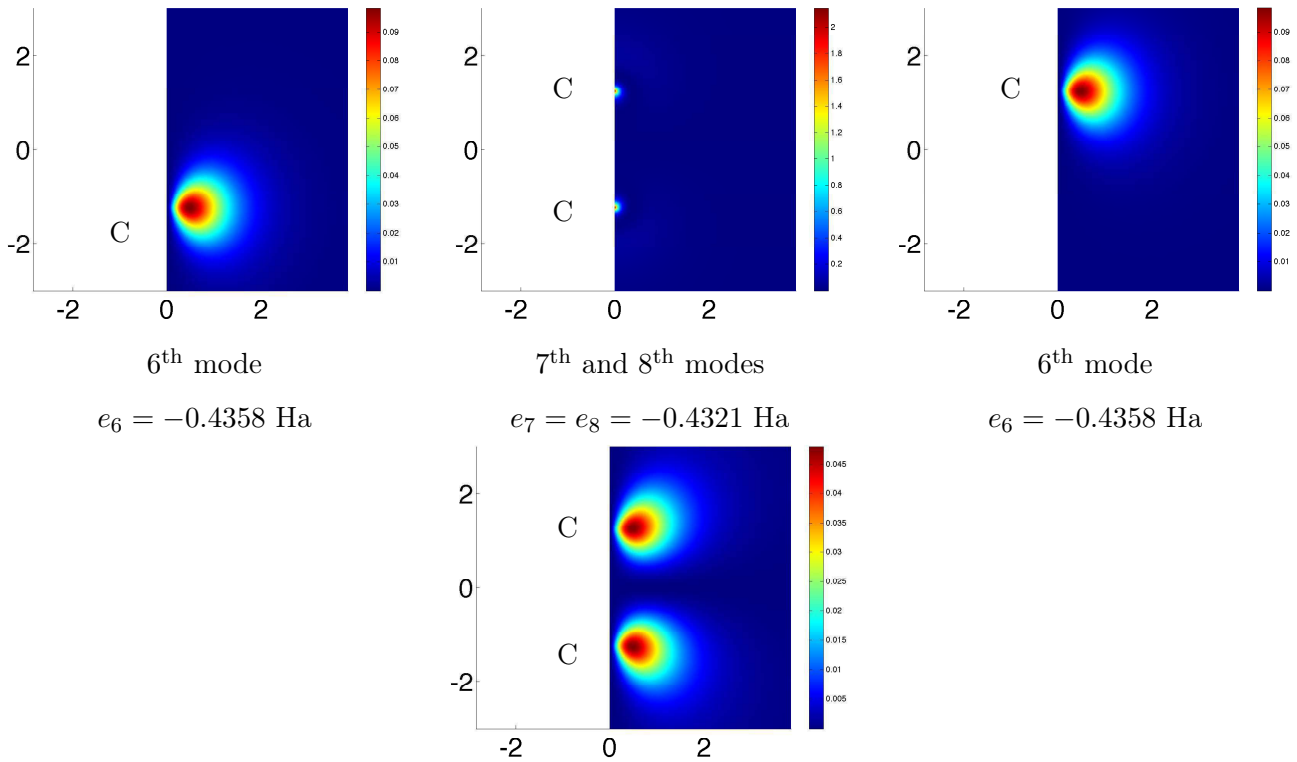


$6^{\text{th}}$ mode

$e_6 = -0.4358$ Ha

$7^{\text{th}}$ and $8^{\text{th}}$ modes

$e_7 = e_8 = -0.4321$ Ha

$6^{\text{th}}$ mode

$e_6 = -0.4358$ Ha

$9^{\text{th}}$, $10^{\text{th}}$, $11^{\text{th}}$ and $12^{\text{th}}$ modes

$e_9 = e_{10} = e_{11} = e_{12} = -0.4283$ Ha

Figure 4.7: Individual probability of presence for the different modes of the C atom and the $C_2$ molecule (HF model)

We focus on the energy of the system to determine the nuclei positions at equilibrium.

## 4.3 Prediction of molecular geometry

We compute the total energy of the system by the Hartree-Fock model and by the configuration interaction model. The positions of the nuclei at equilibrium match the minimum of the total energy.

For instance, for an isolated molecule of $H_2$, Figure 4.8 represents the total energy of the $H_2$ molecule as function of the bond length. We estimate the equilibrium bond length would be $1.41\,a_0$, which is in concordance with literature data [DG89]. We note that to determine the equilibrium bond length to the nearest $0.01\,a_0$, we need estimate of the total energy of the system to the nearest $10^{-4}$ Ha. To predict this quantity to the nearest $0.001\,a_0$, we should need estimation of the total energy of the system to the nearest $10^{-6}$ Ha.

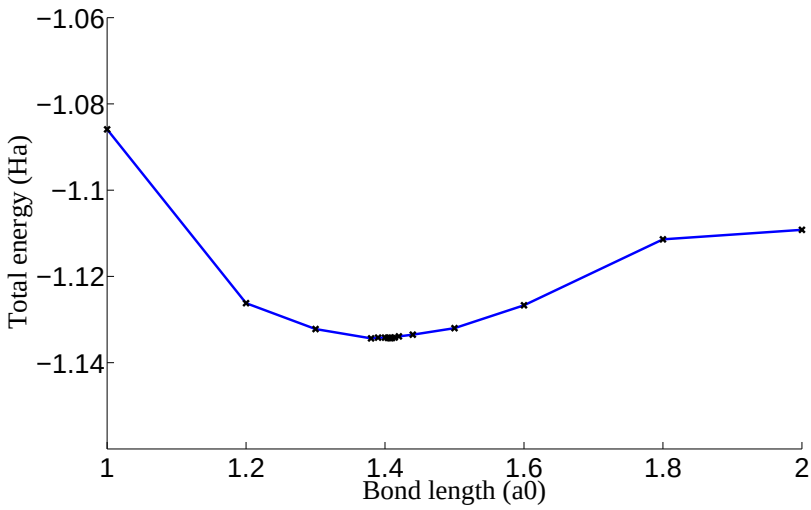


Figure 4.8: Total energy of the $H_2$ molecule as function of the bond length ($R = 2000\,a_0$ and `dof` $= 200000$)

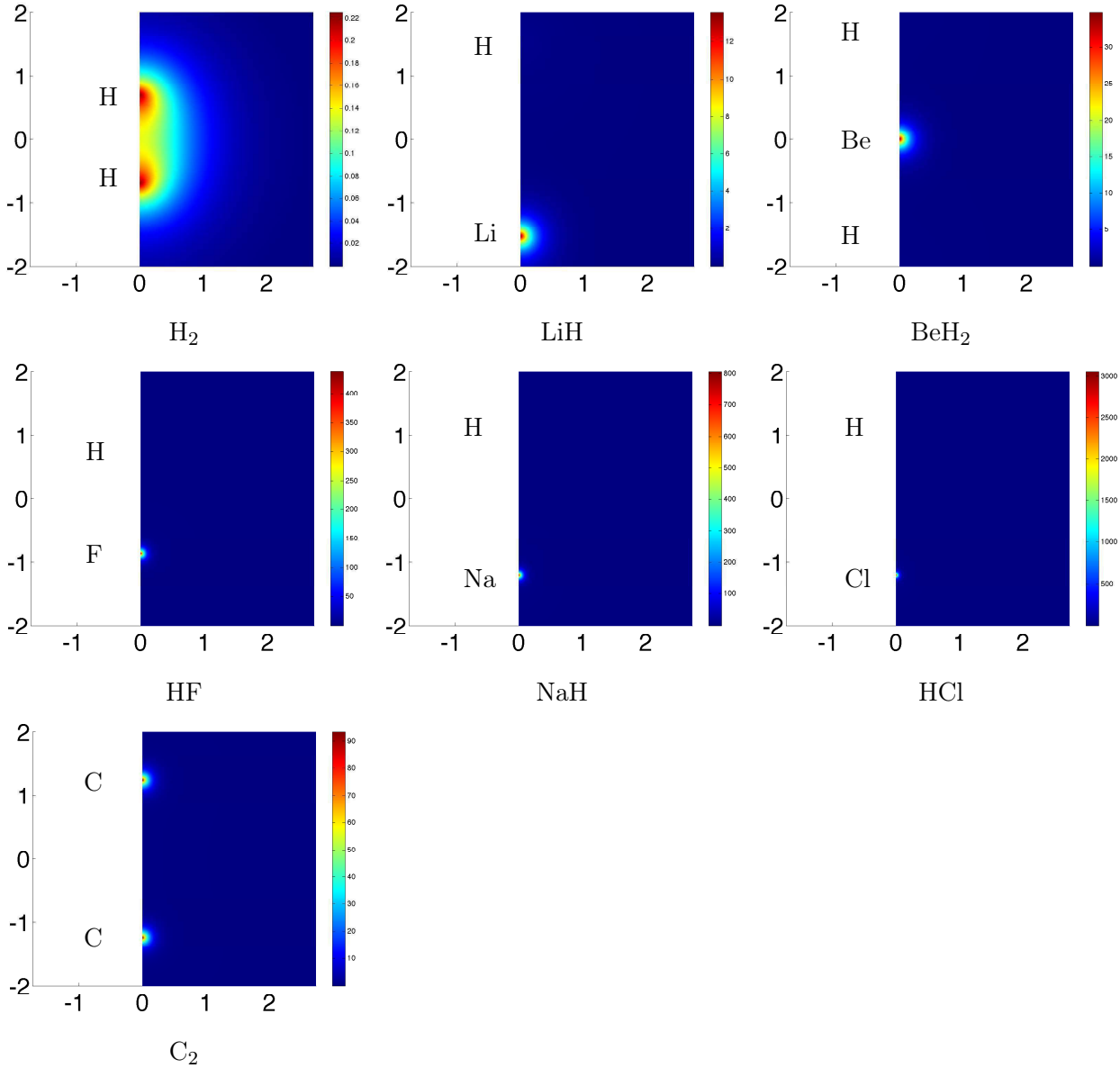


Figure 4.9: Computed electronic density for different molecules by HF

## 4.4 Mechanical properties

The first mechanical quantity we derive from quantum computations is the stress tensor defined by equation (1.2). To evaluate the derivative of the energy with respect to the deformation, we can compute the fundamental energy for different positions of the nuclei near the equilibrium position, as illustrated on Figure 4.8. The value of the energy is estimated in each case and a plot of energy *vs* deformation is obtained. The slope of this curve is the derivative of the energy with respect to the deformation. The shortcoming of this method is the need to compute many times the same molecule for different bond lengths.

### 4.4.1 Stress computation

Computing the forces at a given configuration without calculating at neighboring configurations can be done from the perturbation expression of the energy using the Hellmann-Feynman theorem [Fey39]. The stress tensor $\sigma$ is defined as:

$$\frac{\delta E}{\Omega} = tr\left(\sigma.\varepsilon\right)$$

where $E$ is the total energy of the system, $\Omega$ the volume associated with this energy and $\varepsilon$ is the homogenized deformation due to the nuclei displacements $\delta X_{N_j}$ such that $\delta X_{N_j} = \varepsilon\left(X_{N_j}\right)$. From equation (1.33), a variation of the total Hamiltonian $\delta H$ implies a variation of the wave function $\delta\Psi$ and of the total energy $\delta E$ which satisfies:

$$\left(H - E\right)\delta\Psi + \left(\delta H - \delta E\right)\Psi = 0. \tag{4.3}$$

As $\Psi$ is the normalized solution of the Schrödinger problem, considering the product of equation (4.3) with $\Psi^*$, we have:

$$\delta E = \left(\delta H\Psi, \Psi\right). \tag{4.4}$$

Considering there is no external electric field, the variation of the total energy of the system is expressed as a function of the variation of the total hamiltonian:

$$\delta H = \delta V_{en} + \delta V_{nn} = \sum_{C=1}^{N_n}\left(\nabla_{X_C} V_{Ce} + \sum_{\substack{K=1\\K\neq C}}^{N_n} \nabla_{X_C} V_{CK}, \varepsilon\left(X_C\right)\right)$$

where $X_C$ is the coordinate of the nucleus $C$. The interaction potentials (defined page 14) reads $V_{Ce} = \dfrac{-Z_C}{|x - X_C|}$ and $V_{CK} = \dfrac{Z_C Z_K}{|X_C - X_K|}$. The gradients read:

$$\nabla_{X_C} V_{Ce} = -Z_C \frac{x - X_C}{|x - X_C|^3} \qquad \text{and} \qquad \nabla_{X_C} V_{CK} = Z_C Z_K \frac{X_C - X_K}{|X_C - X_K|^3}. \tag{4.5}$$

Therefore,

$$\delta E = \sum_{C=1}^{N_n} \left( \int_{\mathbb{R}^{3N_e}} -Z_C \frac{x - X_C}{|x - X_C|^3} |\Psi_e|^2 dx + \sum_{\substack{K=1 \\ K \neq C}}^{N_n} Z_C Z_K \frac{X_C - X_K}{|X_C - X_K|^3}, \varepsilon\left(X_C\right) \right). \tag{4.6}$$

We see through this formula that the variation of the nucleus-electron interaction energy due to the deformation is the mean of the Coulomb potential gradient with respect to the deformation weighted by the probability of presence of the particles. To identify the stress tensor, we express the variation of the energy as the trace of a tensor:

$$\delta E = \operatorname{tr} \left[ \sum_{C=1}^{N_n} \left( \int_{\mathbb{R}^{3N_e}} -Z_C \frac{x - X_C}{|x - X_C|^3} |\Psi_e|^2 dx + \sum_{\substack{K=1 \\ K \neq C}}^{N_n} Z_C Z_K \frac{X_C - X_K}{|X_C - X_K|^3} \right) \otimes \varepsilon\left(X_C\right) \right]. \tag{4.7}$$

As $a \otimes A(b) = [a \otimes b] . A^T$, the stress tensor reads:

$$\sigma = \frac{1}{\Omega} \sum_{C=1}^{N_n} \left( \int_{\mathbb{R}^{3N_e}} -Z_C \frac{x - X_C}{|x - X_C|^3} |\Psi_e|^2 dx + \sum_{\substack{K=1 \\ K \neq C}}^{N_n} Z_C Z_K \frac{X_C - X_K}{|X_C - X_K|^3} \right) \otimes_S X_C. \tag{4.8}$$

The stress tensor is built-up from three effects:

- the interaction between nuclei,
- the interaction between nuclei and electrons,
- the interaction between nuclei and the external electric field.

Considering the Hartree-Fock approximation, it can be expressed as:

$$\sigma^{HF} = \frac{1}{\Omega} \sum_{C=1}^{N_n} \left( \left( -Z_C \frac{x - X_C}{|x - X_C|^3} |\Psi_e|^2 \Phi, \Phi \right) + \sum_{\substack{K=1 \\ K \neq C}}^{N_n} Z_C Z_K \frac{X_C - X_K}{|X_C - X_K|^3} \right) \otimes_S X_C. \tag{4.9}$$

This can be computed easily from the HF available integrals. Additionnally, using the configuration interaction approximation, we have:

$$\sigma^{CI} = \frac{1}{\Omega}\sum_{C=1}^{N_n}\left(\sum_{A=1}^{N_d}\sum_{B=1}^{N_d}\alpha_A\alpha_B^*\left(-Z_C\frac{x-X_C}{|x-X_C|^3}|\Psi_e|^2\Phi^A,\Phi^B\right)+\sum_{\substack{K=1\\K\neq C}}^{N_n}Z_CZ_K\frac{X_C-X_K}{|X_C-X_K|^3}\right)\otimes_S X_C. \tag{4.10}$$

We get thus the following result: Provided nuclei positions and the solution of the Schrödinger equation, the stress tensor $\sigma$ can be estimated from nucleus-nucleus and nucleus-electron dipoles. As a generalization from atomic electrostatics, the dipoles are added for each atomic particle but are weighted by the probability of presence for electrons.

### 4.4.2 Elasticity tensor computation

The elasticity tensor describes the linear elastic behavior of the material:

$$\sigma = C\left(\varepsilon\right).$$

It can be computed from the second-order variation of the energy of the system submitted to an homogeneous deformation defined before, and appears as the coefficient of the quadratic expansion of the strains:

$$\delta^2 E = \mathrm{tr}\left[C\left(\varepsilon\right).\varepsilon\right].$$

As $\Psi_e$ is the normalized solution of the Schrödinger equation, it can be shown from Equation (4.3) that:

$$\delta^2 E = 2\left(\left(\delta H-\delta E\right)\delta\Psi^{\perp},\Psi\right)+\left(\delta^2 H\Psi,\Psi\right) \tag{4.11}$$

where $\delta\Psi^{\perp} = -\left(H-E\right)^{-\perp}\left(\delta V-\delta E\right)\Psi$ and $\left(H-E\right)^{-\perp}$ stands for the orthogonal inverse of this operator.

$$\delta^2 E = -2\left(\left(\nabla_{X_N}V_{NK},\varepsilon\left(X_N\right)\right)-\left(\left(\nabla_{X_N}V_{Ne},\varepsilon\left(X_N\right)\right)\Psi,\Psi\right)^2\left(H-E\right)^{-\perp}\Psi,\Psi\right)$$
$$+\left(D^2_{X_NX_M}\left(V_{NK}+V_{Ne}\right)\left(\Psi,\Psi\right)\left(\varepsilon\left(X_N\right)\right),\varepsilon\left(X_M\right)\right)$$

The elasticity tensor $C$ is calculated by the following expression:

$$C = +\frac{1}{\Omega}\left(-2\left(\left(Z_N Z_M \frac{X_N - X_M}{|X_N - X_M|^3}, X_N\right) - \left(\left(-Z_C \frac{x - X_N}{|x - X_N|^3}\frac{\Psi_m}{E_m - E_0}\Psi_m\right), \Psi_m\right)\Psi_0\right)\right.$$
$$\left. + \left(D^2_{X_N X_M} V\Psi, \Psi\right)\right) \otimes (X_N \otimes X_M)\,. \quad (4.12)$$

The elasticity tensor requires a configuration interaction computation. It reads:

$$C = +\frac{1}{\Omega}\left(-2\left(\left(Z_N Z_M \frac{X_N - X_M}{|X_N - X_M|^3}, X_N\right) - \left(\alpha_0\alpha_m\left(-Z_N \frac{x - X_N}{|x - X_N|^3}\frac{\Phi_m}{E_m - E_0}, \Phi^m\right)\alpha_m\Phi^m\right)\alpha_0\Phi^0\right)\right.$$
$$\left. + \left(D^2_{X_N X_M} V\alpha_A\Phi^A, \alpha_B\Phi^B\right)\right) \otimes (X_N \otimes X_M)\,. \quad (4.13)$$

We obtain thus the following result: $\mathbb{C}$ is built up from quadrupole contributions, with classical terms for the atoms and weighted by the wave functions for the electrons. The quadrupole tensors are defined by:

$$D^2_{X_N X_M} V_{Ne} = \frac{Z_N}{|x - X_N|^{3/2}}\left(I - \frac{3}{2}\frac{x - X_N}{|x - X_N|} \otimes 1\right), \quad (4.14)$$

$$D^2_{X_N X_M} V_{NM} = \frac{Z_N Z_M}{|X_N - X_M|^{3/2}}\left(I - \frac{3}{2}\frac{X_N - X_M}{|X_N - X_M|} \otimes \frac{X_N - X_M}{|X_N - X_M|}\right). \quad (4.15)$$

At that scale, $\sigma$ depends on the Hessian matrices of the interaction potential with respect to the position of the nuclei. Thus, the elasticity properties of the systems depends on quadripoles. They are derived from an elastic potential, and all materials are hyperelastic. The remaining problem is to define the volume $\Omega$ in which the energy $E$ is localized. For crystal cases, this volume can be considered to be the elementary cell volume. For molecule cases, the problem is more difficult. *A priori*, molecular wave functions are defined in an unbounded domain. Stress field cannot be established locally, therefore we do not evaluate, in that case, the stress and elasticity tensors, but the bond force and the bond stiffness.

## 4.5 Numerical results

Table 4.2 presents our numerical results for $H_2$, LiH, $BeH_2$ molecules.

## 4.6 Three-dimensional computations

To tackle more complex systems, we need to perform three-dimensional computations. We test the feasibility of such computations. For instance, Figure 4.10 illustrates the three modes of

the $BeH_2$ molecule computed in a three-dimensional domain. These computations require high-performance computers and long computation time.

## 4.7 Summary

In this chapter, we have computed the ground state of isolated systems by determining their one-electron wave functions which match the mimimal energy of the system. From this information, we have derived different characteristics: the electronic energy, the positions of the nuclei, the mechanical and electrical properties of the molecules. Comparing the results with the literature, the proposed numerical approach seems promising.

We face two main challenges: increase the accuracy of the results and tackle large systems. As presented in Chapters 2 and 3, we have applied twice the Galerkin method and reduce the solution space to $\Omega_{CI} \cap \Omega_h$. To increase the accuracy of the results, the two major options consists in enlarging the space $\Omega_{CI}$ by adding determinants to the linear combination, or in enlarging the space $\Omega_h$ by increasing the radius of the FEM domain, adding nodes to the mesh or by increasing the order of the trial function polynomials.

To estimate the accuracy of our results and to optimize computations, *i.e.* to get the best estimation possible without increasing too much the computational cost, we propose *a posteriori* error estimates in the next chapter.

We have presented in Chapter 3 the main possibilities to tackle large systems. Here, we focus only on results for some isolated atoms and molecules, but most systems interact with their environment. Appendix J provides details of the method that is applied to model perfect solid crystals.

Table 4.2: Numerical results

| **Molecule** | $\mathbf{H_2}$ | **LiH** | $\mathbf{BeH_2}$ |
|---|---|---|---|
| HF bond length (in $a_0$) | 1.41 | 2.98 | 2.52 |
| HF total energy (in Ha) | -1.1343 | -7.9905 | -2.052 |
| HF bonding forces (in a.u.) | $F^z_{H_1} = -0.2467$ | $F^z_{Li} = -1.3239$ | $F^z_{Be} = 0.0001$ |
| | $F^z_{H_2} = 0.2467$ | $F^z_H = 60.562768$ | $F^z_H = 84.3572$ |
| HF dipolar moment (in debye) | 0.00 | 6.84 | 0.00 |

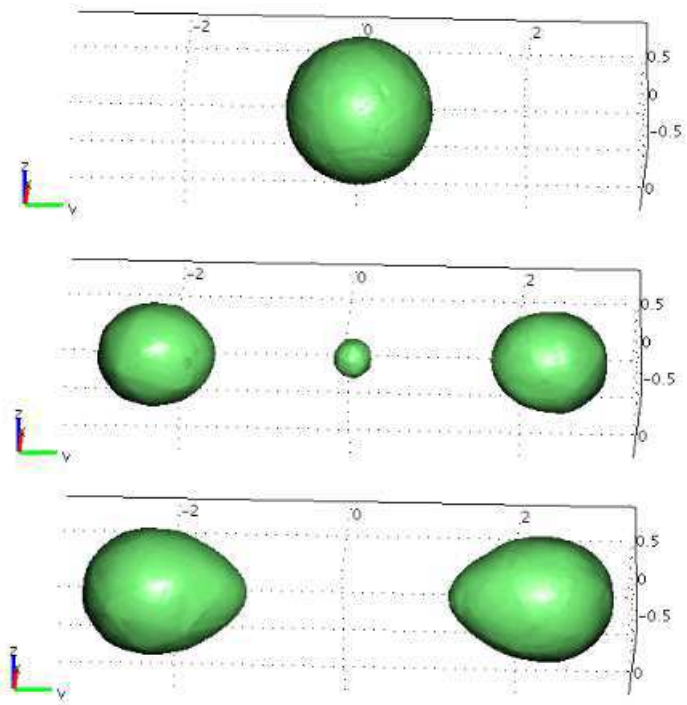


Figure 4.10: Surfaces of isoprobability of presence $|\varphi_i|^2 = 0.03$ for the ground-state modes of the $BeH_2$ molecule (positions of the atoms: $H(0;-2.52;0)$ $Be(0;0;0)$ $H(0;2.52;0)$)

# Chapter 5

# Error indicator for quantum mechanics quantities of interest

Chapter 4 provides estimation of some nanometric characteristics using the Hartree-Fock or the post Hartree-Fock equations and the finite element method. The goal was to describe molecular systems through their wave functions, and to determine their mechanical characteristics.

As for experimental approach, this numerical simulation cannot provide exact information. Estimating the accuracy of the results is of great interest to assess their reliability. Defining the sources of error allows the optimization of the modeling and the numerical strategy, and the achievement of a compromise between model accuracy and computational costs.

In the first part of this chapter, we list the difference sources of error in our numerical computations. Then, we briefly present available tools for error estimation, and overview the previous works about error estimation for *ab initio* computations. In the last part of this chapter, we apply the dual-weighted residual method to estimate the computational errors.

## 5.1 How exact are our results ?

The accuracy of a computation is estimated through some quantities of interest. Quantum computations can provide various quantities, and the accuracy of the computation can differ

with the quantity considered.

### 5.1.1 Different quantities of interest

The goal of quantum computations is to describe a system by its wave function. To encapsulate this description into a unique quantity, we concentrate on the average weighted by the probability of presence of the electrons of any function $F(x)$ of the distribution of the electrons and assume that the corresponding function is bounded:

$$\langle F(x) \rangle = \int F(x) P(x) \, dx. \tag{5.1}$$

Thus, we consider the average of the function $F_0(x) = 1$ weighted by the probability of presence of the electrons, *i.e.* the electronic energy of the system:

$$\langle 1 \rangle = \int \Psi_e^*(x) . \Psi_e(x) \, dx = E_e, \tag{5.2}$$

or the average of the functions $F_1(x) = x$, $F_2(x) = x^2$ or $F_3(x) = x^3$ weighted by the probability of presence of the electrons:

$$\langle x \rangle = \int \Psi_e^*(x) \, x \Psi_e(x) \, dx, \tag{5.3}$$

$$\langle x^2 \rangle = \int \Psi_e^*(x) \, x^2 \Psi_e(x) \, dx, \tag{5.4}$$

$$\langle x^3 \rangle = \int \Psi_e^*(x) \, x^3 \Psi_e(x) \, dx. \tag{5.5}$$

Error estimates can be established for quantities of major interest in a special context *e.g.* the mechanical properties, or it can focus on the most penalizing quantity to qualify a computation used for different applications. Whatever the quantity considered, we require a reliable assessment strategy.

Our results can be evaluated by comparing them with literature data. This comparison can qualify the accuracy but it is difficult to make profit from it to improve the accuracy, or to optimize the computer effort. To improve our estimations, we should identify the sources of errors and evaluate the influence of each source.

Quantum computations do not involve empirical parameters but rely on several approximations (see Chapter 2 and Chapter 3). In the next section, we investigate the different origins of error, and how important they seem to be in our computations.

### 5.1.2 The various origins of error

[ZY04] underlines three main sources of error in FEM models of quantum problems. The first one is the spectrum approximation of the Schrödinger spectrum due to the bounded domain. The second one is the error due to the finite-dimensional piecewise basis, and the third one is due to the iterative algorithm.

We can detail more precisely the different sources of errors solving the quantum mechanics problems by the strategy introduced in Figure 5.1.

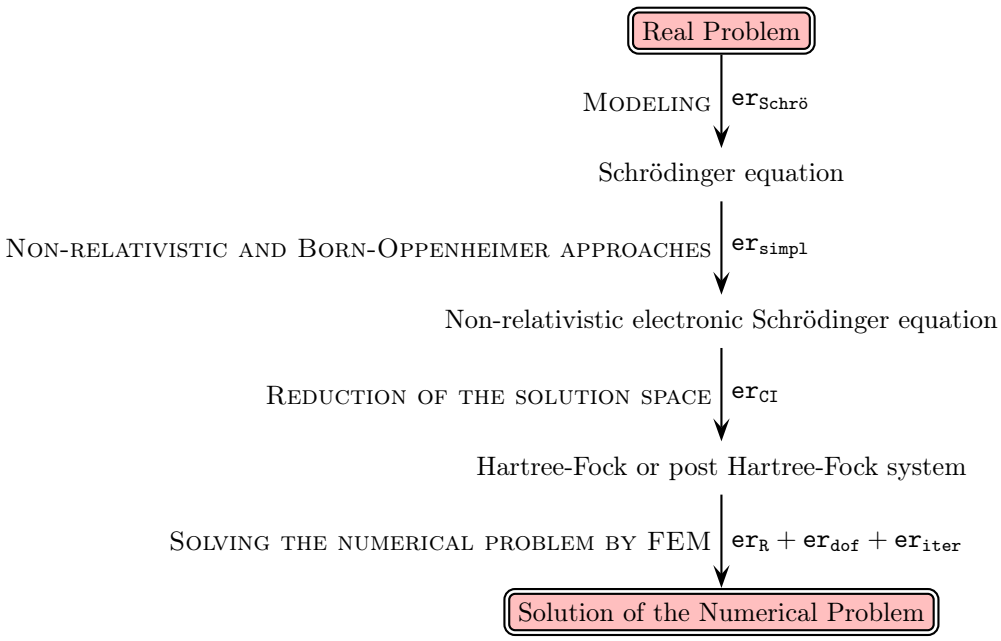


Figure 5.1: From the real problem to the numerical solution

A first source of error $\mathtt{er}_{\mathtt{Schrö}}$ comes from the Schrödinger modelization of the real problem. Then, the Schrödinger problem is simplified using the Born-Oppenheimer hypothesis and the non-relativistic assumption; what induces an error $\mathtt{er}_{\mathtt{simp}}$. The solution of the simplified Schrödinger

equation is approximated by the Hartree-Fock system, the solution space is reduced, and an error $\mathtt{er}_{\mathtt{CI}}$ is induced. Physicists called this error correlation energy. In HF solution, the probability of finding simultaneously the electron 1 in $x_1$ and the electron 2 in $x_2$ reads as the product of two probabilities $P_{12}(x_1, x_2) = |\Phi_1(x_1)|^2 |\Phi_2(x_2)|^2$, thus these two random events are mathematically non correlated. The Hartree-Fock problem is defined on an unbounded domain, but we solved it by FEM on a bounded one. We denote $\mathtt{er}_{\mathtt{R}}$ the error due to the bounded domain. We denote respectively $\mathtt{er}_{\mathtt{dof}}$ and $\mathtt{er}_{\mathtt{iter}}$ the errors due to the approximation by discretization on the FEM domain, and to the iterative method aiming at convergence.

To describe these numerous sources of error, we can contemplate them in the classical model verification and validation process illustrated by Figure 5.2.

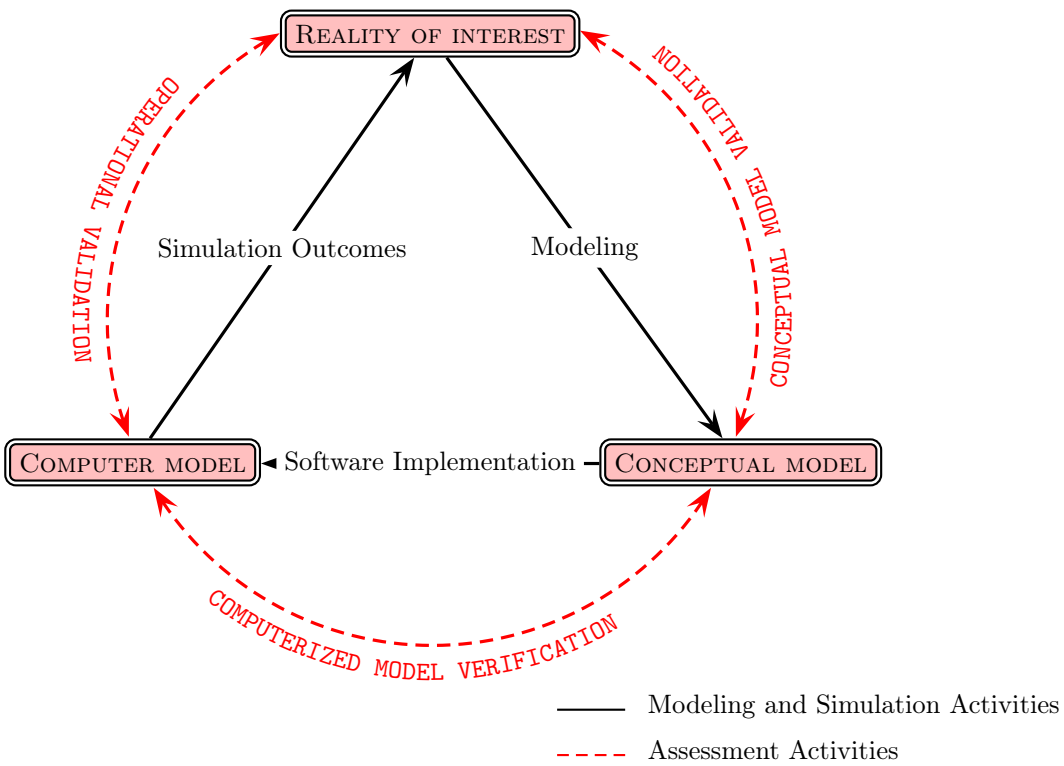


Figure 5.2: Simplified view of the model verification and validation process [Sch79, Sar09]

The real problem is modelized by a mathematical problem, which is implemented to get a computer model. This computer model is supposed to output simulation describing the real system. Here, the part of the error due to the modelization of the problem is the sum of $\mathtt{er}_{\mathtt{Schrö}}$, $\mathtt{er}_{\mathtt{simpl}}$, and $\mathtt{er}_{\mathtt{CI}}$. The validation of the Schrödinger model is out of the scope of our work. The software implementation of the simplified Hartree-Fock model involves error due to the FEM numerical characteristics: $\mathtt{er}_{\mathtt{FEM}} = \mathtt{er}_{\mathtt{R}} + \mathtt{er}_{\mathtt{dof}} + \mathtt{er}_{\mathtt{iter}}$. We can notice that using *ab initio* models, contrary to classical models, no empirical parameters are involved in the computations and in the source of errors.

In Chapter 4, we have compared our estimation to the literature and show their concordance (see page 81). Here, we vary the FEM numerical characteristics to observe their impact on the results. Figures 5.3, 5.4 and Table 5.1 provides the energy estimation of the Helium atom for different numerical parameters: the number of degrees of freedom, the radius of the FEM domain, and for different numbers of determinants in the CI expansion.

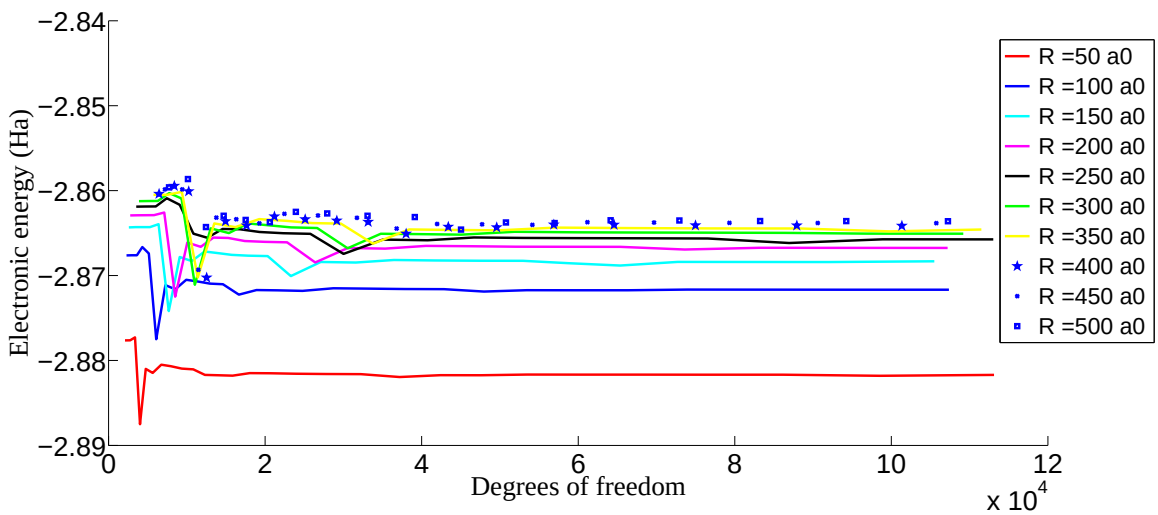


Figure 5.3: Estimation of the helium ground-state electronic energy with respect to the number of degrees of freedom used for each function for different FEM domain radii: $E_e\,(R,\,dof)$

On Figure 5.3, we note that the energy estimation converges when the number of degrees of freedom is increased. We increase enough the number of nodes to obtain an estimation of the

electronic energy to the nearest $10^{-5}\,Ha$. Figure 5.4 shows the influence of the FEM domain radius on the energy estimation.

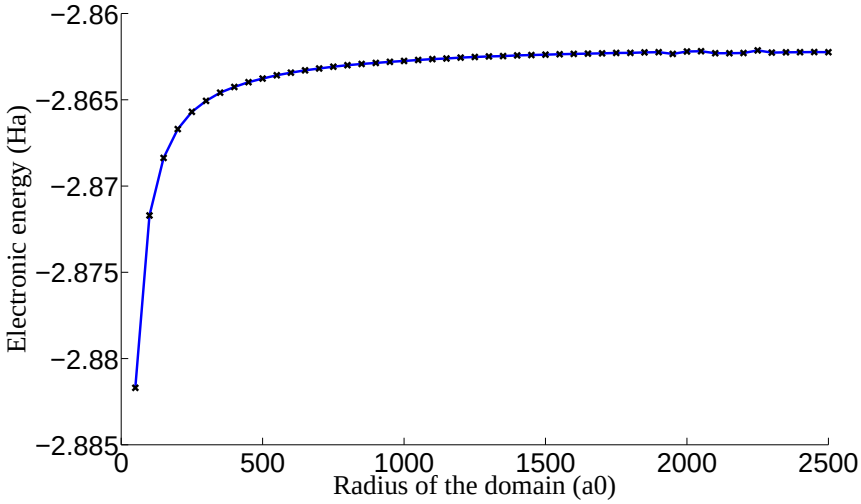


Figure 5.4: Estimation of the helium ground-state electronic energy with respect to the FEM domain radius: $E_e\,(R)$

Between the FEM radii of $1000\,a_0$ and $1250\,a_0$, the estimation varies by $2.10^{-4}$ Ha. Between the FEM radii of $1250\,a_0$ and $1500\,a_0$, the estimation varies by $10^{-4}$ Ha. We conclude a FEM radius of $2000\,a_0$ allows to get consistent results at the nearest $10^{-4}$ Ha imposing a minimum number of 180000 nodes. Using a larger radius would need a larger number of nodes. For instance, a radius of $2500\,a_0$ requires 230 000 nodes to get a result at the nearest $10^{-4}$ Ha.

We examine the different terms of electronic energy separately on Figure 5.5. We can see that the influent term on the dependance on the FEM radius is the term involving the electron-electron interaction, *i.e.* $G_{ij}$ terms. – As introduced in Chapter 2, a third way to improve result accuracy is by enlarging the CI solution space. Table 5.1 presents the electronic energy estimation for different CI linear combinations. The exactitude of the results is improved by increasing the number of determinants.

These results show the variability of the numerical estimation. To improve the estimation, we have increased the solution space, which implies to increase the computation time, and the

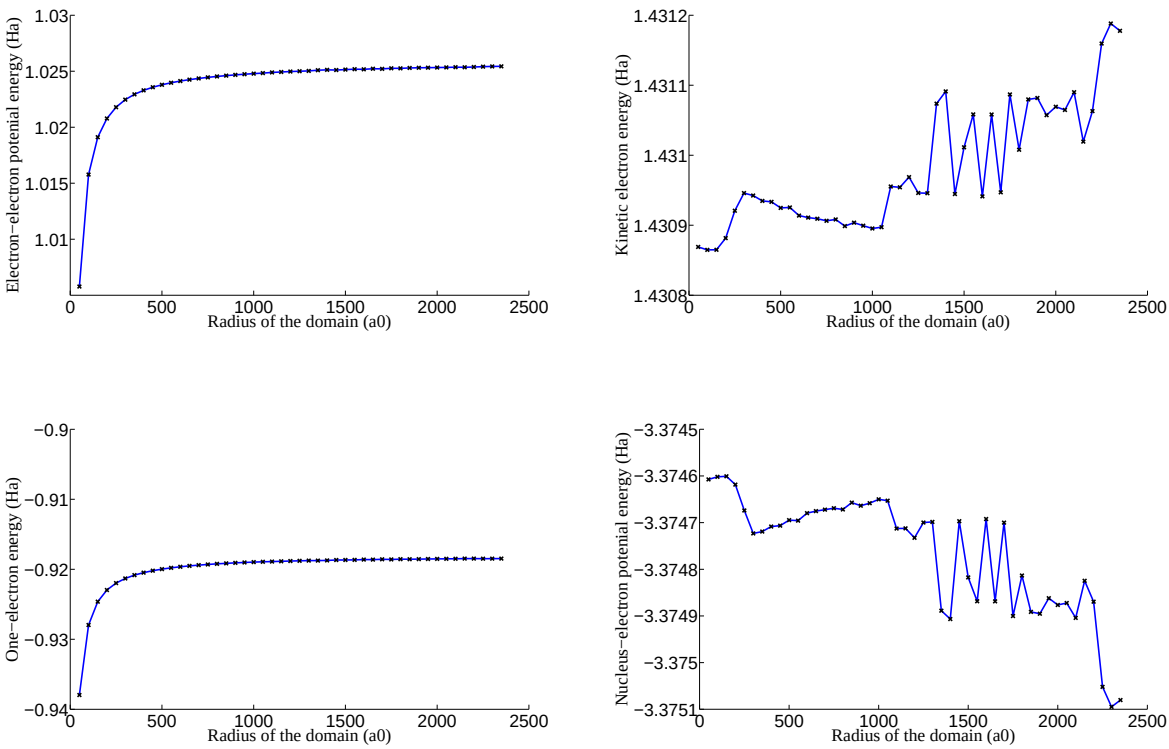


Figure 5.5: Influence of the FEM domain radius on the different terms of the helium ground-state electronic energy

| | |
|---|---|
| 1 det | -2.86412 |
| 5 det | -2.86415 |
| 15 det | -2.86432 |

Table 5.1: Estimation of the helium ground-state electronic energy (in Ha) for different numbers of determinants involved in the CI linear combination ($R = 2000\, a_0$)

memory requirement. Error estimation is an efficient tool to evaluate results, and so decide if it is pertinent to refine the model or not, and which strategy is more convenient. In the next section, we briefly overview some error estimation techniques.

## 5.2 A very short overview of the state of the art

The error estimation state of the art is only briefly presented here. Details can be provided by [AO00].

### 5.2.1 Error estimate

The goal of error estimate is to compare the exact problem $Ax = b$, defining the solution $x$ by the operator $A$ and the right-hand side $b$ with the approximate problem $A_h x_h = b_h$, which defines the approximate solution $x_h$ by the approximate operator $A_h$ and the approximate right-hand side $b_h$. We call approximation error the quantity $e = x - x_h$, it cannot be computed as the exact solution $x$ is unknown.

*A priori* error estimation methods deal with the truncaton error $\tau = A_h (x - x_h)$. They assume some stability properties of the surrogate operator $A_h$, but also interpolation errors. Here, we apply *a posteriori* error methods based on the residual $\rho = A (x - x_h)$. In that case, some stability properties of the unperturbed operator $A$ are required.

Main error estimators proposed in the literature can be classified into four categories:

- methods based on equilibrium residuals [BR78a, BR78b];
- methods based on error in mechanical behaviour relationship [Lad95];
- methods based on dual analysis [BR01];
- methods based on hierarchical basis [BS93].

These different methods are detailed in [Ver96]. We choose an approach based on dual analysis and develop it hereafter.

Traditionally, error estimate aimed at evaluating effects of numerical approximations, for instance error estimate due to the approximation of the continuous exact operator $A$ by a discrete approximated one $A_h$.

Error in model qualifies error due to the simplification of a reference mathematical model to a simplified mathematical one [Cha07]. A cascade of hierarchized models can be defined [OVM99], and the reference model can be chosen among this hierarchy. Some casual reference models and their surrogate models are given by Table 5.2. The analysis of model error can be made with respect to a specific quantity of interest [CO97, VO01, OP02, OBN+05], or with a global standpoint [OZ97, Ain98]. Model and discretization errors cand be handled separately or simulatenously [BE03].

| Reference model | Simplified model | |
|---|---|---|
| heterogeneous model | homogeneous model | [OZ97, OVM99, VO01] |
| 3D model | 2D model | [CO97] |
| viscoelastic model | elastic model | [Cha07] |
| atomic model | continuum model | [PBO06, KM12] |
| Schrödinger model | Hartree-Fock model | |
| Multiconfiguration model | Hartree-Fock model | [Fri03, Lew04] |
| CI model | Hartree-Fock model | |

Table 5.2: Some examples of simplication of reference model

Beyond error estimate theory developped in a mathematical framework, error estimates have been proposed specifically for many disciplines. Hereafter, we focus on works about error estimate in the context of atomic computations.

### 5.2.2 Error estimate for *ab initio* computations

The accuracy of the first quantum computations was examined using the virial theorem [Huo65]. In the case of HF, numerical errors have been analyzed in [MT03] and modeling errors as compared with the Thomas-Fermi model have already been studied in [Bac92]. The intention is to

extend such estimation techniques of the modeling error to more sophisticated approximations such as CI approximation. Without error estimation, some methods have actually been proposed to optimize CI estimations in [CRS+98, BMT05, FB60], but these methods are rather heuristic or limited to symmetric configurations. [Fri03] and [Lew04] introduce relevant mathematical results about CI optimization in the multiconfiguration strategy context.

The objective here is to propose a general approach taking advantage of the recent progress in error estimation techniques [BE03, OP02, OPW+03]. The goal is not to develop new solution techniques for the calculation of electronic structures of materials, a research topic of high interest and actively being studied (see for example [SCS10] and references therein) but to propose a new strategy that would help optimizing the precision of the calculation with respect to its complexity.

## 5.3 A first investigation of error indicators with respect to mechanical and quantum quantities of interest

In the subsequent paragraphs we explore the approach based on duality arguments to investigate different quantities of interest [BR01, BR03]. Because of time limitations we have not been able to perform the associated computations but we believe that the theoretical aspects discussed below deserve to be presented here.

We shall consider three quantities : the ground energy, the probability of presence and finally the evaluation of mechanical stresses.

### 5.3.1 Error indicator for the ground energy

For the sake of simplicity, exact solutions or solutions obtained from a refined model will be used without any subscript and approximate solutions will be equipped with the subscript $h$. Thus the wave function $\Psi$ and ground energy $E$ are exact solution of the Schrödinger equation whose weak form is:

$$\frac{1}{2}\left(\nabla_x \Psi, \nabla_x \delta\Psi\right) + \left(V\Psi, \delta\Psi\right) = E\left(\Psi, \delta\Psi\right) + \delta E\left(1 - |\Psi|^2\right),$$

and the approximate solutions $\Psi_h$ and $E_h$ are solutions of the following weak form on a smaller

function space according to the Galerkin approximation:

$$\frac{1}{2}\left(\nabla_x \Psi_h, \nabla_x \delta\Psi_h\right) + \left(V\Psi_h, \delta\Psi_h\right) = E_h\left(\Psi_h, \delta\Psi_h\right) + \delta E_h\left(1 - |\Psi_h|^2\right).$$

$\Psi_h$ may either come from the Hartree-Fock solution or the CI scheme or from a finite element approximation.

To find a representation of the error in ground energy, we use the following functional:

$$J\left(E, \Psi\right) = E|\Psi, \Psi|^2 \tag{5.6}$$

which is equal to $E$ according to the normalization of the wave function. Associated with this functional, we consider the following Lagrangian $\mathcal{L}$ with adjoint state $(z, E_z)$:

$$\mathcal{L}\left(E, \Psi, E_z, z\right) = J\left(\Psi\right) + \frac{1}{2}\left(\nabla\psi, \nabla z\right) + \left(V\Psi, z\right) - E\left(\Psi, z\right) + E_z\left(1 - \left(\Psi, \Psi\right)\right). \tag{5.7}$$

If we write the optimality equations for this Lagrangian: $\delta\mathcal{L} = 0$, we find the following equations:

$$\begin{cases} (\Psi, \Psi) = (\Psi, z) \\ E = E_z \\ z = \Psi \end{cases} \tag{5.8}$$

which means that here, for the ground energy estimation, the adjoint state is equal to the wave function itself. But more interestingly, the following error representation is easily obtained:

$$E - E_h = \mathcal{L}\left(E_h, \Psi_h, E_{h,z}, \Psi_{h,z}\right) - \mathcal{L}\left(E, \Psi, E_z, z\right). \tag{5.9}$$

A Taylor expansion of the Lagrangian around the approximate solution is performed. Rannacher shows that the residual term is usually of the third order and may be neglected. We will assume that this is actually the case, although this term may be fully computed in our case. Thus, to first order, we obtain by computing the first order derivative of the Lagrangian:

$$\begin{aligned} E - E_h \quad = \quad & \frac{1}{2}\left(\left(E - E_h\right)\left(\left(\Psi_h, \Psi_h\right) - \left(\Psi_h, z_h\right)\right) - E_h\left(\Psi - \delta\Psi_h, z_h\right)\right) \\ & + \frac{1}{2}\left(\nabla\left(\Psi - \delta\Psi_h\right), \nabla z_h\right) + \left(V\left(\Psi - \delta\Psi_h\right), z_h\right) \\ & + 2\left(E_h - E_{z_h}\right)\left(\Psi - \delta\Psi_h, \Psi_h\right) - E_h\left(\Psi_h, z - \delta z_h\right) \\ & + \frac{1}{2}\left(\nabla\Psi_h, \nabla\left(z - \delta z_h\right)\right) + \left(V\Psi_h, z - \delta z_h\right) + \left(E_z - \delta E_{z_h}\right)\left(-\left(\Psi_h, \Psi_h\right) + 1\right) + R_h \end{aligned}$$

with $R_h$ the so-called residual term. Taking into account the stationarity equations, the preceeding equation is simplified to:

$$E - E_h = -E_h\left(\Psi_h, z - \delta z_h\right) + \frac{1}{2}\left(\nabla\Psi_h, \nabla\left(z - \delta z_h\right)\right) + \left(V\Psi_h, z - \delta z_h\right) + R_h \tag{5.10}$$

where $\delta z_h$ is any quantity belonging to the reduced space of approximation because of the Galerkin projection property. We identify the right hand side of the above equation as the *a posteriori* residual of the approximate solution $\Psi_h$ tested on the difference between the exact adjoint $z$ and any test function $\delta z_h$ belonging to the space of approximation.

In the finite element literature, it is classical to choose $\delta z_h$ as the interpolant of $z$ and then to rely on interpolation errors. But from a practical point of view, the test function $z - \delta z_h$ is usually chosen on a refined mesh during post-processing. Here we are satisfied by invoking a refined model: for instance if the $z_h$ solution has been obtained via the Hartree-Fock scheme, $z - \delta z_h$ will be obtained by the CI formulation where wave functions orthogonal to the original approximation are built. Let us call $z_h^\perp$ this wave function. Then the following error indicator is obtained:

$$|E - E_h| \leq \left|\frac{1}{2}\left(\nabla\Psi_h, \nabla z_h^\perp\right) + \left(V\Psi_h, z_h^\perp\right)\right|. \tag{5.11}$$

It should be noted that although the multidimensional Schrödinger equation is used, the quantities in the right hand side may be computed by the Hartree-Fock approach and the associated integrals. Let us assume for instance that $\Psi_h$ has been computed from a HF approach:

$$\Psi_h = \frac{1}{\sqrt{N_e!}}\det\left[\tilde{\Phi}_h\right]. \tag{5.12}$$

Then $z_h^\perp$ is computed on the CI basis with $N_v$ virtual modes and $N_d$ determinants:

$$z_h^\perp = \sum_{A=1}^{N_d} \alpha_A \det\left[\tilde{\Phi}_v^A\right], \tag{5.13}$$

and the indicator is computed correspondingly by :

$$\frac{1}{2}\left(\nabla\Psi_h, \nabla z_h^\perp\right) + \left(V\Psi_h, z_h^\perp\right) = \sum_{A=1}^{N_d} \alpha_A \left[\frac{1}{2}\left(\nabla\Phi_h, \nabla\Phi_{A_h}^v\right) + \left(V_{ne}\Phi_h, \Phi_{A_h}^v\right) - \left(\left(G_h - \mathrm{tr}G_h I\right)\left(\Phi_h\right), \Phi_{A_h}^v\right)\right] \tag{5.14}$$

where the orthogonality between $\Psi_h$ and $z_h^\perp$ has been taken into account.

### 5.3.2 Error indicator for the probability of presence

We continue with error representation with another quantity, the wave function $\Psi$ itself. To reach this goal still following the dual-weighted residual method argument, we choose among many possibilities the following functional:

$$J(\Psi) = \int_\Omega |\Psi|^2 dx \tag{5.15}$$

intended to estimate the electronic density on a given subdomain $\Omega$ chosen eventually close to a given stack of nuclei to investigate bonding. We have:

$$\left(J'(\Psi), \delta\Psi\right) = \int_\Omega \left(\Psi\delta\Psi^* + \Psi^*\delta\Psi\right) dx. \tag{5.16}$$

The same formal Lagrangian $\mathcal{L}$ is used:

$$\mathcal{L}(E, \Psi, E_z, z) = J(\Psi) + \frac{1}{2}(\nabla\psi, \nabla z) + (V\Psi, z) - E(\Psi, z) + E_z(1 - (\Psi, \Psi)), \tag{5.17}$$

and the stationarity of $\mathcal{L}$ provides the following equations:

$$\begin{cases} -\frac{1}{2}\Delta z + Vz - Ez = 2E_z\Psi - J'(\Psi) \\ (\Psi, z) = 0 \\ E_z = \frac{1}{2}(J'(\Psi), \Psi) = \frac{1}{2}\int_\Omega |\Psi|^2 dx. \end{cases} \tag{5.18}$$

The dual Lagrange multiplier $E_z$ is equal to half the probability of presence. The adjoint state $z$, which is now distinct from $\Psi$, should satisfy the following Schrödinger equation with a right hand side:

$$-\frac{1}{2}\Delta z + Vz - Ez = J(\Psi)\Psi - J'(\Psi). \tag{5.19}$$

We can define $J^{\Psi^\perp} = J'(\Psi) - (J'(\Psi), \Psi)\Psi$ as the right hand side of the adjoint state equation. It is important to notice that the second stationary equation implies that $z$ must be chosen orthogonal to $\Psi$ so that the adjoint problem of the Schrödinger equation is well posed, at least if the ground state is not degenerated (non-multiple eigenvalue). We will assume that such is the case here and we remark that Larson has published an approach to deal with error estimate for degenerated eigenmodes [Lar00].

We can proceed with error representation of the electronic density, in a similar way as above, by developing the difference between the exact and approximate Lagrangian:

$$J - J_h = \mathcal{L}\left(E_h, \Psi_h, E_{h,z}, z_h\right) - \mathcal{L}\left(E, \Psi, E_z, z\right). \tag{5.20}$$

By taking into account simultaneously the stationarity of the Lagrangian and the Galerkin property, we arrive at:

$$\begin{aligned} J\left(\Psi\right) - J\left(\Psi_h\right) &= \frac{1}{2}\left[\frac{1}{2}\left(\nabla\Psi_h, \nabla\delta z_h^{\perp}\right) + \left(V\Psi_h, \delta z_h^{\perp}\right) - E_h\left(\Psi_h, \delta z_h^{\perp}\right)\right] \\ &+\frac{1}{2}\left[-\left(\delta\Psi_h^{\perp}, J'\left(\Psi_h\right) - \left(J'\left(\Psi_h\right), \Psi_h\right)\Psi_h\right) + \frac{1}{2}\left(\nabla\delta\Psi_h^{\perp}, \nabla z_h\right) + \left(V\delta\Psi_h^{\perp}, z_h\right) - E_h\left(\delta\Psi_h^{\perp}, z_h\right)\right] \end{aligned} \tag{5.21}$$

where, apart from the third order term $R_h$, two *a posteriori* residuals appear: the first one with respect to the direct and approximate wave $\Psi_h$ and the other one with respect to the approximate dual state $z_h$. It is interesting to simplify the right hand side for the adjoint state:

$$-\left(\delta\Psi_h^{\perp}, J'\left(\Psi_h\right) - \left(J'\left(\Psi_h\right), \Psi_h\right)\Psi_h\right) = -\left(\delta\Psi_h^{\perp}, J'\left(\Psi_h\right)\right) = -\int_{\Omega}\left(\delta\Psi^{\perp}\Psi_h^{*} + \delta\Psi_h^{\perp^{*}}\Psi_h\right)dx \tag{5.22}$$

where orthogonality between different states has been accounted for. It should be pointed that the last integral does not vanish only for two waves $\delta\Psi_h$ and $\Psi_h$ which are not orthogonal on the domain $\Omega$.

This equation leads to the error indicator:

$$\begin{aligned} \left|J\left(\Psi\right) - J\left(\Psi_h\right)\right| \leq \frac{1}{2}&\left|\left(\Psi_h^{\perp}, J^{\Psi_h^{\perp}}\right) + \frac{1}{2}\left(\nabla\Psi_h^{\perp}, \nabla z_h\right) + \left(V\Psi_h^{\perp}, z_h\right) - E_h\left(\Psi_h^{\perp}, z_h\right)\right| \\ &+ \frac{1}{2}\left|\frac{1}{2}\left(\nabla\Psi_h, \nabla z_h^{\perp}\right) + \left(V\Psi_h, z_h^{\perp}\right) - E_h\left(\Psi_h, z_h^{\perp}\right)\right| \end{aligned} \tag{5.23}$$

where $\Psi_h^{\perp}$, $z_h^{\perp}$ are appropriate test functions orthogonal to the original approximate solution. We have seen that the CI scheme for instance just provide such orthogonal waves which can thus be employed to indicate the error on the functional when the HF approximation is looked for.

We would like to remark again that all the integrals involved in the evaluation of both residuals are integrals of the same type as the one involved in the HF or MC formulations and thus can be evaluated similarly.

### 5.3.3 Error indicator for the mechanical stresses

We conclude this chapter with the estimation of error for mechanical quantities such as the stresses whose expression has been derived in the preceeding chapter. To reach this goal we choose the following quadratic functional where $a$ is any constant vector and a summation is implied with respect to the nuclei $X_A$:

$$J(\Psi) = ((\nabla_{X_A} V(X_A), a)\Psi, \Psi). \tag{5.24}$$

This functional allows to explore error on each component of the mechanical stress, or on a criterium such as the Von-Mises criterium. The gradient J' is given by:

$$\left(J'(\Psi), \delta\Psi\right) = \int_{\mathbb{R}^{3N_e}} (\nabla_{X_A} V, a)(\Psi\delta\Psi^* + \Psi^*\delta\Psi)\, dx. \tag{5.25}$$

It is recalled that the gradient with respect to the nuclei position $X_A$ of the Coulomb potential acts actually as a dipole:

$$\nabla_{X_A} V = -\frac{x - X_a}{|x - X_A|^3}.$$

Here we consider only the component of the stresses which contribute to its estimation through the wave function, where the electrostatic dipole is weighted by the square of the wave function. This is thus a quadratic functional which is now used. The Lagrangian is built along the same lines, as mentionned now several times:

$$\mathcal{L}(E, \Psi, E_z, z) = J(\Psi) + \frac{1}{2}(\nabla\psi, \nabla z) + (V\Psi, z) - E(\Psi, z) + E_z(1 - (\Psi, \Psi)). \tag{5.26}$$

Its stationarity implies that:

$$\begin{cases} E_z = \frac{1}{2}(J'(\Psi), \Psi) = \frac{1}{2}J(\Psi) \\ -\frac{1}{2}\Delta z + Vz - Ez = J(\Psi)\Psi - J'(\Psi) \\ (\Psi, z) = 0. \end{cases} \tag{5.27}$$

Now the dual Lagrange multiplier $E_z$ is equal to half the studied stress component. Another interesting result is obtained: The adjoint state is orthogonal to the direct wave and its right hand side is given by a dipole potential minus its average probability.

Following similar computations as above the following error indicator is provided:

$$|J(\Psi) - J(\Psi_h)| \leq \frac{1}{2}\left| -\left(\delta\Psi_h^{\perp}, J'(\Psi_h)^{\Psi_h^{\perp}}\right) + \frac{1}{2}\left(\nabla\delta\Psi_h^{\perp}, \nabla z_h\right) + \left(V\delta\Psi_h^{\perp}, z_h\right) - E_h\left(\delta\Psi_h^{\perp}, z_h\right)\right| + \frac{1}{2}\left|\frac{1}{2}\left(\nabla\Psi_h, \nabla\delta z_h^{\perp}\right) + \left(V\Psi_h, \delta z_h^{\perp}\right) - E_h\left(\Psi_h, \delta z_h^{\perp}\right)\right| \quad (5.28)$$

where it is recalled that the chosen functional $J$ used gives the quantum mechanics contribution to the stress tensor through the dipole.

Similar considerations may be developped for the elasticity tensor but will be omitted here.

It should be noted one more time that although the multidimensional Schrödinger equation is used, the quantities in the right hand side may be computed by the Hartree-Fock approach and the associated integrals.

# Conclusions and Perspectives

This dissertation introduces an original approach to model the behavior of a material at the nanoscale. At the bottom of the scale ladder for mechanics of materials, this scale allows the exploration of local defects, interfaces,... It does not satisfy Newtonian mechanics, but quantum mechanics. This work proposes to solve the Schrödinger equation by applying twice the Galerkin approach. First, the Schrödinger equation is solved in the Hartree-Fock or the configuration interaction solution space. Second, both these electronic problems have been implemented to be variationally solved in a finite-dimensional space by the FEM. This FEM approach allows the computation of the electronic structure in a real-space basis and the local refinement of the basis where it is most needed. The numerical model is solved by Newton's method. From the approximate wave functions, the behavior of the system has been mechanically characterized at the nanoscale. The numerical strategy has been validated for simple and isolated systems: atoms and linear molecules. To evaluate the accuracy of the results and optimize computation efforts, error estimates have been proposed for both numerical and model approximations and for different quantities of interest. The finite element strategy in this context is promising to optimize computations.

To conclude this exploratory dissertation at the frontier between mechanics, physics, and applied mathematics, many perspectives can be proposed. They can be classified into three main categories. The first goal is to optimize the existent tool, the second one to transform it into a muti-scale tool, and the last one to design a numerical tool able to tackle "real-world" problems.

### Optimization of the numerical tool

The model can be numerically optimized for two objectives: increasing the accuracy of the results or increasing the size of the modelized systems.

To gain in acuracy, error estimate could be improved to better optimize our computations, and to propose other dedicated error estimates for various quantities of interest and possibly a local model refinement.

To gain in terms of memory requirement and tackle large systems, different strategies detailed in Section 3.4 could be explored to reduce the number of degrees of freedom. A first strategy reduces the number of unknowns by computing only the valence modes, knowing the core modes from previous computations of isolated atoms. A second strategy simplifies the test functions using proper generalized decomposition. The last proposition consists in reducing the size of the stiffness matrix by applying domain decomposition, or localized model refinement.

### Multi-scale modeling

The Hartree-Fock method is appropriate to study systems of several atoms. To study larger electronic systems, DFT or Monte Carlo methods would be more convenient. Therefore, we plan to equip our numerical tool with DFT or Monte-Carlo solvers.

Then, these different methods could be coupled to study large systems providing precision of the Hartree-Fock method, or to determine efficiently some DFT functionals by solving an inverse problem from a Hartree-Fock solution.

This multi-scale simulation would find great interest in using methods such as the Arlequin method, a superposition method that uses energetic and volume coupling of the information provided by different scales or models. This strategy can couple two continuum models, or even a discrete atomic model with a continuum one [PCDB09]. With a same approach, coupling a continuum electronic model with a discrete atomic model could be proposed.

### Engineering applications

In the long term, it would be of great interest to provide a tool sharp enough to be used as a foundation stone to model complex materials. This challenge will be possible only with a

highly-optimized tool and a high-performance computer. Many engineering applications could be explored. As detailed in Introduction, this nanoscale information could be for instance useful to take into account defects in crystallized materials, to explore interfacial performances or to model complex nano-structures such as concrete.

To conclude the work presented here which have focused only on the numerical simulations, we highlight that for "real-world" applications, numerical simulations should be employed in parallel with experimental studies. The laboratory MSSMat offers a high expertise in nanoscopic experimentation as well using scanning electron microscopy, transmission electron microscopy, atomic force microscopy, tunneling effect microscopy, nanoindentation, or X-ray diffractometry. In a such context, a numerical tool exploring that scale could allow a dialog between experiments and simulations.

# Bibliography


[AC08] A. Ammar and F. Chinesta. Circumventing curse of dimensionality in the solution of highly multidimensional models encountered in quantum mechanics using meshfree finite sums decomposition. *Lecture Notes in Computational Science and Engineering*, 65:1–17, 2008.

[Ack95] J. Ackermann. Finite-element-method expectation values for correlated two-electron wave functions. *Physical Review A*, 52(3):1968–1976, 1995.

[ACV98] G. Allaire, C. Conca, and M. Vanninathan. The Bloch transform and applications. *ESAIM Proceedings*, 3:65–84, 1998.

[AER94] J. Ackermann, B. Erdmann, and R. Roitzsch. A self-adaptive multilevel finite element method for the stationary Schrödinger equation in three space dimensions. *Journal of Chemical Physics*, 101(9):7643–7650, 1994.

[AF05] P. Atkins and R. Friedman. *Molecular Quantum Mechanics*. Oxford University Press, 2005.

[AGL03] A. Aspuru-Guzik and W.A. Lester. *Handbook of Numerical Analysis, Volume X, Special Volume: Computational Chemistry*, chapter Quantum Monte Carlo methods for the solution of the Schrödinger equation for molecular systems, pages 485–535. North-Holland, 2003.

[AHM10] R. Alizadegan, K.J. Hsia, and T.J. Martinez. A divide and conquer real space finite-element Hartree-Fock method. *Journal of Chemical Physics*, 132:034101, 2010.

[Ain98] M. Ainsworth. A posteriori error estimation for fully discrete hierarchic models of elliptic boundary value problems on thin domains. *Numerical Mathematics*, 80(325), 1998.

[AMCK06a] A. Ammar, B. Mokdad, F. Chinesta, and R. Keunings. A new family of solvers for some classes of multidimensional partial differential equations encountered in kinetic theory modeling of complex fluids. *Journal of Non-Newtonian Fluid mechanics*, 139:153–176, 2006.

[AMCK06b] A. Ammar, B. Mokdad, F. Chinesta, and R. Keunings. A new family of solvers for some classes of multidimensional partial differential equations encountered in kinetic theory modeling of complex fluids. Part II: transient simulation using space-time separated representation. *Journal of Non-Newtonian Fluid mechanics*, 144:98–121, 2006.

[AO00] M. Ainsworth and J.T. Oden. *A posteriori error estimation in finite element analysis*. Wiley, 2000.

[AR93] J. Ackermann and R. Roitzsch. A two-dimensional multilevel adaptive finite element method for the time-independent Schrödinger equation. *Chemical Physics Letters*, 214(1):109 – 117, 1993.

[Ask75] A. Askar. Finite element method for bound state calculations in quantum mechanics. *The Journal of Chemical Physics*, 62(2):732–734, 1975.

[Ast00] R.J. Astley. Infinite elements for wave problems: a review of current formulations and an assessment of accuracy. *International Journal for Numerical Methods in Engineering*, 49(7):951–976, 2000.

[Bac92] V. Bach. Error bound for the Hartree-Fock energy of atoms and molecules. *Communications in Mathematical Physics*, 147:527–548, 1992.

[Bai00] C. Bai. *Scanning tunneling microscopy and its applications*. Springer Verlag, 2000.

[Bal73] A. Baldereschi. Mean-value point in the Brillouin zone. *Physical Review B*, 7(12):5212–5215, 1973.

[Bar05] M. Barrault. *Développement de méthodes rapides pour le calcul de structures électroniques*. PhD thesis, École Nationale des Ponts et Chaussées, 2005.

[BCHLB07] M. Barrault, E. Cancès, W.W. Hager, and C. Le Bris. Multilevel domain decomposition for electronic structure calculations. *Journal of Computational Physics*, 222:86–109, 2007.

[BD06] J.L. Basdevant and J. Dalibard. *Mécanique quantique*. École Polytechnique, 2006.

[BE03] M. Braack and A. Ern. A posteriori control of modelling errors and discretization errors. *Multiscale Modeling and Simulation*, 1(2):221–238, 2003.

[Bec93] A.D. Becke. A new mixing of Hartree-Fock and local density-functional theories. *Journal of Chemical Physics*, 98(2):1372–1377, 1993.

[Ben98] H. Ben Dhia. Multiscale mechanical problems: the Arlequin method. *Comptes-Rendus de l'Académie des Sciences II B*, 326(12):899–904, 1998.

[Bla00] X. Blanc. *Mathematical models and methods for ab-initio quantum chemistry*, chapter A mathematical insight into ab initio simulations of the solid phase, pages 133–158. Lecture Notes in Chemistry, vol.74, Springer edition, 2000.

[Blo28] F. Bloch. Über die Quantenmechanik der elektronen in Kristallgittern. *Zeitschrift für Physik*, 52, 1928.

[BM07] R.J. Bartlett and M. Musial. Coupled-cluster theory in quantum chemistry. *Reviews of Modern Physics*, 79:291–352, 2007.

[BMB09] M. Bozlar, F. Miomandre, and J. Bai. Electrochemical synthesis and characterization of carbon nanotube/modified polypyrrole hybrids using a cavity microelectrode. *Carbon*, 47:80–84, 2009.

[BMT05] D. Bressanini, G. Morosi, and S. Tarasco. An investigation of nodal structures and the construction of trial wave functions. *Journal of Chemical Physics*, 123, 2005.

[BO27] M. Born and R. Oppenheimer. Zur quantentheorie der molekeln. *Annalen der Physics*, 84:457–484, 1927.

[Bon64] A. Bondi. Van der Waals volumes and radii. *Journal of Physical Chemistry*, 68(3):441–451, 1964.

[Bor26] M. Born. Zur quantenmechanik der sto$\beta$vorgänge. *Zeitschrift für Physik A Hadrons and Nuclei*, 37(12):863–867, 1926.

[Boy50] S.F. Boys. Electronic wave functions I. A general method of calculation for the stationary states of any molecular system. *Proceedings of the Royal Society A*, 200:542–554, 1950.

[BR78a] I. Babuška and W.C. Rheinboldt. Error estimates for adaptive finite element computations. *Journal of Numerical Analysis*, 18:736–754, 1978.

[BR78b] I. Babuška and W.C. Rheinboldt. A posteriori error estimates for the finite element method. *Journal of Numerical Methods in Engineering*, 12:1597–1615, 1978.

[BR01] R. Becker and R. Rannacher. An optimal control approach to a posteriori error estimation in finite element methods. *Acta Numerica*, 19:1–102, 2001.

[BR03] W. Bangerth and R. Ranacher. *Adaptive finite element methods for differential equations*. Birkhäuser Basel, 2003.

[Bra50] A. Bravais. Mémoire sur les systèmes formés par des points distribués régulièrement sur un plan ou dans l'espace. *Journal de l'École Polytechnique*, 19:1–128, 1850.

[Bre30] G. Breit. Separation of angles in the two-electron problem. *Physical Review*, 35(6):569–578, 1930.

[Bri53] L. Brillouin. *Wave propagation in the periodic structures*. Dover Publications, 1953.

[BS93] R.E. Bank and R.K. Smith. A posteriori estimates based on hierarchical bases. *SIAM Journal on Numerical Analysis*, 30:921–935, 1993.

[BSH93] M. Braun, W. Schweizer, and H. Herold. Finite-element calculations for the S states of helium. *Physical Review A*, 48(3):1916–1920, 1993.

[BSI11] B. Bhuvaneshwari, S. Sasmal, and N.R. Iyer. Nanoscience to nanotechnology for civil engineering: proof of concepts. In *GEMESED'11 Proceedings of the 4th WSEAS international conference on energy and development - environment - biomedecine*, 2011.

[BSW36] L.P. Bouckaert, R. Smoluchowski, and E. Wigner. Theory of Brillouin zones and symmetry properties of wave functions in crystals. *Physical Review*, 50:58–67, 1936.

[BTS08] W.M. Brown, A.P. Thompson, and P.A. Schultz. Bridging scales from ab initio models to predictive empirical models for complex materials. *Sandia Report*, 2008.

[CA08] F. Chinesta and A. Ammar. On the frontier of the simulation world. When models involve excessive degrees of freedom. *European Journal of Computational Mechanics*, 17(5-7):583–595, 2008.

[CAJL93] K. Cho, A. Arias, J.D. Joannopoulos, and P.K. Lam. Wavelets in electronic structure calculations. *Physical Review Letters*, 71(12):1808–1811, 1993.

[Can98] E. Cancès. *Simulation moléculaire et effets d'environnement. Une perspective mathématique et numérique.* PhD thesis, École Nationale des Ponts et Chaussées, 1998.

[CC73a] D.J. Chadi and M.L. Cohen. Electronic structure of $Hg_{1-x}Cd_xTe$ alloys and charge-density calculations using representative k points. *Physical Review B*, 7(2):692–699, 1973.

[CC73b] D.J. Chadi and M.L. Cohen. Special points in the Brillouin zone. *Physical Review B*, 8(12):5747–5753, 1973.

[CCF+05] A.G. Császár, G. Czakó, T. Furtenbacher, J. Tennyson, V. Szalay, S.V. Shirin, N.F. Zobov, and O.L. Polyansky. On equilibrium structures of the water molecule. *Journal of Chemical Physcis*, 122:214305, 2005.

[CDK+03] E. Cancès, M. Defranceschi, W. Kutzelnigg, C. Le Bris, and Y. Maday. *Handbook of Numerical Analysis, Volume X, Special Volume: Computational Chemistry*, chapter Computational Quantum Chemistry: A primer, pages 3–270. North-Holland, 2003.

[CDL73] C. Cohen-Tannoudji, B. Diu, and F. Laloë. *Mécanique Quantique*. Hermann, 1973.

[Ced10] G. Ceder. Opportunities and challenges for first-principles materials design and applications to Li battery materials. *Materials Research Society Bulletin*, 35:693–701, 2010.

[CH95] E. Clementi and D.W.M. Hofmann. Coulomb-hole-Hartree-Fock functional for molecular systems. *Journal of molecular structure*, 330:17–31, 1995.

[Cha05] C. Chauvin. *Les ondelettes comme fonctions de base dans le calcul de structures électroniques*. PhD thesis, Institut National Polytechnique de Grenoble, 2005.

[Cha07] L. Chamoin. *Encadrement a posteriori de quantités locales dans les problèmes de viscoélasticité linéaire résolus par la Méthode des Éléments Finis*. PhD thesis, École Normale Supérieure de Cachan, 2007.

[CLM06] E. Cancès, C. Le Bris, and Y. Maday. *Méthodes mathématiques en chimie quantique. Une introduction*. Springer, 2006.

[CO97] J.R. Cho and J.T. Oden. Local a posteriori error estimates of hierarchical models for plate- and shell-like structures. *Computer Methods in Applied Mechanics and Engineering*, 149(33), 1997.

[Com11] Computational Chemical Sciences Group, Oak Ridge National Laboratory, http://www.csm.ornl.gov/ccsg/html/projects/madness.html. *MADNESS (Mul-*

*tiresolution ADaptive NumErical Scientific Simulation)*, 2011 (accessed December 5, 2011).

[Cor11] Cornell University - Cornell Center for Materials Research (CCMR), http://dft.physics.cornell.edu/. *DFT++*, 2011 (accessed December 5, 2011).

[Cou84] C. Coulomb. *Tome 1 Mémoires de Coulomb.* Collection de mémoires relatifs à la physique, 1884.

[CRS+98] N. J. Clarke, M. Raimondi, M. Sironi, J. Gerratt, and D.L. Cooper. Optimization of virtual orbitals in the framework of a multiconfiguration spin-coupled wave function. *Theoretical Chemistry Accounts*, 99:8–17, 1998.

[Cry11] Crystal Software Inc, USA, http://www.crystalcom.com/. *CRYSTAL*, 2011 (accessed December 5, 2011).

[CWWZ00] A. Canning, L.W. Wang, A. Williamson, and A. Zunger. Parallel empirical pseudopotential electronic structure calculations for million atom systems. *Journal of Computational Physics*, 160:29–41, 2000.

[Dal96] A. Dal Corso. *Quantum-mechanical ab-initio calculation of the properties of crystalline materials*, chapter Reciprocal space integration and special-point techniques, pages 77–89. Lecture Notes in Chemistry, vol.67, Springer edition, 1996.

[DBD+00] M. Despont, J. Brugger, U. Drechsler, U. Dürig, W. Häberle, M. Lutwyche, H. Rothuizen, R. Stutz, R. Widmet, G. Binning, H. Rohrer, and P. Vettiger. VLSI-NEMS chip for parallel AFM data storage. *Sensors and Actuators*, 80:100–107, 2000.

[DCAJ94] A. Devenyi, K. Cho, T.A. Arias, and J.D. Joannopoulos. Adaptive Riemannian metric for all-electron calculations. *Physical Review B*, 49:13373–13376, 1994.

[DDE+03] J.P. Desclaux, J. Dolbeault, M.J. Esteban, P. Indelicato, and E. Séré. *Handbook of Numerical Analysis, Volume X, Special Volume: Computational Chemistry*,

chapter Computational Quantum Chemistry: A primer, pages 453–484. North-Holland, 2003.

[de 24] L. de Broglie. *Recherches sur la théorie des quanta.* PhD thesis, 1924.

[DG89] R.L. DeKock and H.B. Gray. *Chemical structure and bonding.* University Science Books, 1989.

[DGD02] P. Damle, A.W. Ghosh, and S. Datta. First-principles analysis of molecular conduction using quantum chemistry software. *Chemical Physics*, 281:171–187, 2002.

[DGG09] J. Deng, T.B. Gilbert, and M.W. Gill. Approaching the Hartree-Fock limit by perturbative methods. *Journal of Chemical Physics*, 130:231101, 2009.

[DGR+99] R.E. Doak, R.E. Grisenti, S. Rehbein, G. Schmahl, J.P. Toennies, and Ch. Wöll. Towards realization of an atomic de Broglie microscope: Helium atom focusing using Fresnel zone plates. *Physical Review Letters*, 83(21):4229–4232, 1999.

[DHC91] E.R. Davidson, S.A. Hagstrom, and S.J. Chakravorty. Ground-state correlation energies for two- to ten-electron atomic ions. *Physical Review A*, 44(11):7071–7083, 1991.

[Dir26] P. Dirac. On the theory of Quantum Mechanics. *Proceedings of the Royal Society*, A112:661–667, 1926.

[Dir28] P. Dirac. The quantum theory of the electron. *Proceedings of the Royal Society*, A117:610–624, 1928.

[DKG92] H.-Q. Ding, N. Karasawa, and W.A. Goddard III. Atomic level simulations on a million particles: The cell multipole method for Coulomb and London nonbond interactions. *Journal of Chemical Physics*, 97(6):4309–4315, 1992.

[DL97] M. Defranceschi and C. Le Bris. Computing a molecule: A mathematical viewpoint. *Journal of Mathematical Chemistry*, 21:1–30, 1997.

[dLPZ79] M. de Llano, A. Plastino, and J.G. Zabolitzky. Optimal plane-wave Hartree-Fock states for many-fermion systems. *Physical Review C*, 20(6):2418–2425, 1979.

[DPLP99] T. Darden, L. Perera, L. Li, and L. Pedersen. New tricks for modelers from the crystallography toolkit: the particle mesh Ewald algorithm and its use in nucleic acid simulations. *Structure*, 7:55–60, 1999.

[DPRS83] R. Dovesi, C. Pisani, C. Roetti, and V.R. Saunders. Treatment of Coulomb interactions in Hartree-Fock calculations of periodic systems. *Physical Review B*, 28(10):5781–5792, 1983.

[DvB11] J.S. Dolado and K. van Breugel. Recent advances in modeling for cementitious materials. *Cement and Concrete Research*, 41:711–726, 2011.

[DYP93] T. Darden, D. York, and L. Pedersen. Particle mesh Ewald: An N.log(N) method for Ewald sums in large systems. *Journal of Chemical Physics*, 98(12):10089–10092, 1993.

[EM77] B. Engquist and A. Majda. Absorbing boundary conditions for the numerical simulation of waves. *Mathematics of computation*, 31(139):629–651, 1977.

[Eur11] European program, Commissariat à l'Énergie Atomique, http://inac.cea.fr/_Sim/BigDFT/. *BigDFT*, 2011 (accessed December 5, 2011).

[Ewa21] von P.P. Ewald. Die Berechnung optischer und elektrostatischer Gitterpotentiale. *Annalen der Physics*, 369(3), 1921.

[FB60] J.M. Foster and S.F. Boys. Canonical configuration interaction procedure. *Reviews of Modern Physics*, 32(2):300–302, 1960.

[FCC96] The lifetimes and energies of the first excited singlet states of diadinoxanthin and diatoxanthin. *Biochimica et Biophysica Acta*, 1277:243–252, 1996.

[Fer26] E. Fermi. Sulla quantizzazzione del gas perfetto monoatomico. *Rendiconti Lincei*, 3(145), 1926.

[Fey39] R.P. Feynman. Forces in molecules. *Physical Review*, 56:340–343, 1939.

[Fey99] R.P. Feynman. *Le cours de physique de Feynman : Mécanique, tome 1.* Dunod, 1999.

[FMNR01] W.M.C. Foulkes, L. Mitas, R.J. Needs, and G. Rajagopal. Quantum Monte Carlo simulations of solids. *Reviews of Modern Physics*, 73:33–83, 2001.

[FMS73] G. Fonte, R. Mignani, and G. Schiffrer. Solution of the Hartree-Fock equations. *Communications in Mathematical Physics*, 33:293–304, 1973.

[Fou06] M. Foulkes. Introductory lectures on electrons in solids. Imperial College London, 2006.

[FPZ95] D. François, A. Pineau, and A. Zaoui. *Comportement mécanique des matériaux - élasticité et plasticité.* Hermès, 1995.

[Fre71] A.P. French. *Newtonian mechanics.* Norton, 1971.

[Fri03] G. Friesecke. The multiconfiguration equations for atoms and molecules: charge quantization and existence of solutions. *Archive for Rational Mechanics and Analysis*, 169:35–71, 2003.

[FRRT78] M. Fridman, Y. Rosenfeld, A. Rabinovitch, and R. Thieberger. Finite element method for solving the two-dimensional Schrödinger equation. *Journal of Computational Physics*, 26:169–180, 1978.

[Gau11] Gaussian, Inc., USA, http://www.gaussian.com/. *Gaussian*, 2011 (accessed December 5, 2011).

[GD09] A. Górecka-Drzazga. Miniature and MEMS-type vacuum sensors and pumps. *Vacuum*, pages 1419–1426, 2009.

[GH07] J.-J. Greffet and C. Henkel. Coherent thermal radiation. *Contemporary Physics*, 48(4):183–194, 2007.

[GM94] W. Greiner and B. Muller. *Quantum Mechanics (Theoretical Physics)*. Springer, 1994.

[God88] M.J. Godfrey. Stress field in quantum systems. *Physical Review B*, 37(17):10176–10183, 1988.

[Gou95] S.H. Gould. *Variational methods for eigenvalue problems: an introduction to the methods of Rayleigh, Ritz, Weinstein, and Aronszajn*. Dover Publications, 1995.

[GP92] G. Galli and M. Parrinello. Large scale electronic structure calculations. *Physical Review Letters*, 69:3547–3550, 1992.

[Gri62] R.E. Grim. *Applied clay mineralogy*. McGraw-Hill, 1962.

[Hal91] G.G. Hall. The Lennard-Jones paper of 1929 and the foundations of molecular orbital theory. *Advances in quantum chemistry*, 22:1–6, 1991.

[HCA12] J. Hermet, P. Cortona, and C. Adamo. New range-separated hybrids based on the TCA density functional. *Chemical Physics Letters*, pages 145–149, 2012.

[HK64] P. Hohenberg and W. Kohn. Inhomogeneous electron gas. *Physical Review*, 136(3B):864–871, 1964.

[Hla97] J. Hladik. *Mécanique Quantique*. Masson, 1997.

[HTIF06] T. Hoshi, R. Takayama, Y. Iguchi, and T. Fujiwara. Large-scale electronic-structure theory and nanoscale defects formed in cleavage process of silicon. *Physica B*, 376-377:975–978, 2006.

[Huo65] W.M. Huo. Electronic structure of CO and BF. *The Journal of Chemical Physics*, 43(2):624–647, 1965.

[HWC06] J. Hafner, C. Wolverton, and G. Ceder. Toward computational materials design: the impact of density functional theory on materials research. *Materials Research Society Bulletin*, 31:659–664, 2006.

[HWRV05] D.R. Hamann, X. Wu, K.M. Rabe, and D. Vanderbilt. Metric tensor formulation of strain in density-functional perturbation theory. *Physical Review B*, 71, 2005.

[IO99] T. Ishida and K. Ohno. Force analysis by molecular orbitals - partition of the Hellmann-Feynman force into one-electron orbital contributions. *Journal of Molecular Structure*, 461-462:335–349, 1999.

[IV01] Y. Ishikawa and M.J. Vilkas. Relativistic quantum mechanics of many-electron systems. *Journal of Molecular Structure*, 573:139–169, 2001.

[Jao08] B. Jaoul. *Étude de la plasticité et application aux métaux.* Presse des Mines, Collection Sciences de la matière, 2008.

[JGP93] B.G. Johnson, P.M.W. Gill, and J.A. Pople. The performance of a family of density functional methods. *The Journal of Chemical Physics*, 98:5612–5626, 1993.

[Joh09] C. Johnson. *Numerical solutions of partial differential equations by the finite element method.* Dover Publications, 2009.

[JT03] M.J.T. Jordan and K.C. Thompson. The response of a molecule to an external electric field: predicting structural and spectroscopic change. *Chemical Physics Letters*, 370:14–20, 2003.

[Kit04] C. Kittel. *Introduction to solid state physics.* John Wiley Sons Inc, 2004.

[KM93] T. Koga and K. Matsui. Optimal Hylleraas wave functions. *Zeitschrift für Physik D*, 27:97–102, 1993.

[KM12] D. El Kass and R. Monneau. Atomic to continuum passage for nanotubes. Part II: error estimates. 2012.

[KOB+02] G. Klimeck, F. Oyafuso, T.B. Boykin, R.C. Bowen, and P. von Allmen. Development of a nanoelectronic 3-D (NEMO 3-D) simulator for multimillion atom simulations and its application to alloyed quantum dots. *Computer Modeling in Engineering and Sciences*, 3(5):601–642, 2002.

[Kob12] J. Kobus. A finite difference Hartree-Fock program for atoms and diatomic molecules. *Computer Physics Communications*, 2012.

[Kum00] P. Kumar. Finite element method computations in unbounded domains with nonzero but uniform far field decay. *Computers and Structures*, 75:457–462, 2000.

[Lad95] P. Ladevèze. Les bases de la méthode des erreurs en relation de comportement pour le contrôle adaptatif des calculs éléments finis. *Rapport interne n°163,LMT-Cachan*, 1995.

[Lar00] M.G. Larson. A posteriori and a priori error analysis for finite element approximations of self-adjoint elliptic eigen-value problems. *SIAM Journal of Numerical Analysis*, 38(2):608–625, 2000.

[LC88] L. Lemaitre and J.-L. Chaboche. *Mécanique des matériaux solides.* Dunod, 1988.

[LCT72] P.-J. Lin-Chung and S. Teitler. Relativistic pseudopotential method. *Physical Review B*, 6(4):1419–1425, 1972.

[Le 05] C. Le Bris. *Systèmes multi-échelles : modélisation et simulation.* Springer, 2005.

[Leo88] J.-F. Leon. Excited states for Coulomb systems in the Hartree-Fock approximation. *Communications in Mathematical Physics*, 120:261–268, 1988.

[Lew02] M. Lewin. The multiconfiguration methods in quantum chemistry: Palais-Smale condition and existence of minimizers. *Comptes-Rendus de l'Académie des Sciences Paris, Série I*, pages 299–304, 2002.

[Lew04] M. Lewin. Solutions of the multiconfiguration equations in quantum chemistry. *Archive for Rational Mechanics and Analysis*, 171:83–114, 2004.

[Lio87] P.L. Lions. Solutions of Hartree-Fock equations for Coulomb systems. *Communications in Mathematical Physics*, 109:33–97, 1987.

[LL05] C. Le Bris and J.L. Lions. From atoms to crystals: a mathematical journey. *Bulletin of the American Mathematical Society*, 42(3):291–363, 2005.

[LMZ91] P. Lazzeretti, M. Malagoli, and R. Zanasi. Coupled Hatree-Fock calculations of magnetic properties of the benzene molecule. *Journal of Molecular Structure*, 234:127–145, 1991.

[LOS10] B. Langwallner, C. Ortner, and E. Süli. Existence and convergence results for the Galerkin approximation of an electronic density functional. *Mathematical Models and Methods in Applied Sciences*, 20(12):2237–2265, 2010.

[Low55] P.-O. Lowdin. Quantum theory of many-particle sysems. I. Physical interpretations by means of density matrices, natural spin-orbitals, and convergence problems in the method of configurational interaction. *Physical Review*, 97(6), 1955.

[LS77] E.H. Lieb and B. Simon. The Hartree-Fock theory for Coulomb systems. *Communications in Mathematical Physics*, 53:185–194, 1977.

[LS85] F.S. Levin and J. Shertzer. Finite-element solution of the Schrödinger equation for the helium ground state. *Physical Review A*, 32(6):3285–3290, 1985.

[LSP+11] J.S. Lundeen, B. Sutherland, A. Patel, C. Stewart, and C. Bamber. Direct measurement of the quantum wavefunction. *Nature*, 474:188–191, 2011.

[Men69] D. Mendelejew. *Ueber die Beziehungen der Eigenschaften su den Atomgewichten der Elemente. In: Zeitschrift für Chemie.* 1869.

[MGC93] F. Mauri, G. Galli, and R. Car. Orbital formulation for electronic-structure calculations with linear system-size scaling. *Physical Review B*, 47:9973–9976, 1993.

[MH09] D. Marx and J. Hutter. *Ab initio molecular dynamics.* Cambridge University Press, 2009.

[MHH12] M. Miyasita, K. Higuchi, and M. Higuchi. An alternative scheme for calculating the unrestricted Hartree-Fock equation: Application to the boron and neon atoms. *Physica B*, 407:2758–2762, 2012.

[MMC90] H.D. Meyer, U. Manthe, and L.S. Cederbaum. The multi-configurational time-dependent Hartree approach. *Chemical Physics Letters*, 165(1):73–78, 1990.

[Mor06] M. Moreaud. *Propriétés morphologiques multi-échelles et prévision du comportement diélectrique de nanocomposites.* PhD thesis, École des Mines de Paris, 2006.

[MP34] C. Moller and M.S. Plesset. Note on an approximation treatment for many-electrons systems. *Physical Review*, 46:618–622, 1934.

[MP76] H.J. Monkhorst and J.D. Pack. Special points for Brillouin-zone integrations. *Physical Review B*, 13(12):5188–5192, 1976.

[MP89] M. Methfessel and A.T. Paxton. High-precision sampling for Brillouin-zone integration in metals. *Physical Review B*, 40(6):3616–3621, 1989.

[MR08] Y. Maday and U. Razafison. A reduced basis method applied to the restricted Hartree-Fock equations. *Comptes-Rendus de l'Académie des Sciences Paris, Série I*, 346:243–248, 2008.

[MT03] Y. Maday and G. Turinici. Error bars and quadratically convergent methods for the numerical simulation of the Hartree-Fock equations. *Numerische Mathematik*, 94(4):739–770, 2003.

[NB76] S. Nordholm and G. Bacskay. Generalized finite element method applied to the calculation of continuum states. *Chemical Physcis Letters*, 42(2):259–263, 1976.

[NFP+11] S. Nikolov, H. Fabritius, M. Petrov, M. Friák, L. Lymperakis, C. Sachs, D. Raabe, and J. Neugebauer. Robustness and optimal use of design principles of arthropod exoskeletons studied by ab initio-based multiscale simulations. *Journal of the Mechanical Behavior of Biomedical Materials*, 4:129–145, 2011.

[NLK86] D. Neuhauser, K. Langanke, and S.E. Koonin. Hartree-Fock calculations of atoms and molecular chains in strong magnetic fields. *Physical Review A*, 33(3):2084–2086, 1986.

[NM85a] O.H. Nielsen and R.M. Martin. Quantum-mechanical theory of stress and force. *Physical Review B*, 32(6):3780–3791, 1985.

[NM85b] O.H. Nielsen and R.M. Martin. Stresses in semiconductors: *Ab initio* calculations on Si, Ge and GaAs. *Physical Review B*, 32(6):3792–3805, 1985.

[NMCO08] F. Nascimiento, P. Mei, L. Cardoso, and J. Otubo. Grain size effect on the structural parameters of the stress induced $e_{hcp}$- martensite in iron-based shape memory alloy. *Materials Research*, 11(1):63–67, 2008.

[Nou10] A. Nouy. A priori model reduction through Proper Generalized Decomposition for solving time-dependent partial differential equations. *Computer Methods in Applied Mechanics and Engineering*, 199:160–1626, 2010.

[NP06] L. Navarro and E. Pérez. Paul Ehrenfest: The genesis of the adiabatic hypothesis, 1911-1914. *Archive for History of Exact Sciences*, 60:209–267, 2006.

[OBN+05] J.T. Oden, I. Babuška, F. Nobile, Y. Feng, and R. Tempone. Theory and methodology for estimation and control of errors due to modeling, approximation, and uncertainty. *Computer Methods in Applied Mechanics and Engineering*, 194:195–204, 2005.

[ODMG95] P. Ordejón, D.A. Drabold, R.M. Martin, and M.P. Grumbach. Linear system-size scaling methods for electronic-structure calculations. *Physical Review B*, 51:1456–1476, 1995.

[OM76] N.S. Ostlund and D.L. Merrifield. Ghost orbitals and the basis set extension effects. *Chemical Physics Letters*, 39(3):612–614, 1976.

[OP02] J.T. Oden and S. Prudhomme. Estimation of modeling error in computational mechanics. *Journal of Computational Physics*, 182:496–515, 2002.

[OPNZ00] A.A. Oliferenko, V.A. Palyulin, A.V. Neiman, and N.S. Zefirov. A new topological model for the calculation of partial atomic charges. *Doklady Chemistry*, 375:281–284, 2000.

[OPW+03] J.T. Oden, S. Prudhomme, T. Westermann, J. Bass, and M.E. Botkin. Estimation of eigenfrequencies for elasticity and shell problems. *Mathematical Models and Methods in Applied Sciences*, 13(3):323–344, 2003.

[OT11] T. Ozaki and M. Toyoda. Accurate finite element method for atomic calculations based on density functional theory and Hartree-Fock method. *Computer Physics Communications*, 182:1245–1252, 2011.

[OVM99] J.T. Oden, K. Vemaganti, and N. Moës. Hierarchical modeling of heterogeneous solids. *Computer Methods in Applied Mechanics and Engineering*, 172(1-4):3–25, 1999.

[OZ97] J.T. Oden and T.I. Zohdi. Analysis and adaptive modeling of highly heterogeneous elastic structures. *Computer Methods in Applied Mechanics and Engineering*, 148:367, 1997.

[PA08] P. Pyykkö and M. Atsumi. Molecular single-bond covalent radii for elements 1-118. *Chemistry-A European Journal*, 15(1):186–197, 2008.

[Pau25] W. Pauli. Über den Zusammenhang des Abschlusses der Elektronengruppen im Atom mit der Komplexstruktur der Spektren. *Zeitschrift für Physik*, 31:765–783, 1925.

[PB82] G.D. Purvis and R.J. Bartlett. A full coupled-cluster singles and doubles model: The inclusion of disconnected triples. *Journal of Chemical Physics*, 76(4):1910–1919, 1982.

[PBE96] J.P. Perdew, K. Burke, and M. Ernzerhof. Generalized gradient approximation made simple. *Physical Review Letters*, 77(18):3865–3868, 1996.

[PBO06] S. Prudhomme, P.T. Bauman, and J.T. Oden. Error control for molecular statics problems. *International Journal for Multiscale Computational Engineering*, 4(5-6):647–662, 2006.

[PCDB09] S. Prudhomme, L. Chamoin, H. Ben Dhia, and P.T. Bauman. An adaptive strategy for the control of modeling error in two-dimensional atomic-to-continuum coupling simulations. *Computer methods in applied mechanics and engineering*, 198, 2009.

[Pic89] W.E. Pickett. Pseudopotential methods in condensed matter applications. *Computer Physics Reports*, 9(3):115 – 197, 1989.

[PJS94] D.R. Plante, W.R. Johnson, and J. Sapirstein. Relativistic all-order many-body calculations of the n=1 and n=2 states of heliumlike ions. *Physical Review A*, 49(5):3519–3530, 1994.

[PKS+09] R. Pellenq, A. Kushima, R. Shahsavari, K.J. Van Vliet, M.K. Buehler, S. Yip, and F.-J. Ulm. A realistic molecular model of cement hydrates. *Proceedings of the National Academy of Sciences*, 106(38):16102–16107, 2009.

[P.P82] P.Pulay. Improved SCF convergence acceleration. *Journal of Computational Chemistry*, 3:556–560, 1982.

[PS05] J.E. Pask and P.A. Sterne. Finite element methods in ab initio electronic structure calculations. *Modelling and Simulation in Materials Science and Engineering*, 13:R71–R96, 2005.

[PSK08] M. Praprotnik, L. Delle Site, and K. Kremer. Multiscale simulation of soft matter: from scale bridging to adaptive resolution. *Annual Review of Physical Chemistry*, 59:545–571, 2008.

[PTA+92] M.C. Payne, M.P. Teter, D.C. Allan, T.A. Arias, and J.D. Joannopoulos. Iterative minimization techniques for ab initio total-energy calculations: molecular dynamics and conjugate gradients. *Reviews of Modern Physics*, 64(4):1045–1097, 1992.

[RC04] S. Ragot and P. Cortona. Correlation energy of many-electron systems: a modified Coll-Salvetti approach. *Journal of Chemical Physics*, 121(16), 2004.

[RJR+07] F. Reichel, L.P.H. Jeurgens, G. Richter, P.A. van Aken, and E.J. Mittemeijer. The origin of high-mismatch orientation relationships for ultra-thin oxide overgrowths. *Acta Materialia*, 55:6027–6037, 2007.

[RMG65] S. Rolland, J.F. Le Men, and L. Galatry. Énergies, fonctions propres et moment dipolaire d'une molécule diatomique polaire dans un champ électrique uniforme. *Le Journal de Physique*, 26:297–302, 1965.

[Roo51] C.C.J. Roothaan. New developments in molecular orbital theory. *Reviews of modern physics*, 23(2):69–89, 1951.

[RSL63] R.M. Pitzer R.M. Stevens and W.N. Lipscomb. Perturbed Hartree-Fock calculations. I. Magnetic susceptibility and shielding in the LiH molecule. *Journal of Chemical Physics*, 38(2):550–560, 1963.

[Rui05a] M.B. Ruiz. Hylleraas method for many-electron atoms. I. The Hamiltonian. *International Journal of Quantum Chemistry*, 101:246–260, 2005.

[Rui05b] M.B. Ruiz. Hylleraas method for many-electron atoms. II. Integrals over wave functions with one interelectronic coordinate. *International Journal of Quantum Chemistry*, 101:261–273, 2005.

[Sar09] R.G. Sargent. Verification and validation of simulation models. In *Proceedings of the 2009 winter simulation conference*, pages 162–176, 2009.

[SB02] K. Schwarz and P. Blaha. Quantum mechanical computations at the atomic scale for material sciences. In *Fifth World Congress on Computational Mechanics*, 2002.

[Sch26a] E. Schrödinger. Quantization as an eigenvalue problem. *Annalen der Physik*, 79, 1926.

[Sch26b] E. Schrödinger. An undulatory theory of the mechanics of atoms and molecules. *Physical Review*, 28(6):1049–1070, 1926.

[Sch79] S. Schlesinger. Terminology for model credibility. *Simulation*, 32(3), 1979.

[Sch09] R. Schneider. Analysis of the projected coupled cluster method in electronic structure calculation. *Numerische Mathematik*, 113:433–471, 2009.

[Sch11] Schrödinger, Inc., http://www.schrodinger.com/. *Jaguar Schrödinger*, 2011 (accessed December 5, 2011).

[Scr95] A. Scrinzi. A 3-dimensional finite elements procedure for quantum mechanical applications. *Computer Physics Communications*, 86:67–80, 1995.

[SCS10] Y. Saad, J.R. Chelikowsky, and S.M. Shontz. Numerical methods for electronic structure calculations of materials. *SIAM Review*, 52(1):3–54, 2010.

[SH73] V.R. Saunders and I.H. Hillier. A "level-shifting" method for converging closed shell Hartree-Fock wave functions. *International Journal of Quantum Chemistry*, 7:699–705, 1973.

[Sla24] J.C. Slater. Compressibility of the alkali halides. *Physical Review*, 23(4):488–500, 1924.

[Sla29] J.C. Slater. Theory of complex spectra. *Physical Review*, 34:1293–1322, 1929.

[Sla30] J.C. Slater. Atomic shielding constants. *Physical Review*, 36:57–64, 1930.

[Sla32] J.C. Slater. Analytic atomic wave functions. *Physical Review*, 42:33–43, 1932.

[Sla37] J.C. Slater. Wave functions in periodic potential. *Physical Review*, 51(10):846–851, 1937.

[Sla51] J.C. Slater. Magnetic effects and the Hartree-Fock equation. *Physical Review*, 82(4):538–541, 1951.

[SM63] R.L. Smith and J.W. Miser. Compilation of the properties of lithium hydride. *Lewis Research Center, NASA*, 1963.

[SO90a] D. Sundholm and J. Olsen. Large multiconfigurational Hartree-Fock calculations on the hyperfine structure of Li($^2S$) and Li($^2P$). *Physical Review A*, 42:2614–2621, 1990.

[SO90b] D. Sundholm and J. Olsen. Nuclear quadrupole moments of $^{33}$S and $^{35}$S. *Physical Review A*, 42:1160–1164, 1990.

[SO93] D. Sundholm and J. Olsen. Finite-element multiconfiguration Hartree-Fock calculations of the atomic quadrupole moments of excited states of Be, Al, In, Ne, Ar, Kr, and Xe. *Physical Review A*, 47:2672–2679, 1993.

[SO95] D. Sundholm and J. Olsen. Finite-element multiconfiguration Hartree-Fock calculations of electron affinities of manganese. *Chemical Physics Letters*, 233:115–122, 1995.

[SO96] A. Szabo and N. Ostlund. *Modern Quantum Chemistry: Introduction to Advanced Electronic Structure Theory.* Dover Publications, 1996.

[Szc01] A. Szczech. Extrema of Hartree-Fock type functionals. *Reports on Mathematical Physics*, 48(3):397–406, 2001.

[TCA08a] V. Tognetti, P. Cortona, and C. Adamo. Increasing physical constraints and improving performances in a parameter-free GGA functional. *Chemical Physics Letters*, 460:536–539, 2008.

[TCA08b] V. Tognetti, P. Cortona, and C. Adamo. A new parameter-free correlation functional based on an average atomic reduced density gradient analysis. *Journal of Chemical Physics*, 128:034101, 2008.

[Thi03] J.M. Thijssen. *Computational Physics.* Cambridge University Press, 2003.

[Tho11] A. Thorel. *Un certain regard sur les matériaux - Les relations entre l'élaboration, la microstructure et les propriétés des matériaux.* Presse des Mines, Collection Sciences de la matière, 2011.

[TJ96] A.Y. Toukmaji and J.A. Board Jr. Ewald summation techniques in perspective: a survey. *Computer Physics Communications*, 95:73–92, 1996.

[TSP98] M. Tokman, D. Sundholm, and P. Pyykkö. Nuclear quadrupole moments of gallium isotopes obtained from finite-element MCHF calculations on the $4p^2\mathrm{P}_{3/2}$ state of Ga. *Chemical Physics Letters*, 291:414–418, 1998.

[TT95a] E. Tsuchida and M. Tsukada. Electronic-structure calculations based on the finite-element method. *Physical Review B*, 52(8):5573–5578, 1995.

[TT95b] E. Tsuchida and M. Tsukada. Real space approach to electronic-structure calculations. *Solid State Communications*, 94(1):5–8, 1995.

[TT96] E. Tsuchida and M. Tsukada. Adaptive finite-element method for electronic-structure calculations. *Physical Review B*, 54(11):7602–7605, 1996.

[TT98] E. Tsuchida and M. Tsukada. Large-scale electronic-structure calculations based on the adaptive finite-element method. *Journal of the Physical Society of Japan*, 62(11):3844–3858, 1998.

[TTAS11] B.Y. Tian, B. Tie, A. Aubry, and X.Y. Su. Elastic wave propagation in periodic cellular structures. *Computer Modeling in Engineering and Sciences*, 76, 2011.

[VAS11] VASP Group, Universität Wien, http://cms.mpi.univie.ac.at/vasp/. *VASP*, 2011 (accessed December 5, 2011).

[vBG80] U. von Barth and C.D. Gelatt. Validity of the frozen-core approximation and pseudopotential theory for cohesive energy calculations. *Physical Review B*, 21:2222–2228, 1980.

[Ver96] R. Verfürth. *A review of a posteriori error estimation and adaptive mesh-refinement techniques.* Wiley/Teubner, 1996.

[vHWvdK03] R.P.J. van Hees, T.J. Wijffels, and L.J.A.R. van der Klugt. Thaumasite swelling in historic mortars: field observations and laboratory research. *Cement and Concrete Composites*, 25:1165–1171, 2003.

[VO01] K. Vemaganti and J.T. Oden. Estimation of local modeling error and goal-oriented modeling of heterogeneous materials. *Journal of Computational Physics*, 164(22), 2001.

[Wei02] J.H. Weiner. *Statistical mechanics of elasticity.* Dover Publications, 2002.

[WM80] H.-J. Werner and W. Meyer. A quadratically convergent multiconfiguration-self-consistent field method with simultaneous optimization of orbitals and CI coefficients. *Journal of Chemical Physics*, 73(5):2342–2356, 1980.

[YC82] M.T. Yin and M.L. Cohen. Theory of ab initio pseudopotential calculations. *Physical review B*, 25(12):7403–7412, 1982.

[YDP93] D.M. York, T.A. Darden, and L.G. Pedersen. The effect of long-range electrostatic interactions in simulations of macromolecular crystals: A comparison of the Ewald and truncated list methods. *Journal of Chemical Physics*, 99(10):8345–8348, 1993.

[You01] D. Young. *Computational chemistry: A practical guide for applying techniques to real-world problems.* Hardcover, 2001.

[ZT05] O.C. Zienkiewicz and R.L. Taylor. *The finite element method.* Butterworth-Heinemann, 2005.

[ZY04] W. Zheng and L.-A. Ying. Finite element approximations to the discrete spectrum of the Schrödinger operator with the Coulomb potential. *SIAM Journal on Numerical Analysis*, 42(1), 2004.

[ZYD04] W. Zheng, L. Ying, and P. Ding. Numerical solutions of the Schrödinger equation for the ground lithium by the finite element method. *Applied Mathematics and Computation*, 153:685–695, 2004.

# Appendices

# Appendix A

# A brief description of microscopes

To investigate experimentally the structure of a material, there are two main approaches available which are microscopy or physico-chemical analyses. In this Appendix, we present a brief summary of the different families of microscopes employed to obtain images of samples.

### Optical microscopy

Historically, the first technique developped was optical or light microscopy. It uses visible light transmitted through or reflected from the sample. A single or multiple lenses magnify the view of the sample. Optical microscopy has three major limitations. Only dark and strongly refracting objects can be observed. The resolution is limited by diffraction approximately around $0,2\,\mu$m (and to 2000$\times$ magnification). Points outside the focal plane give an unfocused image which reduces the clarity of the picture.

Because resolution depends on the wavelength of the input wave according to Bragg's law, an idea was to develop microscopes with a low-wavelength input wave. X-ray microscopy has a better resolution than optical microscopy, but it is less common than electron microscopy which has a better resolution.

### Electron microscopy

Electron microscopes produce electronically magnified images of samples. They use an electron beam, which is focused by electrostatic and electromagnetic fields used as "lenses". The wavelength of electrons is about 100,000 times shorter than the visible light wavelength. Therefore, the diffraction limit is lower and their magnification is better. It can go to 2,000,000×.

The original form of electron microscopes is the transmission electron microscope (TEM). It uses a high-voltage electron beam (40 to 400 keV) which is partially scattered by the specimen. The transmitted electron beam contains information about the structure of the specimen. It is projected onto a viewing screen coated with a fluorescent material, such as phosphorus, or scintillating material such as zinc sulfide.

The resolution of TEM is limited by spherical aberration. However, hardwares correcting this aberration have been developed to create the High Resolution TEM (HRTEM). This new technology gives images with resolution below $0,5.10^{-10}$ m.

With the scanning electron microscope (SEM), the electron beam does not contain information about the specimen. The electron beam loses energy in contact with the specimen which converts it into other forms such as the emission of low-energy electrons (conventionally used signal), light emission (cathodoluminescence) or X-ray emission. The SEM maps the intensity of any of these signals.

Its resolution is generally about one order of magnitude poorer than the one of a TEM. However, SEMs are interesting since they provide a great depth of field, and give a good three-dimensional representation of the sample.

TEMs and SEMs are the most widely used electron microscopes. Among other electron microscopes, the Reflection Electron Microscope (REM) detects the reflected beam of elastically scattered electrons. The Low-Voltage Electron Microscope (LVEM) uses a relatively low electron voltage of 5 kV. The weakness of the voltage improves the contrast of the image, which reduces or even eliminates the need to stain polymers to enhance contrast. Generally, the samples need to be thinner (20-65 nm) than samples for TEM microscopes.

Electron microscopes require stable high-voltage supplies, stable currents for electromagnetic lens, pumped vacuum systems, cooling water circulation through the lenses, and special devices to cancel the external magnetic field.

Beyond light or electrons, other particles can be used to ray the sample. Particle accelerators use magnetic and electric fields to propel charged particles to high speed. They provide high quality wave source: high intensity, large wavelength spectrum, high stability. With X-ray diffraction, they allow for the study of cristallography. To get a high resolution, the atomic de Broglie microscope is currently being developed. It will use neutral Helium atoms as probe particles and will give a nanometer-order resolution [DGR+99].

Another microscopy is the scanning probe microscopy.

### Scanning probe microscopy

Scanning probe microscopes are based on atomic-scale interactions. It does not focus on the interaction between a wave and the sample, but between a probe and the sample. A probe tip scans the sample in the vicinity of it to collect information and build a picture of it.

The resolution varies depending on the technique used. It is limited by the size of the volume of interaction between the probe and the sample, which is largely dependent on the size of the probe. Currently, probes with a tip radius of 5-10 nm can be produced.

Scanning tunneling microscopy (STM) relies on quantum tunneling. It allows the aquisition of the map of the electronic densities for conductor materials. According to [Bai00], a good STM resolution is 0.1 nm lateral resolution and 0.01 nm depth resolution.

Atomic force microscopy (AFM) gives the topography of the surface of the sample. It is based on the attractions and repulsions between the atoms of the surface of the sample and the probe tip. Depending on the application, it can be used in contact (static) modes or in non-contact (dynamic) modes where the cantilever is vibrated. The resolution is about 10 nm lateral resolution and 0.1 nm depth resolution. It can be used for non-conductor materials.

Scanning near-field optical microscope collects evanescent waves at the vicinity of the sample (at a distance much smaller than the wavelength of the light). With this technique, the critical parameter is the size of the detector aperture. The resolutions are about 20 nm for lateral directions and 2-5 nm for the vertical direction.

# Appendix B

# Periodic Table

The periodic table is a tabular presentation of the 118 known chemical elements. Although there were precursors, the periodic table is generally credited to Mendeleev [Men69].

Elements are presented by increasing atomic number, the number of protons in the nucleus. By definition, each element has a specific atomic number. For uncharged atoms, the number of electrons is equal to the atomic number. Thus, provided the number and the nature of atoms to be simulated, this table allows for the determination of the total number of electrons in the system.

The horizontal rows are called periods. The vertical columns lump together elements with similar properties *e.g.* alkali metals, halogens, noble gases. Therefore, the horizontal rows contain some gaps.

| | | | | | | | | | | | | | | | | | |
|---|---|---|---|---|---|---|---|---|---|---|---|---|---|---|---|---|---|
| $^{1}$H | | | | | | | | | | | | | | | | | $^{2}$He |
| $^{3}$Li | $^{4}$Be | | | | | | | | | | | $^{5}$B | $^{6}$C | $^{7}$N | $^{8}$O | $^{9}$F | $^{10}$Ne |
| $^{11}$Na | $^{12}$Mg | | | | | | | | | | | $^{13}$Al | $^{14}$Si | $^{15}$P | $^{16}$S | $^{17}$Cl | $^{18}$Ar |
| $^{19}$K | $^{20}$Ca | $^{21}$Sc | $^{22}$Ti | $^{23}$V | $^{24}$Cr | $^{25}$Mn | $^{26}$Fe | $^{27}$Co | $^{28}$Ni | $^{29}$Cu | $^{30}$Zn | $^{31}$Ga | $^{32}$Ge | $^{33}$As | $^{34}$Se | $^{35}$Br | $^{36}$Kr |
| $^{37}$Rb | $^{38}$Sr | $^{39}$Y | $^{40}$Zr | $^{41}$Nb | $^{42}$Mo | $^{43}$Tc | $^{44}$Ru | $^{45}$Rh | $^{46}$Pd | $^{47}$Ag | $^{48}$Cd | $^{49}$In | $^{50}$Sn | $^{51}$Sb | $^{52}$Te | $^{53}$I | $^{54}$Xe |
| $^{55}$Cs | $^{56}$Ba | $^{57}$La | $^{72}$Hf | $^{73}$Ta | $^{74}$W | $^{75}$Re | $^{76}$Os | $^{77}$Ir | $^{78}$Pt | $^{79}$Au | $^{80}$Hg | $^{81}$Tl | $^{82}$Pb | $^{83}$Bi | $^{84}$Po | $^{85}$At | $^{86}$Rn |
| $^{87}$Fr | $^{88}$Ra | $^{89}$Ac | | | | | | | | | | | | | | | |

| | | | | | | | | | | | | | |
|---|---|---|---|---|---|---|---|---|---|---|---|---|---|
| $^{58}$Ce | $^{59}$Pr | $^{60}$Nd | $^{61}$Pm | $^{62}$Sm | $^{63}$Eu | $^{64}$Gd | $^{65}$Tb | $^{66}$Dy | $^{67}$Ho | $^{68}$Er | $^{69}$Tm | $^{70}$Yb | $^{71}$Lu |
| $^{90}$Th | $^{91}$Pa | $^{92}$U | $^{93}$Np | $^{94}$Pu | $^{95}$Am | $^{96}$Cm | $^{97}$Bk | $^{98}$Cf | $^{99}$Es | $^{100}$Fm | $^{101}$Md | $^{102}$No | $^{103}$Lw |

Table B.1: Periodic table of the elements

# Appendix C

# Atomic units

Using the international system of units is cumbersome to describe the nanoscale quantities. It is more convenient to employ the so-called atomic units system.

Two families of atomic units exist: the Hartree atomic units and the Rydberg atomic units, which differ in the choice of the mass unit and the charge unit. In the Hartree system, the mass unit and the charge unit are respectively the electron rest mass $m_e$ and the elementary charge $e$. In the Rydberg system, they are $2m_e$ and $\frac{e}{\sqrt{2}}$. In this dissertation, we use only the Hartree system.

Table C.1 specifies the physical constants chosen as the fundamental units in the Hartree system.

| **Dimension** | **Name** | **Symbol** | **Value in SI units** |
|---|---|---|---|
| Mass | Electron rest mass | $m_e$ | $9,110.10^{-31}$ kg |
| Charge | Elementary charge | $e$ | $1,603.10^{-19}$ C |
| Angular momentum | Reduced Planck's constant | $\hbar = \frac{h}{2\pi}$ | $1,055.10^{-34}$ J.s |
| Electric constant | Coulomb's constant | $\kappa = \frac{1}{4\pi\varepsilon_0}$ | $8,988.10^{9}$ kg.m$^3$.s$^{-2}$.C$^{-2}$ |

Table C.1: Fundamental units of the Hartree atomic system

We highlight that all the elementary quantities (length, time, mass, electric current, thermodynamic temperature, amount of substance and luminous intensity) not have an atomic unit. For example, for electromagnetic studies, the atomic units system is complemented by some SI units or cgs units.

From the four fundamental atomic units, we can derive other units. Table C.2 mentions some derived atomic units.

| **Dimension** | **Name** | **Symbol** | **Expression** | **Value in SI units** |
|---|---|---|---|---|
| Length | Bohr radius | $a_0$ | $\frac{4\pi\varepsilon_0\hbar^2}{m_e e^2}$ | $5,292.10^{-11}$ m |
| Energy | Hartree energy | Ha | $\frac{\hbar^2}{m_e a_0^2} = m_e \left(\frac{e^2}{4\pi\varepsilon_0\hbar}\right)^2$ | $4,360.10^{-18}$ J |
| Time | | | $\frac{\hbar}{E_h}$ | $2,419.10^{-17}$ s |
| Electric field | | | $\frac{E_h}{e.a_0}$ | $5,142.10^{11}$ V.m$^{-1}$ |
| Force | | | $\frac{E_h}{a_0}$ | $8,239.10^{-8}$ N |
| Pressure | | | $\frac{E_h}{a_0^3}$ | $2,942.10^{13}$ Pa |

Table C.2: Derived units of the atomic system

# Appendix D

# Electron configurations of the atoms

Appendix B contains the periodic table, which gives the number of protons specific to each chemical element. For uncharged systems, the number of electrons in the electronic cloud is equal to the number of protons in the nucleus. Beyond the number of electrons, the key information is the electron configuration, *i.e.* the distribution of the electrons in the spectrum of the one-electron eigenmodes.

The electron configuration can be established by the Aufbau principle, also called the "building-up" principle. This Appendix lists the electron configurations of the 94 atoms which occur naturally on Earth.

Among all the electrons of the electronic cloud, the chemical properties are determined by the valence electrons, *i.e.* the electrons related to the outermost modes far from the nucleus. Therefore, atoms with the same valence configuration exhibit similar properties.

| Element | | Z | Electron Configuration | Element | | Z | Electron Configuration |
|---|---|---|---|---|---|---|---|
| Hydrogen | H | 1 | $1s^1$ | Cadmium | Cd | 48 | $[Kr]\ 5s^2\ 4d^{10}$ |
| Helium | He | 2 | $1s^2$ | Indium | In | 49 | $[Kr]\ 5s^2\ 4d^{10}\ 5p^1$ |
| Lithium | Li | 3 | $1s^2\ 2s^1$ | Tin | Sn | 50 | $[Kr]\ 5s^2\ 4d^{10}\ 5p^2$ |
| Beryllium | Be | 4 | $1s^2\ 2s^2$ | Antimony | Sb | 51 | $[Kr]\ 5s^2\ 4d^{10}\ 5p^3$ |
| Boron | B | 5 | $1s^2\ 2s^2\ 2p^1$ | Tellurium | Te | 52 | $[Kr]\ 5s^2\ 4d^{10}\ 5p^4$ |
| Carbon | C | 6 | $1s^2\ 2s^2\ 2p^2$ | Iodine | I | 53 | $[Kr]\ 5s^2\ 4d^{10}\ 5p^5$ |
| Nitrogen | N | 7 | $1s^2\ 2s^2\ 2p^3$ | Xenon | Xe | 54 | $[Kr]\ 5s^2\ 4d^{10}\ 5p^6$ |
| Oxygen | O | 8 | $1s^2\ 2s^2\ 2p^4$ | Caesium | Cs | 55 | $[Xe]\ 6s^1$ |
| Fluorine | F | 9 | $1s^2\ 2s^2\ 2p^5$ | Barium | Ba | 56 | $[Xe]\ 6s^2$ |
| Neon | Ne | 10 | $1s^2\ 2s^2\ 2p^6$ | Lanthanum | La | 57 | $[Xe]\ 6s^2\ 5d^1$ |
| Sodium | Na | 11 | $1s^2\ 2s^2\ 2p^6\ 3s^1$ | Cerium | Ce | 58 | $[Xe]\ 6s^2\ 4f^1\ 5d^1$ |
| Magnesium | Mg | 12 | $1s^2\ 2s^2\ 2p^6\ 3s^2$ | Praseodymium | Pr | 59 | $[Xe]\ 6s^2\ 4f^3$ |
| Aluminium | Al | 13 | $1s^2\ 2s^2\ 2p^6\ 3s^2\ 3p^1$ | Neodymium | Nd | 60 | $[Xe]\ 6s^2\ 4f^4$ |
| Silicon | Si | 14 | $1s^2\ 2s^2\ 2p^6\ 3s^2\ 3p^2$ | Promethium | Pm | 61 | $[Xe]\ 6s^2\ 4f^5$ |
| Phosphorus | P | 15 | $1s^2\ 2s^2\ 2p^6\ 3s^2\ 3p^3$ | Samarium | Sm | 62 | $[Xe]\ 6s^2\ 4f^6$ |
| Sulfur | S | 16 | $1s^2\ 2s^2\ 2p^6\ 3s^2\ 3p^4$ | Europium | Eu | 63 | $[Xe]\ 6s^2\ 4f^7$ |
| Chlorine | Cl | 17 | $1s^2\ 2s^2\ 2p^6\ 3s^2\ 3p^5$ | Gadolinium | Gd | 64 | $[Xe]\ 6s^2\ 4f^7\ 5d^1$ |
| Argon | Ar | 18 | $1s^2\ 2s^2\ 2p^6\ 3s^2\ 3p^6$ | Terbium | Tb | 65 | $[Xe]\ 6s^2\ 4f^9$ |
| Potassium | K | 19 | $[Ar]\ 4s^1$ | Dysprosium | Dy | 66 | $[Xe]\ 6s^2\ 4f^{10}$ |
| Calcium | Ca | 20 | $[Ar]\ 4s^2$ | Holmium | Ho | 67 | $[Xe]\ 6s^2\ 4f^{11}$ |
| Scandium | Sc | 21 | $[Ar]\ 4s^2\ 3d^1$ | Erbium | Er | 68 | $[Xe]\ 6s^2\ 4f^{12}$ |
| Titanium | Ti | 22 | $[Ar]\ 4s^2\ 3d^2$ | Thulium | Tm | 69 | $[Xe]\ 6s^2\ 4f^{13}$ |
| Vanadium | V | 23 | $[Ar]\ 4s^2\ 3d^3$ | Ytterbium | Yb | 70 | $[Xe]\ 6s^2\ 4f^{14}$ |
| Chromium | Cr | 24 | $[Ar]\ 4s^1\ 3d^5$ | Lutetium | Lu | 71 | $[Xe]\ 6s^2\ 4f^{14}\ 5d^1$ |

| | | | | | | | |
|---|---|---|---|---|---|---|---|
| Manganese | Mn | 25 | $[Ar]\ 4s^2\ 3d^5$ | Hafnium | Hf | 72 | $[Xe]\ 6s^2\ 4f^{14}\ 5d^2$ |
| Iron | Fe | 26 | $[Ar]\ 4s^2\ 3d^6$ | Tantalum | Ta | 73 | $[Xe]\ 6s^2\ 4f^{14}\ 5d^3$ |
| Cobalt | Co | 27 | $[Ar]\ 4s^2\ 3d^7$ | Tungsten | W | 74 | $[Xe]\ 6s^2\ 4f^{14}\ 5d^4$ |
| Nickel | Ni | 28 | $[Ar]\ 4s^2\ 3d^{10}$ | Rhenium | Re | 75 | $[Xe]\ 6s^2\ 4f^{14}\ 5d^5$ |
| | | | or $[Ar]\ 4s^1\ 3d^9$ | | | | |
| Copper | Cu | 29 | $[Ar]\ 4s^1\ 3d^{10}$ | Osmium | Os | 76 | $[Xe]\ 6s^2\ 4f^{14}\ 5d^6$ |
| Zinc | Zn | 30 | $[Ar]\ 4s^2\ 3d^{10}$ | Iridium | Ir | 77 | $[Xe]\ 6s^2\ 4f^{14}\ 5d^7$ |
| Gallium | Ga | 31 | $[Ar]\ 4s^2\ 3d^{10}\ 4p^1$ | Platinum | Pt | 78 | $[Xe]\ 6s^1\ 4f^{14}\ 5d^9$ |
| Germanium | Ge | 32 | $[Ar]\ 4s^2\ 3d^{10}\ 4p^2$ | Gold | Au | 79 | $[Xe]\ 6s^1\ 4f^{14}\ 5d^{10}$ |
| Arsenic | As | 33 | $[Ar]\ 4s^2\ 3d^{10}\ 4p^3$ | Mercury | Hg | 80 | $[Xe]\ 6s^2\ 4f^{14}\ 5d^{10}$ |
| Selenium | Se | 34 | $[Ar]\ 4s^2\ 3d^{10}\ 4p^4$ | Thallium | Tl | 81 | $[Xe]\ 6s^2\ 4f^{14}\ 5d^{10}\ 6p^1$ |
| Bromine | Br | 35 | $[Ar]\ 4s^2\ 3d^{10}\ 4p^5$ | Lead | Pb | 82 | $[Xe]\ 6s^2\ 4f^{14}\ 5d^{10}\ 6p^2$ |
| Krypton | Kr | 36 | $[Ar]\ 4s^2\ 3d^{10}\ 4p^6$ | Bismuth | Bi | 83 | $[Xe]\ 6s^2\ 4f^{14}\ 5d^{10}\ 6p^3$ |
| Rubidium | Rb | 37 | $[Kr]\ 5s^1$ | Polonium | Po | 84 | $[Xe]\ 6s^2\ 4f^{14}\ 5d^{10}\ 6p^4$ |
| Strontium | Sr | 38 | $[Kr]\ 5s^2$ | Astatine | At | 85 | $[Xe]\ 6s^2\ 4f^{14}\ 5d^{10}\ 6p^5$ |
| Yttrium | Y | 39 | $[Kr]\ 5s^2\ 4d^1$ | Radon | Rn | 86 | $[Xe]\ 6s^2\ 4f^{14}\ 5d^{10}\ 6p^6$ |
| Zirconium | Zr | 40 | $[Kr]\ 5s^2\ 4d^2$ | Francium | 87 | Fr | $[Rn]\ 7s^1$ |
| Niobium | Nb | 41 | $[Kr]\ 5s^1\ 4d^4$ | Radium | Ra | 88 | $[Rn]\ 7s^2$ |
| Molybdenum | Mo | 42 | $[Kr]\ 5s^1\ 4d^5$ | Actinium | Ac | 89 | $[Rn]\ 7s^2\ 6d^1$ |
| Technetium | Tc | 43 | $[Kr]\ 5s^2\ 4d^5$ | Thorium | Th | 90 | $[Rn]\ 7s^2\ 6d^2$ |
| Ruthenium | Ru | 44 | $[Kr]\ 5s^1\ 4d^7$ | Protactinium | Pa | 91 | $[Rn]\ 7s^2\ 5f^2\ 6d^1$ |
| Rhodium | Rh | 45 | $[Kr]\ 5s^1\ 4d^8$ | Uranium | U | 92 | $[Rn]\ 7s^2\ 5f^3\ 6d^1$ |
| Palladium | Pd | 46 | $[Kr]\ 4d^{10}$ | Neptunium | Np | 93 | $[Rn]\ 7s^2\ 5f^4\ 6d^1$ |
| Silver | Ag | 47 | $[Kr]\ 5s^1\ 4d^{10}$ | Plutonium | Pu | 94 | $[Rn]\ 7s^2\ 5f^6$ |

# Appendix E

# Quantum numbers

In classical mechanics, the characteristics of a material can range continously whereas quantum mechanics provide the quantization of observable quantities. Quantum numbers describe any quantum system by a discrete set of integers or half-integers. This Appendix describes briefly these numbers, for complements we refer to [Hla97, AF05].

Each operator $A$ that commutes with the Hamiltonian (*i.e.* satisfies the relation $AH = HA$) can be associated with a quantum number. An electronic wave function in an atom can be completely described by a set of four independent quantum numbers, but this set is not unique. Among the different models, we present here the set proposed by the Hund-Mulliken molecular orbital theory which describes electrons by the four quantum numbers $n$, $l$, $m$ and $m_s$.

The principal or first quantum number $n$ labels the $n$th eigenvalue of Hamiltonian with the contribution due to angular momentum left out. Therefore, it always have a positive integer value.

The azimuthal quantum number $l$, also known as the angular quantum number or the second quantum number gives the magnitude of the orbital angular momentum as: $L^2 = \bar{h}l(l+1)$. In the literature, an eigenmode for which $l = 0$ is called a s orbital, in the case of $l = 1$, $l = 2$ or $l = 3$, they are called respectively a p orbital, a d orbital or a f orbital.

The magnetic quantum number $m$ yields the projection of the orbital angular momentum

along a specific axis $L_z$. The values of $m$ range from $-l$ to $l$ with integer steps between them.

The spin projection quantum number $m_s$ gives the projection of the spin angular momentum $S$ along the specific axis: $S_z = m_s\bar{h}$. For an electronic wave function, the values of $m_s$ can be $-\frac{1}{2}$ or $\frac{1}{2}$.

According to Hund's rules, two electrons can never have the same set of quantum numbers.

# Appendix F

# The weak form of the Hartree-Fock system

This Appendix presents the calculation to get the weak form of the Hartree-Fock system from the Schrödinger equation. For the sake of clarity, the calculation is detailed in the case of a system comprising one nucleus with $Z$ protons located in $X$, and two electrons located respectively in $x_1$ and $x_2$. The two electrons are described by the wave function $\Psi_e$:

$$\begin{array}{rcccl} \Psi_e & : & x = (x_1, x_2) & \longmapsto & \Psi_e(x) \\ & & \mathbb{R}^6 & \longrightarrow & \mathbb{C}. \end{array}$$

The eigenpair $(\Psi_e, E_e)$ is solution of the Schrödinger problem (section 2.5):

$$\begin{aligned} \frac{1}{2}\left(\nabla_x \Psi_e, \nabla_x \delta\Psi_e\right) + \left(\left(V_{en} + V_{ee}\right)\Psi_e, \delta\Psi_e\right) = E_e\left(\Psi_e, \delta\Psi_e\right) + \frac{\delta E_e}{2}\left[\left(\Psi_e, \Psi_e\right) - 1\right] \\ + \delta\lambda\left[\Psi_e(x_{\sigma(1)}, x_{\sigma(2)}) - \mathrm{sg}\left(\sigma\right)\Psi_e(x_1, x_2)\right], \\ \forall \delta\Psi_e \in \mathsf{W},\ \forall \delta E_e \in \mathsf{W}^{E_e},\ \forall \delta\lambda \in \mathsf{W}^{\lambda}, \end{aligned} \quad \text{(F.1)}$$

where $E_e$ appears as a Lagrange multiplier associated with the unit norm of $\Psi_e$. $\delta E_e$ and $\delta\lambda$ are two test Lagrange multipliers.

The Hartree-Fock method solves the Schrödinger equation in the space $\mathsf{W}^{HF}$. The wave function $\Psi_e$ is approximated by a Slater determinant $\Psi_e^{HF}$ built from two orthonormal one-

electron wave functions $\varphi_1$ and $\varphi_2$ defined in $\mathbb{R}^3$:

$$\begin{cases} \Psi_e \sim \Psi_e^{HF} = \dfrac{1}{\sqrt{2}} \begin{vmatrix} \varphi_1(x_1) & \varphi_1(x_2) \\ \varphi_2(x_1) & \varphi_2(x_2) \end{vmatrix} \\ \int_{\mathbb{R}^3} \varphi_1^* \varphi_1 = \int_{\mathbb{R}^3} \varphi_2^* \varphi_2 = 1 \\ \int_{\mathbb{R}^3} \varphi_1^* \varphi_2 = \int_{\mathbb{R}^3} \varphi_2^* \varphi_1 = 0 \end{cases} \quad \text{where} \quad \begin{cases} \varphi_1 : x_1 \mapsto \varphi_1(x_1) \\ \qquad \mathbb{R}^3 \to \mathbb{C} \\ \varphi_2 : x_2 \mapsto \varphi_2(x_2) \\ \qquad \mathbb{R}^3 \to \mathbb{C}. \end{cases} \tag{F.2}$$

The normality and anti-symmetry of the solution is ensured by the form of the Hartree-Fock trial function. The orthonormalization of the one-electron wave functions is imposed by the Lagrange multipliers $\Lambda_{11}$, $\Lambda_{22}$ and $\Lambda_{12}$. We denote $\Phi = \begin{bmatrix} \varphi_1 \\ \varphi_2 \end{bmatrix}$ and $\Lambda = \begin{bmatrix} \Lambda_{11} & \Lambda_{12} \\ \Lambda_{21} & \Lambda_{22} \end{bmatrix}$. The Hartree-Fock problem reads:

$$\frac{1}{2}\left(\nabla_x \Psi_e^{HF}, \nabla_x \delta\Psi_e^{HF}\right) + \left((V_{en} + V_{ee})\, \Psi_e^{HF}, \delta\Psi_e^{HF}\right) = \delta\left[\mathrm{tr}\left[\frac{\Lambda}{2} \cdot \left(\left(\int_{\mathbb{R}^3} \Phi \otimes \Phi\right) - I\right)\right]\right].$$

We express this problem as a function of the one-electron wave functions. The electronic kinetic energy reads:

$$\left(\nabla_x \Psi_e^{HF}, \nabla_x \delta\Psi_e^{HF}\right) = \left(\nabla_{x_1} \Psi_e^{HF}, \nabla_{x_1} \delta\Psi_e^{HF}\right) + \left(\nabla_{x_2} \Psi_e^{HF}, \nabla_{x_2} \delta\Psi_e^{HF}\right)$$

where

$$\begin{aligned} \left(\nabla_{x_1} \Psi_e^{HF}, \nabla_{x_1} \delta\Psi_e^{HF}\right) &= \left(\nabla_{x_1}\varphi_1(x_1)\,\varphi_2(x_2) - \varphi_1(x_2)\,\nabla_{x_1}\varphi_2(x_1), \nabla_{x_1}\delta\varphi_1(x_1)\,\varphi_2(x_2)\right. \\ &\quad \left. + \nabla_{x_1}\varphi_1(x_1)\,\delta\varphi_2(x_2) - \delta\varphi_1(x_2)\,\nabla_{x_1}\varphi_2(x_1) - \varphi_1(x_2)\,\nabla_{x_1}\delta\varphi_2(x_1)\right) \\ \left(\nabla_{x_1} \Psi_e^{HF}, \nabla_{x_1} \delta\Psi_e^{HF}\right) &= \frac{1}{2}\left(\nabla_{x_1}\varphi_1(x_1), \nabla_{x_1}\delta\varphi_1(x_1)\right), \end{aligned}$$

therefore

$$\left(\nabla_x \Psi_e^{HF}, \nabla_x \delta\Psi_e^{HF}\right) = \left(\nabla_x \Phi, \nabla_x \delta\Phi\right).$$

Now, we focus on the interactions between the electrons and the nucleus:

$$\left(V_{en}\Psi_e^{HF}, \delta\Psi_e^{HF}\right) = \left(\frac{-Z}{|X - x_1|}\Psi_e^{HF}, \delta\Psi_e^{HF}\right) + \left(\frac{-Z}{|X - x_2|}\Psi_e^{HF}, \delta\Psi_e^{HF}\right)$$

where

$$\begin{aligned}
\left(\frac{-Z}{|X-x_1|}\Psi_e^{HF}, \delta\Psi_e^{HF}\right) &= \Bigg[\frac{-Z}{2|X-x_1|}\left(\varphi_1(x_1)\varphi_2(x_2) - \varphi_1(x_2)\varphi_2(x_1)\right), \\
&\quad \delta\varphi_1(x_1)\varphi_2(x_2) + \varphi_1(x_1)\delta\varphi_2(x_2) - \delta\varphi_1(x_2)\varphi_2(x_1) - \varphi_1(x_2)\delta\varphi_2(x_1)\Bigg] \\
&= \left(\frac{-Z}{2|X-x_1|}\varphi_1, \delta\varphi_1\right) + \left(\frac{-Z}{2|X-x_1|}\varphi_2, \delta\varphi_2\right)
\end{aligned}$$

so

$$\left(V_{en}\Psi_e^{HF}, \delta\Psi_e^{HF}\right) = \left(\frac{-Z}{|X-x_1|}\Phi, \delta\Phi\right) + \left(\frac{-Z}{|X-x_2|}\Phi, \delta\Phi\right).$$

Finally, we look into the interaction between electrons:

$$\begin{aligned}
\left(V_{ee}\Psi_e^{HF}, \delta\Psi_e^{HF}\right) &= \left(\frac{1}{|x_1-x_2|}\Psi_e^{HF}, \delta\Psi_e^{HF}\right) \\
&= \Bigg(\frac{1}{2|x_1-x_2|}\left(\varphi_1(x_1)\varphi_2(x_2) - \varphi_1(x_2)\varphi_2(x_1)\right), \\
&\quad \delta\varphi_1(x_1)\varphi_2(x_2) + \varphi_1(x_1)\delta\varphi_2(x_2) - \delta\varphi_1(x_2)\varphi_2(x_1) - \varphi_1(x_2)\delta\varphi_2(x_1)\Bigg) \\
&= \left(\frac{|\varphi_1|^2}{|x_1-x_2|}\varphi_2, \delta\varphi_2\right) + \left(\frac{|\varphi_2|^2}{|x_1-x_2|}\varphi_1, \delta\varphi_1\right) \\
&\quad - \left(\frac{\varphi_1\varphi_2}{|x_1-x_2|}\varphi_2, \delta\varphi_1\right) - \left(\frac{\varphi_1\varphi_2}{|x_1-x_2|}\varphi_1, \delta\varphi_2\right) \\
&= \left(\left(\operatorname{tr}(G)\, I - G\right)\Phi, \delta\Phi\right).
\end{aligned}$$

The orthonormalization of the one-electron wave functions by the Lagrange multipliers leads to:

$$\begin{aligned}
\delta\left[\operatorname{tr}\left(\tfrac{\Lambda}{2}\cdot\left(\left(\int_{\mathbb{R}^3}\Phi\otimes\Phi\right) - I\right)\right)\right] &= \operatorname{tr}\left[\tfrac{\delta\Lambda}{2}\cdot\left(\int_{\mathbb{R}^3}(\Phi\otimes\Phi) - I\right)\right] + \operatorname{tr}\left[\tfrac{\Lambda}{2}\cdot\left(\int_{\mathbb{R}^3}(\delta\Phi\otimes\Phi) + \int_{\mathbb{R}^3}(\Phi\otimes\delta\Phi)\right)\right] \\
&= \operatorname{tr}\left[\tfrac{\delta\Lambda}{2}\cdot\left(\int_{\mathbb{R}^3}(\Phi\otimes\Phi) - I\right)\right] + \operatorname{tr}\left[\Lambda\cdot\int_{\mathbb{R}^3}(\Phi\otimes\delta\Phi)\right] \\
&= \operatorname{tr}\left[\tfrac{\delta\Lambda}{2}\cdot\left(\int_{\mathbb{R}^3}(\Phi\otimes\Phi) - I\right)\right] + (\Lambda\Phi, \delta\Phi).
\end{aligned}$$

Therefore, the weak form of the Hartree-Fock problem reads:

$$\left(-\frac{1}{2}\nabla\Phi, \nabla\delta\Phi\right) + \left(\left(V_{en} + \operatorname{tr}(G)\, I - G\right)\Phi, \delta\Phi\right) = (\Lambda\Phi, \delta\Phi) + \operatorname{tr}\left[\delta\Lambda\cdot\left(I - \int_{\mathbb{R}^3}\Phi\otimes\Phi^*\right)\right],$$

$$\forall\delta\Phi\in\mathsf{W}^{\Phi},\ \forall\delta\Lambda\in\mathsf{W}^{\Lambda}. \quad \text{(F.3)}$$

# Appendix G

# Setting up the Hartree-Fock system

This Appendix details the calculation to obtain the strong form of the Hartree-Fock system from the Schrödinger equation. For the sake of clarity, the calculation is exposed for the case of a system composed of one nucleus of $Z$ protons located in $X$ and two electrons located respectively in $x_1$ and $x_2$. The two electrons are described by a unique wave function $\Psi_e$:

$$\begin{array}{rcccc} \Psi_e & : & x = (x_1, x_2) & \longmapsto & \Psi_e\,(x) \\ & & \mathbb{R}^6 & \longrightarrow & \mathbb{C} \end{array}$$

which is solution of the following system:

$$\begin{cases} -\dfrac{1}{2}\Delta_x \Psi_e + \left( \dfrac{-Z}{|X - x_1|} + \dfrac{-Z}{|X - x_2|} + \dfrac{1}{|x_1 - x_2|} \right) \Psi_e = E_e \Psi_e, \\ \int_{\mathbb{R}^6} |\Psi_e|^2 dx = 1, \\ \Psi_e(x_{\sigma(1)}, x_{\sigma(2)}) = \mathrm{sg}\,(\sigma)\, \Psi_e(x_1, x_2). \end{cases} \tag{G.1}$$

The Hartree-Fock method solves the Schrödinger equation in a reduced space $\mathsf{W}^{HF}$. The Hartree-Fock strategy approximates the wave function $\Psi_e$ by a Slater determinant $\Psi_e^{HF}$ built from two orthonormal one-electron wave functions $\varphi_1$ and $\varphi_2$ defined in $\mathbb{R}^3$:

$$\begin{cases} \Psi_e \sim \Psi_e^{HF} = \dfrac{1}{\sqrt{2}} \begin{vmatrix} \varphi_1(x_1) & \varphi_1(x_2) \\ \varphi_2(x_1) & \varphi_2(x_2) \end{vmatrix} \\ \int_{\mathbb{R}^3} \varphi_1^* \varphi_1 = \int_{\mathbb{R}^3} \varphi_2^* \varphi_2 = 1 \\ \int_{\mathbb{R}^3} \varphi_1^* \varphi_2 = \int_{\mathbb{R}^3} \varphi_2^* \varphi_1 = 0 \end{cases} \quad \text{where} \quad \begin{cases} \begin{array}{rcccc} \varphi_1 & : & x_1 & \mapsto & \varphi_1\,(x_1) \\ & & \mathbb{R}^3 & \to & \mathbb{C} \\ \varphi_2 & : & x_2 & \mapsto & \varphi_2\,(x_2) \\ & & \mathbb{R}^3 & \to & \mathbb{C}. \end{array} \end{cases} \tag{G.2}$$

By choosing a Hartree-Fock trial function, the conditions of normality and anti-symmetry of the wave function $\Psi_e$ are automatically satisfied.

The ground-state eigenpair $(\Psi_e^{HF}, E_e^{HF})$ minimizes the electronic energy:

$$E_e^{HF} = \left( -\frac{1}{2}\Delta_x \Psi_e + \left( \frac{-Z}{|X-x_1|} + \frac{-Z}{|X-x_2|} + \frac{1}{|x_1-x_2|} \right) \Psi_e^{HF}, \Psi_e^{HF} \right).$$

We express this energy as a function of the one-electron wave functions:

$$\begin{aligned} E_e^{HF} \quad = \quad & \left( -\frac{1}{2}\Delta_x \frac{1}{\sqrt{2}} \left(\varphi_1(x_1)\varphi_2(x_2) - \varphi_2(x_1)\varphi_1(x_2)\right), \frac{1}{\sqrt{2}} \left(\varphi_1(x_1)\varphi_2(x_2) - \varphi_2(x_1)\varphi_1(x_2)\right) \right) \\ & + \left( \frac{-Z}{|X-x_1|} \frac{1}{\sqrt{2}} \left(\varphi_1(x_1)\varphi_2(x_2) - \varphi_2(x_1)\varphi_1(x_2)\right), \frac{1}{\sqrt{2}} \left(\varphi_1(x_1)\varphi_2(x_2) - \varphi_2(x_1)\varphi_1(x_2)\right) \right) \\ & + \left( \frac{-Z}{|X-x_2|} \frac{1}{\sqrt{2}} \left(\varphi_1(x_1)\varphi_2(x_2) - \varphi_2(x_1)\varphi_1(x_2)\right), \frac{1}{\sqrt{2}} \left(\varphi_1(x_1)\varphi_2(x_2) - \varphi_2(x_1)\varphi_1(x_2)\right) \right) \\ & + \left( \frac{1}{|x_1-x_2|} \frac{1}{\sqrt{2}} \left(\varphi_1(x_1)\varphi_2(x_2) - \varphi_2(x_1)\varphi_1(x_2)\right), \frac{1}{\sqrt{2}} \left(\varphi_1(x_1)\varphi_2(x_2) - \varphi_2(x_1)\varphi_1(x_2)\right) \right) \end{aligned}$$

Using the orthonormality of the one-electron wave functions, we can express simply the electronic energy. The Hartree-Fock problem reads:

$$\begin{cases} \min \left\{ E_e^{HF} = -\left( \frac{1}{2}\Delta_{x_1}\varphi_1(x_1), \varphi_1(x_1) \right) - \left( \frac{1}{2}\Delta_{x_2}\varphi_2(x_2), \varphi_2(x_2) \right) \right. \\ \qquad + \left( \frac{-Z}{|X-x_1|}\varphi_1(x_1), \varphi_1(x_1) \right) + \left( \frac{-Z}{|X-x_2|}\varphi_2(x_2), \varphi_2(x_2) \right) \\ \qquad \left. + \left( \left( \frac{\varphi_1(x_1)}{|x_1-x_2|}, \varphi_1(x_1) \right) \varphi_2(x_2), \varphi_2(x_2) \right) - \left( \left( \frac{\varphi_1(x_1)}{|x_1-x_2|}, \varphi_2(x_1) \right) \varphi_1(x_2), \varphi_2(x_2) \right) \right\}, \\ 1 = (\varphi_1, \varphi_1) = (\varphi_2, \varphi_2), \\ 0 = (\varphi_1, \varphi_2) = (\varphi_2, \varphi_1). \end{cases}$$

We solve this problem with the Euler-Lagrange equations, and impose the orthonormalization constraint using the Lagrange multipliers $\Lambda_{11}$, $\Lambda_{12}$ and $\Lambda_{22}$:

$$\begin{aligned} \mathcal{L}(\varphi_1, \varphi_2, \Lambda_{11}, \Lambda_{12}, \Lambda_{22}) = E_e^{HF} + \Lambda_{11} \left( 1 - \int_{\mathbb{R}^3} \varphi_1 \varphi_1^* \right) + \Lambda_{12} \int_{\mathbb{R}^3} \varphi_1^* \varphi_2 \\ + \Lambda_{12} \int_{\mathbb{R}^3} \varphi_2^* \varphi_1 + \Lambda_{22} \left( 1 - \int_{\mathbb{R}^3} \varphi_2^* \varphi_2 \right). \end{aligned} \tag{G.3}$$

Minimizing this Lagrangian, we get:

$$d\mathcal{L} = \frac{\partial \mathcal{L}}{\partial \varphi_1} d\varphi_1 + \frac{\partial \mathcal{L}}{\partial \varphi_2} d\varphi_2 + \frac{\partial \mathcal{L}}{\partial \Lambda_{11}} d\Lambda_{11} + \frac{\partial \mathcal{L}}{\partial \Lambda_{22}} d\Lambda_{22} + \frac{\partial \mathcal{L}}{\partial \Lambda_{12}} d\Lambda_{12} = 0,$$

and then the following system called the Hartree-Fock system:

$$\begin{cases} -\frac{1}{2}\Delta_x\varphi_1 - \frac{Z}{|X-x|}\varphi_1 + \frac{|\varphi_2(x_1)|^2}{|x_1-x|}\varphi_1 - \frac{\varphi_1(x_1)\varphi_2(x_1)}{|x_1-x|}\varphi_2 - \Lambda_{11}\varphi_1 - \Lambda_{12}\varphi_2 = 0, \\ -\frac{1}{2}\Delta_x\varphi_2 - \frac{Z}{|X-x|}\varphi_2 + \frac{|\varphi_1(x_1)|^2}{|x_1-x|}\varphi_2 - \frac{\varphi_1(x_1)\varphi_2(x_1)}{|x_1-x|}\varphi_1 - \Lambda_{12}\varphi_1 - \Lambda_{22}\varphi_2 = 0, \\ 1 - \int_{\mathbb{R}^3}\varphi_1^*\varphi_1 = 0, \\ \int_{\mathbb{R}^3}\varphi_1^*\varphi_2 = 0, \\ \int_{\mathbb{R}^3}\varphi_2^*\varphi_1 = 0, \\ 1 - \int_{\mathbb{R}^3}\varphi_2^*\varphi_2 = 0. \end{cases}$$

We denote $\Phi = \begin{bmatrix} \varphi_1 \\ \varphi_2 \end{bmatrix}$, $\Lambda = \begin{bmatrix} \Lambda_{11} & \Lambda_{12} \\ \Lambda_{21} & \Lambda_{22} \end{bmatrix}$, $G = \begin{bmatrix} G_{11} & G_{12} \\ G_{21} & G_{22} \end{bmatrix} = \begin{bmatrix} \frac{|\varphi_1(x_1)|^2}{|x_1-x|} & \frac{\int \varphi_1^*(x_1)\varphi_2(x_1)}{|x_1-x|} \\ \frac{\int \varphi_2^*(x_1)\varphi_1(x_1)}{|x_1-x|} & \frac{|\varphi_2(x_1)|^2}{|x_1-x|} \end{bmatrix}$.
The Hartree-Fock system reads:

$$\begin{cases} -\frac{1}{2}\Delta_x\Phi - \frac{Z}{|X-x|}\Phi + (\mathrm{tr}\,(G)\,I - G)\Phi - \Lambda\Phi = 0, \\ \int_{\mathbb{R}^3}\Phi\otimes\Phi = I. \end{cases}$$

In the general case of a system with $N_e$ wave functions, we get a similar system with the following conditions:

$$\begin{cases} \mathcal{L}\left(\Phi,\Lambda\right) = \left(H\Psi_e^{HF}, \Psi_e^{HF}\right) + \mathrm{tr}\left[\Lambda\cdot\left(I - \int_{\mathbb{R}^3}\Phi\otimes\Phi^* dx\right)\right], \\ \Psi_e^{HF}\left(x_1,...,x_{N_e}\right) = \frac{1}{\sqrt{N_e!}}\det\left[\Phi\left(x_1\right),...,\Phi\left(x_{N_e}\right)\right]_{i\in[1;N_e]}. \end{cases}$$

# Appendix H

# The Two-dimensional equations

Appendix F introduced how to get the Fock system:

$$\boxed{\begin{array}{ll} \left(-\frac{1}{2}\nabla_{x_e}\Phi, \nabla_{x_e}\delta\Phi\right) + (V_{en}\Phi, \delta\Phi) + ((\mathrm{tr}\,(G)\,I - G)\,\Phi, \delta\Phi) = (\Lambda\Phi, \delta\Phi)\,, & \forall\delta\Phi \in \mathsf{W}^{\Phi}, \\ \mathrm{tr}\left[\nabla_{x_e}G \cdot \nabla_{x_e}\delta G^T\right] = \mathrm{tr}\left[(4\pi\Phi \otimes \Phi^*) \cdot \delta G^T\right], & \forall\delta G \in \mathsf{W}^{G}, \\ \mathrm{tr}\left[\left(I - \int_{\mathbb{R}^3}\Phi \otimes \Phi^*\right) \cdot \delta\Lambda^T\right] = 0, & \forall\delta\Lambda \in \mathsf{W}^{\Lambda}. \end{array}}$$

This system is defined in a three-dimensional space $(r, \theta, z)$. For isolated atoms or isolated linear molecules *i.e.* molecules in which all bond angles are 180 degrees, we can determine analytically the dependence with respect to $\theta$ of each one-electron wave function. For each one-electron wave function $\varphi_i$, it is defined from its magnetic quantum number $m_i$.

We therefore assume that each wave function is the product of an unknown in-plane function $\varphi_i^{rz}(r, z)$ and an *a priori* known angular function $\varphi_i^{\theta}(\theta) = e^{im_i\theta}$:

$$\varphi_i(r, \theta, z) = e^{im_i\theta}\varphi_i^{rz}(r, z).$$

We compute by the FEM the functions $\varphi_i^{rz}$ in the plane $(r, z)$. We introduce in this Appendix how the different equations are modified to be expressed only in the $(r, z)$ plane.

We express the operator nabla $\nabla_x$ defined in the three-dimensional space $(r, \theta, z)$ as a function analytically known from the differential operator $\nabla_{rz}$ defined in the two-dimensional space $(r, z)$:

$$\nabla_x\varphi_i \quad = \quad \frac{\partial\varphi_i}{\partial r}e_r + \frac{\partial\varphi_i}{\partial\theta}\frac{e_\theta}{r} + \frac{\partial\varphi_i}{\partial z}e_z,$$

$$
\begin{aligned}
\nabla_x \varphi_i &= e^{im_i\theta}\left(\frac{\partial \varphi_i^{rz}}{\partial r}e_r + \frac{\partial \varphi_i^{rz}}{\partial z}e_z\right) + im_i e^{im_i\theta}\varphi_i^{rz}(r,z)\frac{e_\theta}{r},\\
\nabla_x \varphi_i &= e^{im_i\theta}\nabla_{rz}\varphi_i^{rz} + im_i e^{im_i\theta}\varphi_i^{rz}(r,z)\frac{e_\theta}{r}.
\end{aligned}
$$

We take the same approach for the Green interaction terms $G_{ij}(r,\theta,z) = e^{i(m_i-m_j)\theta}G_{ij}^{rz}(r,z)$:

$$
\begin{aligned}
\nabla_x G_{ij} &= \frac{\partial G_{ij}}{\partial r}e_r + \frac{\partial G_{ij}}{\partial \theta}\frac{e_\theta}{r} + \frac{\partial G_{ij}}{\partial z}e_z,\\
\nabla_x G_{ij} &= e^{i(m_i-m_j)\theta}\left(\frac{\partial G_{ij}^{rz}}{\partial r}e_r + \frac{\partial G_{ij}^{rz}}{\partial z}e_z\right) + i(m_i-m_j)e^{i(m_i-m_j)\theta}G_{ij}^{rz}(r,z)\frac{e_\theta}{r},\\
\nabla_x G_{ij} &= e^{i(m_i-m_j)\theta}\nabla_{rz}G_{ij}^{rz} + i(m_i-m_j)e^{i(m_i-m_j)\theta}G_{ij}^{rz}(r,z)\frac{e_\theta}{r}.
\end{aligned}
$$

Therefore, in the two-dimensional space, the Fock system becomes:

$$
\boxed{
\begin{aligned}
&\left(\sum_{j=1}^{N_e} e^{i(m_j-m_i)\theta}\Lambda_{ij}\varphi_j^{rz}, \delta\varphi_i^{rz}\right) = -\frac{1}{2}\left[(\nabla_{rz}\varphi_i^{rz}, \nabla_{rz}\delta\varphi_i^{rz}) - \left(\frac{m_i^2}{r^2}\varphi_i^{rz}, \delta\varphi_i^{rz}\right)\right]\\
&\qquad\qquad + \left(\left(\left(V_{en} + \operatorname{tr}(G)\right)I - G\right)\varphi_i^{rz}, \delta\varphi_i^{rz}\right), \qquad \forall \delta\varphi_i^{rz} \in \mathsf{W}^{\varphi_i^{rz}},\\
&\operatorname{tr}\left[\nabla_{rz}G_{ij}^{rz}.\nabla_{rz}\delta G_{ij}^{rz}\right] - \frac{(m_i-m_j)^2}{r^2}\left(G_{ij}^{rz}, \delta G_{ij}^{rz}\right) = \operatorname{tr}\left[\left(4\pi\varphi_i^{rz}\otimes\varphi_j^{rz^*}\right).\delta G_{ij}^{rz^T}\right], \quad \forall \delta G_{ij}^{rz} \in \mathsf{W}^{G_{ij}^{rz}},\\
&\operatorname{tr}\left[\left(I_{ij} - e^{i(m_i-m_j)}\left(\int_{\mathbb{R}^3}\varphi_i^{rz}\otimes\varphi_j^{rz^*}\right)\right).\delta\Lambda_{ij}^T\right] = 0, \qquad \forall \delta\Lambda_{ij}^{rz} \in \mathsf{W}^{\Lambda_{ij}^{rz}}.
\end{aligned}
}
$$

# Appendix I

# Magnetic properties

We can benefit from quantum computations to estimate magnetic properties such as the magnetic moment and the magnetizability [Sla51, RSL63, AF05]. We derive them from the total energy $E$ when the Schrödinger equation takes the magnetic field into account. The magnetic moment $m$ and the magnetizability tensor $\xi$ can be defined respectively as the opposite of the derivative of the energy with respect to the magnetic field $B$ at the first order and at the second order:

$$m = -\frac{\partial E}{\partial B}, \tag{I.1}$$

$$\xi = -\frac{\partial^2 E}{\partial B \partial B}. \tag{I.2}$$

The magnetic potential of a system under the application of an external magnetic field $B$ reads [NLK86]:

$$V_e^{mag}(x_k) = e\, i\, (\nabla_{x_k} . \wedge B)\, x_k, \tag{I.3}$$

$$V_n^{mag}(X_j) = e\, i\, Z_j\, (\nabla_{x_k} . \wedge B)\, X_j. \tag{I.4}$$

From equation (1.33), a perturbation of the magnetic field $\delta B$ leads to a perturbation of the potential $\delta V_e = e\, i\, (\nabla_{x_k} . \wedge \delta B)\, x_k$ and a perturbation of the electronic energy:

$$\delta E_e = \left( \left( e\, i\, (\nabla_{x_k} . \wedge \delta B)\, x_k \right) \Psi_e, \Psi_e \right). \tag{I.5}$$

Thus, the electronic magnetic dipole moment denoted by $m_e$ and defined by equation (1.4) reads

$$m_e = -\left( \left( e\, i\, (\nabla_{x_k} . \wedge 1)\, x_k \right) \Psi_e, \Psi_e \right). \tag{I.6}$$

The magnetic dipole moment describes the torque that a magnetic field can exert on the system and the force that the system can exert on electric currents. It is expressed in A.m$^2$ or in J.T$^{-1}$ in the SI system. Considering the Hartree-Fock approximation and the nuclei as particles without speed, the magnetic moment can be expressed as follows:

$$m^{HF} = -\left(\left(e\, i\left(\nabla_{x_k}. \wedge 1\right) x_k\right) \Phi, \Phi\right). \tag{I.7}$$

Using the configuration interaction approximation, it yields that:

$$m^{CI} = -\sum_{A=1}^{N_d} \sum_{B=1}^{N_d} \alpha_A \alpha_B \left(\left(e\, i\left(\nabla_{x_k}. \wedge 1\right) x_k\right) \Phi^A, \Phi^B\right). \tag{I.8}$$

The magnetizability tensor $\xi$ characterizes the ability of a system to be magnetized by any external magnetic field. It is expressed in m$^2$.A$^2$.s$^2$.kg$^{-1}$ or in J.T$^{-2}$ in the SI system, or in $e^2.a_0^2.m_e^{-1}$ in the atomic system. From equation (4.11), we establish:

$$\delta^2 E = \left(\left(e\, i\left(\nabla_{x_k}. \wedge \delta^2 B\right) x_k\right) \Psi_e, \Psi_e\right) + 2\left(\left(e\, i\left(\nabla_{x_k}. \wedge \delta B\right) x_k\right) \otimes \delta\Psi_e, \Psi_e\right) \tag{I.9}$$

therefore the magnetizability tensor defined by equation (I.2) reads:

$$\xi = -\left(\left(e\, i\left(\nabla_{x_k}. \wedge 1\right) x_k\right) \Psi_e, \Psi_e\right) - 2\left(\left(e\, i\left(\nabla_{x_k}. \wedge 1\right) x_k\right) \otimes \frac{\delta\Psi_e}{\delta B}, \Psi_e\right). \tag{I.10}$$

Applying the Hartree-Fock model, it yields that:

$$\xi^{HF} = -\left(\left(e\, i\left(\nabla_{x_k}. \wedge 1\right) x_k\right) \Phi, \Phi\right) - 2\left(\left(e\, i\left(\nabla_{x_k}. \wedge 1\right) x_k\right) \otimes \frac{\delta\Phi}{\delta B}, \Phi\right). \tag{I.11}$$

With the configuration interaction approximation, it reads:

$$\xi^{CI} = -\sum_{A=1}^{N_d} \sum_{B=1}^{N_d} \alpha_A \alpha_B \left[\left(\left(e\, i\left(\nabla_{x_k}. \wedge 1\right) x_k\right) \Phi^A, \Phi^B\right) + 2\left(\left(e\, i\left(\nabla_{x_k}. \wedge 1\right) x_k\right) \otimes \frac{\delta\Phi^A}{\delta B}, \Phi^B\right)\right]. \tag{I.12}$$

# Appendix J

# Crystals: The Bloch theorem

In Chapter 4, we presented numerical results for isolated systems. However, most systems interact with their surroundings. For instance, atoms in crystals present periodic interactions with neighboring atoms. This Appendix focuses on the Bloch theorem which is applied to model and analyze crystal structures.

### The periodic atomic arrangement in crystals

A crystal is a solid material, whose constituent atoms are arranged in an orderly repeating pattern extending in all three spatial dimensions. For example, Figure J.1 represents the LiH crystal, which is composed of lithium and hydrogen atoms perfectly ordered.

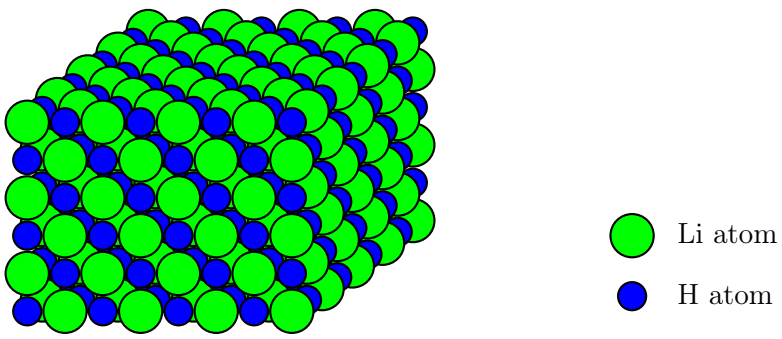


Figure J.1: Scheme of a perfect LiH crystal

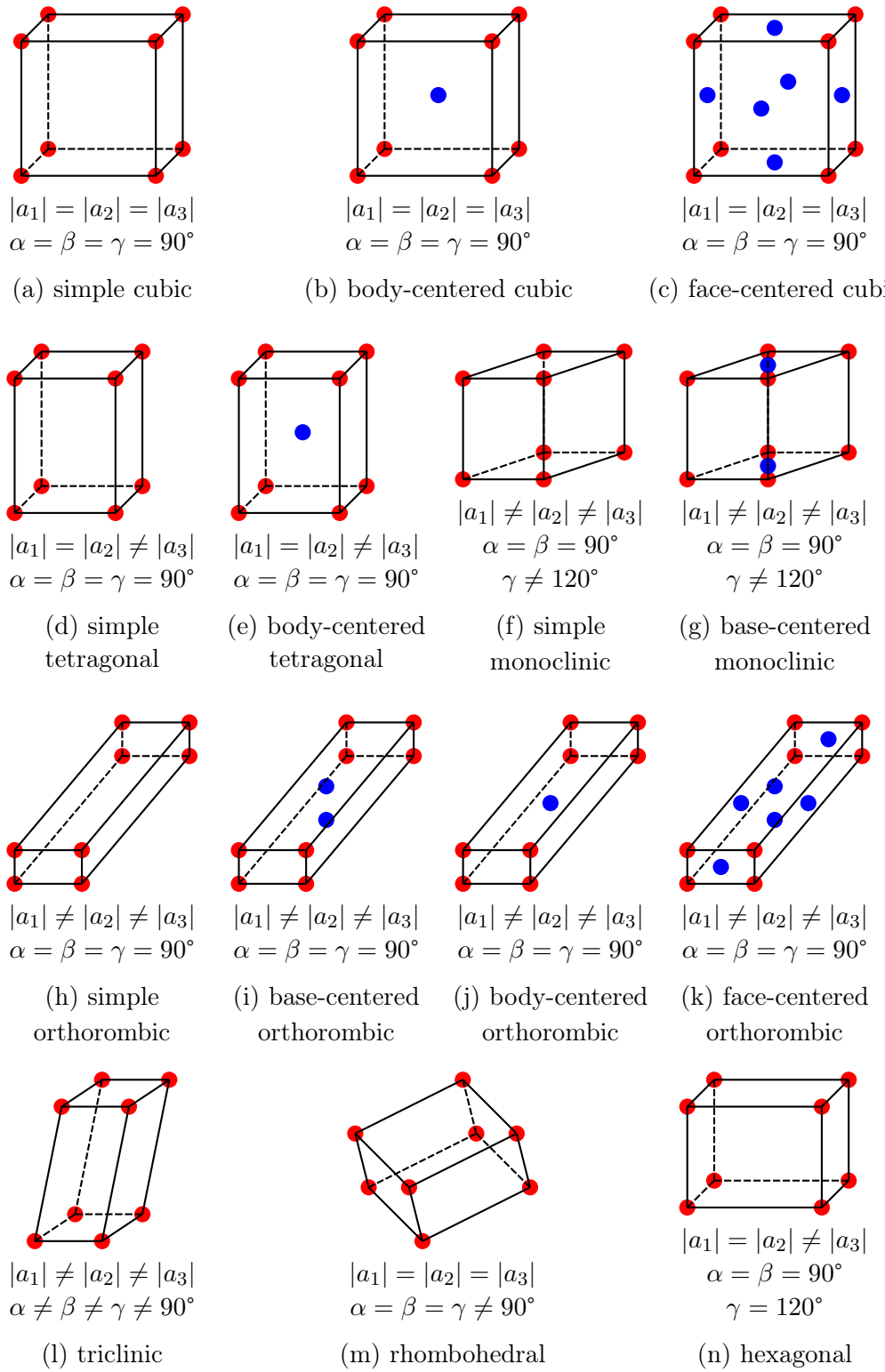


Figure J.2: The 14 three-dimensional Bravais lattices (parallelograms whose lengths of side are $|a_1|$, $|a_2|$ and $|a_3|$, and the angles between the different sides $\alpha$, $\beta$ and $\gamma$)

The periodicity of the lattice is described by a geometrical arrangement and a chemical arrangement.

The geometrical arrangement is defined by a Bravais lattice [Bra50], which is a regular distribution of points in the space respecting the periodicity of the crystal. Provided the positions $X_0$ of the nuclei of the atoms of one cell of the crystal, the positions $X_n$ of the other nuclei of the crystal lattice can be obtained by translation of the first cell:

$$X_n = X_0 + n_i a_i \tag{J.1}$$

with $a_i$ the direction vectors and $n_i$ the number of cells in the direction of $a_i$. The parameters of the lattice are the lengths $|a_i|$ of the primitive vectors and the angles formed by them: $\alpha$, $\beta$ and $\gamma$. For example, Figure J.3 represents the cubic Bravais lattice of the LiH crystal.

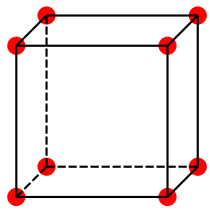

$a_1 = a_2 = a_3 = 2,042.10^{-10}\, m$
$\alpha = \beta = \gamma = 90°$

Figure J.3: Bravais lattice of the LiH crystal

The Bravais lattice can be considered as a vector space where the scalars $n_i$ are only integers. The basis of the Bravais lattice is a set of vectors $a_i$, which are linearly independent in $\mathbb{R}^3$. This basis is not unique, but its volume is unique. The fundamental space is constituted by the points whose coordinates $n_i$ belongs to $[0, 1[$. Generally, it is called the primitive cell.

We can classify lattices with respect to their symmetry group, which describes rotations and translations that do not disturb the lattice. Therefore, the number of different lattices is infinite but the number of types of lattices is finite. In a one-dimensional space, only one type of lattice exists. Five different types of lattice exist in a two-dimensional space and fourteen different types in a three-dimensional space. They are represented on Figure J.2.

Because a crystal can be composed of different types of atoms, the distribution of points is not sufficient to characterize the whole structure. It is necessary to clarify the chemical arrangement by the description of a periodic cell. The whole structure can be built by translation operations of this cell. Therefore, the cell represented on Figure J.4(a) can not be considered as a periodic cell whereas the cells of Figure J.4(b) and Figure J.4(c) are acceptable. The cell represented on Figure J.4(c) is the elementary cell also called the Wigner-Seitz cell or the Dirichlet zone.

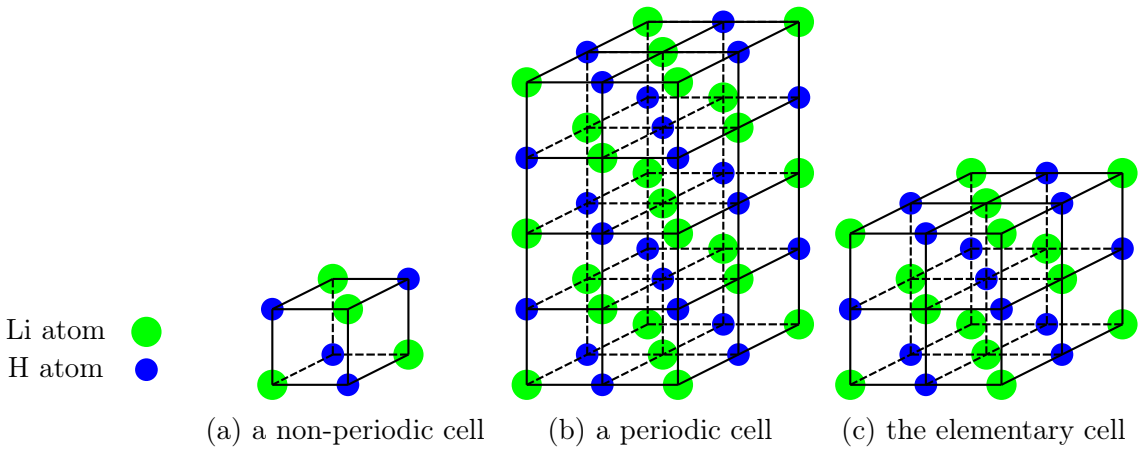


Figure J.4: Different cells of the LiH crystal

Let us consider the electrons of a perfect infinite crystal, the structure is perfectly periodic, but not the wave function of the system. Lots of efforts could be saved by reducing the FEM domain from the entire periodic crystal to a primitive cell by applying the Bloch theorem.

### The Bloch theorem

Numerical computations aim at taking advantage of the periodicity of the lattice to reduce computational costs. The Bloch transformation was introduced in 1928 [Blo28], and it is traditionnally used in the context of solid state physics [AF05]. Nevertheless, this approach is also appealing to analyze other periodic structures *e.g.* honeycombs [ACV98, TTAS11].

The perfect crystal is a periodic strucure $\Omega$ of space dimension $N_c$. Let us define a primitive cell $Q_0$ and a set of basis vectors $\{a_i\}_{i\in[1;N_c]}$, called direct cell basis, such that the entire structure

$\Omega$ can be reconstituted by repeating the primitive cell along the three directions of the direct cell basis. The reciprocal cell $Q_0^*$, called the first Brillouin zone [Bri53] and the reciprocal cell basis $\{a_i^*\}_{i\in[1;N_c]}$ are defined as dual to $Q_0$ and $\{a_i\}_{i\in[1;N_c]}$, and satisfy:

$$\begin{cases} \dfrac{a_i^*.a_j}{|a_i|\,|a_j|} = \delta_{ij} \\ |Q_0|\,|Q_0^*| = 1, \end{cases} \tag{J.2}$$

where $\delta_{ij}$ stands for the Kronecker delta, and $|Q_0|$ and $|Q_0^*|$ are respectively the volumes of the elementary Wigner-Seitz cell and the volume of the first Brillouin cell.

For any non-periodic function $\Psi_e(x)$ defined on $\Omega^{N_e}$, the Bloch theorem states that, for each wave vector $k$ of the first Brillouin zone, the Bloch wave functions $\tilde{\Psi}_e^k(x,k)$ are some periodic functions with the same periodicity as the crystal $\Omega$, which are defined as:

$$\begin{array}{rcccl} \tilde{\Psi}_e^k & : & (x,k) & \longmapsto & \tilde{\Psi}_e^k(x,k) = \sum\limits_{i=1}^{N_c} \Psi_e(x+n_i a_i)\exp^{i(k,x+n_i a_i)} \\ & & \Omega^{N_e}\times {Q_0^*}^{N_e} & \longrightarrow & \mathbb{C}, \end{array} \tag{J.3}$$

from the non-periodic function $\Psi_e(x)$ :

$$\begin{array}{rcccl} \Psi_e & : & x & \longmapsto & \Psi_e(x) \\ & & \Omega^{N_e} & \longrightarrow & \mathbb{C}, \end{array}$$

with $n_i \in \mathbb{Z}$ the number of cells in the direction of the vector $a_i$.

The inverse Bloch transformation provides the value of the wave function $\Psi_e$ at any point $x$ by integrating the Bloch wave functions $\tilde{\Psi}_e^k(x,k)$ over the first Brillouin zone $Q_0^*$:

$$\Psi_e(x) = \frac{1}{|Q_0^*|}\int_{Q_0^*} \tilde{\Psi}_e^k(x,k)\exp^{-i(k,x)}\,dk. \tag{J.4}$$

Thus, by virtue of the Bloch theorem, any non-periodic wave function in a periodic crystal can be decomposed into Bloch wave functions $\tilde{\Psi}_e^k$ that are periodic with periods $a_i$ in the direct space. The strategy to solve a crystal can be summed up by Figure J.5.

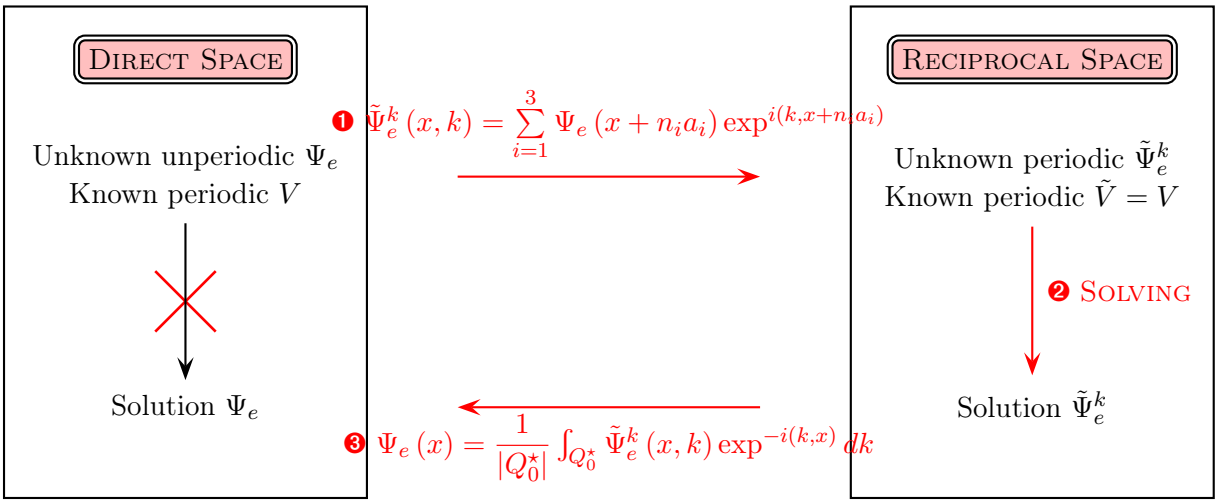


Figure J.5: Modeling a perfect crystal

Let us suppose a three-dimensional perfectly periodic crystal, the crystal wave function is defined in $\mathbb{R}^{3N_e}$ and the Bloch function is defined from a $6N_e$-dimensional space, which is the sum of the $x$-space and the $k$-space. The Schrödinger equation is solved in this $6N_e$-dimensional space to provide the function $\tilde{\Psi}_e^k(x,k)$. From which, we build *a posteriori* the solution $\Psi_e(x)$. Therefore, the problem can be solved only on the elementary cell in the direct space.

To obtain the solution of the problem not only in the elementary cell but also in the whole crystal, we use the periodicity properties of the Bloch functions:

$$\Psi_e(x + n_i.a_i) = \frac{1}{|Q_0^*|} \int_{Q_0^*} \tilde{\Psi}_e^k(x,k) \exp^{-i(k,x+n_i.a_i)} dk. \tag{J.5}$$

### The periodic problem

From the Schrödinger problem (equation 2.5), we deduce that the periodic wave function $\tilde{\Psi}_e$ satisfies:

$$\frac{1}{2}\left(\nabla_x \tilde{\Psi}_e^k, \nabla_x \delta\tilde{\Psi}_e^k\right) + \left(i\,k\nabla_x \tilde{\Psi}_e^k + \frac{1}{2}|k|^2 \tilde{\Psi}_e^k + V_e \tilde{\Psi}_e^k, \delta\tilde{\Psi}_e^k\right) = \tilde{E}_e^k\left(\tilde{\Psi}_e^k, \delta\tilde{\Psi}_e^k\right) + \frac{\delta\tilde{E}_e^k}{2}\left[\left(\tilde{\Psi}_e^k, \tilde{\Psi}_e^k\right) - 1\right]$$
$$+ \delta\tilde{\lambda}^k\left[\tilde{\Psi}_e^k(x_{\sigma(1)}, \ldots, x_{\sigma(N_e)}) - \mathrm{sg}(\sigma)\,\tilde{\Psi}_e^k(x_1, \ldots, x_{N_e})\right],$$

$$\forall \delta\tilde{\Psi}_e^k \in \tilde{\mathsf{W}}^k,\ \forall \delta\tilde{E}_e^k \in \tilde{\mathsf{W}}^{E_e^k},\ \forall \delta\tilde{\lambda}^k \in \tilde{\mathsf{W}}^{\lambda^k}. \quad \text{(J.6)}$$

This equation is highly multi-dimensional. To become tractable numerically, we apply the Hartree-Fock method. The trial function is a Slater determinant built from a vector $\tilde{\Phi}^k$ of one-electron wave functions $\tilde{\varphi}_i^k$. The vector $\tilde{\Phi}^k$ satisfies the following Fock system:

$$\begin{aligned}
&\left(-\frac{1}{2}\nabla_x\tilde{\Phi}^k, \nabla_x\delta\tilde{\Phi}^k\right)\\
&\quad + \left(i\,k\nabla_x\tilde{\Phi}^k + \frac{1}{2}|k|^2\tilde{\Phi}^k + V_{en}\tilde{\Phi}^k + \left(\mathrm{tr}(\tilde{G}^k)I - \tilde{G}^k\right)\tilde{\Phi}^k, \delta\tilde{\Phi}^k\right) = \left(\tilde{\Lambda}^k\tilde{\Phi}^k, \delta\tilde{\Phi}^k\right),\\
&\mathrm{tr}\left[\nabla_x\tilde{G}^k \cdot \nabla_x\delta\tilde{G}^{k^T}\right] = \mathrm{tr}\left[\left(4\pi\tilde{\Phi}^k \otimes \tilde{\Phi}^{k^*}\right) \cdot \delta\tilde{G}^{k^T}\right],\\
&\mathrm{tr}\left[\left(I - \int_{\mathbb{R}^3}\tilde{\Phi}^k \otimes \tilde{\Phi}^{k^*}\right) \cdot \delta\tilde{\Lambda}^{k^T}\right] = 0,\\
&\qquad\qquad \forall \delta\tilde{\Phi}^k \in \tilde{\mathsf{W}}^{\Phi^k}, \forall \delta\tilde{G}^k \in \tilde{\mathsf{W}}^{G^k}, \forall \delta\tilde{\Lambda}^k \in \tilde{\mathsf{W}}^{\Lambda^k}.
\end{aligned} \quad \text{(J.7)}$$

The matrix $\tilde{\Lambda}^k$ contains Lagrange multipliers and on its diagonal, yield the individual electronic energies. $V_{en}$ is the interaction potential between electrons and nuclei. $\tilde{G}^k$ is the interaction matrix due to the interaction between electrons.

**Potential to consider** The electrons of the elementary cell are submitted to the Coulomb potential due not only to the particles of the cell, but to all the particles of the crystal. The interactions between electrons and nuclei are described by a potential that has the perfect periodicity of the Bravais lattice:

$$V_{en}(x + n_i.a_i) = V_{en}(x), \qquad \forall n_i \in \mathbb{Z}. \quad \text{(J.8)}$$

The interaction between an electron localized in $x_i$ and the $N_n$ nuclei of atomic number $Z_j$ localized in $X_j$ and the other electrons localized in $x_k$ of the crystal reads:

$$V_e(x_i) = \sum_{j=1}^{N_n} \frac{-Z_j}{|X_j - x_i|} + \sum_{\substack{k=1\\k\neq i}}^{N_e} \frac{1}{|x_k - x_i|}. \quad \text{(J.9)}$$

For perfect infinite crystals, the number of nuclei $N_n$ is infinite. The difficulty to estimate accurately the Coulomb potential is to take into account enough surrounding nuclei.

Many works have been published on the methods to estimate the Coulomb potential in a periodic structure [DPRS83]. According to [YDP93], it is essential to take into account long-range electrostatic interactions. Truncated list methods (direct truncation and "twin-range" cutoff methods) appear as poor methods. Ewald [Ewa21] proposes to consider the space as repeating unit cells; details about the Ewald sums are provided in [TJ96, DPLP99]. Darden *et al.* [DYP93] compute these sums by a fast $N \times \lg(N)$ algorithm. Another approach is multipole calculations. The space is divided into cells, and each cell is represented by a multipole moment series: charges, dipoles, quadrupoles, octopoles,... This method becomes faster than the exact algorithm when the number of atoms exceeds 300 [DKG92].

The number of eigenmodes is infinite, whereas the electronic density in the crystal is finite. All the modes cannot be occupied. The occupied modes are determined by computing the Fermi energy.

### The Fermi energy

At 0 K, the energy of the system is the minimum of the energy functional that can admit an electronic density matching the number of electrons on the elementary cell. This energy is called the Fermi energy $E_F$:

$$E_F = \min_{E_e} \left\{ \int_{-\infty}^{E_e} \rho(E_e)\, dE_e = N_e \right\}. \tag{J.10}$$

Electrons are fermions so they satisfy the Fermi-Dirac distribution $\mu_T(x) = \dfrac{1}{1+\exp^{-x/k_B T}}$ [Fer26, Dir26]. The electronic density reads:

$$\rho(E_e) = \frac{2}{|\Omega|} \sum_i \int_{Q_0^*} \mu_T' \left( E_e - E_{e_i}^k(k) \right) dk, \tag{J.11}$$

where the factor 2 is used considering a RHF approach. $E_{e_i}^k$ is the spectrum of eigenvalues, whose values depend on the wave number $k$.

$$\rho(E_e) = \frac{2}{|Q_0^*|} \sum_i \int_{Q_0^*} H' \left( E_e - E_{e_i}^k(k) \right) dk \tag{J.12}$$

where $H$ is the Heaviside function defined by:

$$H(x) = \begin{cases} 0, & x < 0, \\ 1, & x \geqslant 0. \end{cases} \tag{J.13}$$

The derivative of this function is a Dirac mass at 0 that we denote $\delta$.

$$\rho(E_e) = \frac{2}{|Q_0^*|} \sum_i \int_{Q_0^*} \delta\left(E_e - E_{e_i}^k(k)\right) dk \tag{J.14}$$

For insulators at the equilibrium state, the surfaces $E_{e_i}^k(k)$ have dedicated rays and do not cross the focus of other eigenvalues. Therefore, $\frac{N_e}{2}$ eigenmodes are fully occupied, the other ones are void. In case of metals, a value $E_e$ can match several eigenmodes, the determination of the Fermi energy is a more delicate problem.

For instance, provided the band structure of a one-dimensional crystal illustrated on Figure J.6, if there are two electrons per cell, only the first eigenmode is doubly occupied. Accordingly, this system is an insulator. If there were three electrons per cell, the first mode is doubly occupied, and the second and third eigenmodes would be both partially occupied. The crystal would be a metal.

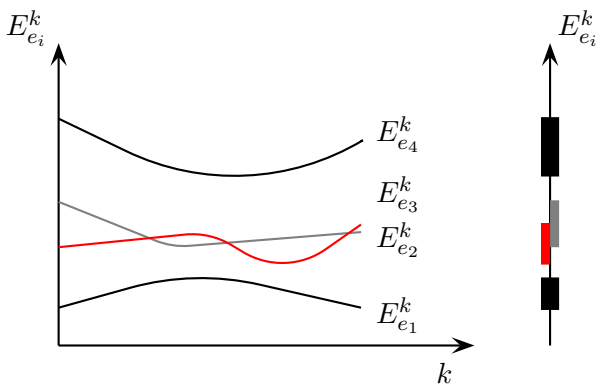


Figure J.6: The band structure of a one-dimensional crystal [Bla00]

### Integration over the Brillouin zone

Once the periodic problem has been solved, the solution $\Phi(x)$ is built by integrating the Bloch functions $\tilde{\Phi}^k(x,k)$ over the Brillouin zone.

To reduce the calculation time, for sufficiently smooth functions, it is possible to perform the integration by estimating the function only in a carefully selected set of a few points in the Brillouin zone called special points [Dal96]. Several sets of special points exist depending on the Bravais lattice and the group symmetry [BSW36]. Historically, the use of the special points was introduced by Baldereschi in 1973. He showed in [Bal73] that the computation of the charge density of semiconductors could be performed by using a single point. Chadi and Cohen [CC73a, CC73b] set up a procedure to generate special-point sets, and proposed sets for the cubic and hexagonal lattices. Monkhorst and Park [MP76] introduced a more systematic strategy based on equally spaced points. The application of the special-point method to metals requires particular care, Methfessel and Paxton deal with this particular case in [MP89].

## Abstract

Since performances of experimental and numerical tools have been largely improved, mechanics of materials can explore smaller and smaller scales. Thus, a better comprehension, or even a prediction, of local phenomena associated with macroscopic deformations are hoped. This dissertation focuses on the smallest scale involved in mechanical behavior of materials, *i.e.* interactions between nuclei due to electrons behavior and especially to valence electrons. The originality of this work is setting up the finite element method as numerical tool to solve this problem. This approach largely used to solve structural mechanics problems provides powerful numerical tools to tackle electronic structures. The Hartree-Fock and post-Hartree-Fock models are employed, and mechanical properties of electronic structures are estimated. These estimates are based on a set of approximations of both model and numerical origins. Error estimates are proposed to analyze the accuracy of the results.

## Résumé

Grâce à l'amélioration des performances des outils expérimentaux et numériques, la mécanique des matériaux peut explorer des échelles de plus en plus fines. Une meilleure compréhension, voire une prédiction, des phénomènes locaux mis en jeu est alors espérée. Cette thèse s'intéresse à la plus petite échelle impliquée dans le comportement mécanique des matériaux, c.-à-d. les interactions entre noyaux dues au comportement des électrons, et notamment des électrons de valence. L'originalité de ce travail est dans la mise en place des éléments finis comme outil numérique de résolution de ce problème. Cette approche largement utilisée dans le domaine de la mécanique des structures fournit de puissants outils numériques permettant de résoudre le problème électronique. Des modèles de Hartree-Fock et post-Hatree-Fock sont implémentés, et les caractéristiques mécaniques des structures électroniques sont estimées. Ces résultats reposent sur de nombreuses approximations dues aussi bien à la modélisation qu'aux approximations numériques. Des estimateurs d'erreur sont développés pour analyser les résultats.